



HAL
open science

Development, characterization and optimization of sustainable green composites with advanced sandwich structure

Chen Chen

► **To cite this version:**

Chen Chen. Development, characterization and optimization of sustainable green composites with advanced sandwich structure. Mechanics of materials [physics.class-ph]. Centrale Lille Institut, 2021. English. NNT: 2021CLIL0034 . tel-04614176

HAL Id: tel-04614176

<https://theses.hal.science/tel-04614176>

Submitted on 17 Jun 2024

HAL is a multi-disciplinary open access archive for the deposit and dissemination of scientific research documents, whether they are published or not. The documents may come from teaching and research institutions in France or abroad, or from public or private research centers.

L'archive ouverte pluridisciplinaire **HAL**, est destinée au dépôt et à la diffusion de documents scientifiques de niveau recherche, publiés ou non, émanant des établissements d'enseignement et de recherche français ou étrangers, des laboratoires publics ou privés.

CENTRALE LILLE

THESE

Présentée en vue

D'obtenir le grade de

DOCTEUR

En

Spécialité : Mécanique

Par

Chen CHEN

DOCTORAT DELIVRE PAR CENTRALE LILLE

Titre de la thèse:

Development, characterization and optimization of sustainable green composites with advanced sandwich structure

Développement, caractérisation et optimisation de composites durables avec une structure sandwich avancée

Soutenue le 09/12/2021 devant le jury d'examen :

Président	M. Nahiene Hamila	Professeur, ENIB
Rapporteur	M. Pierre-jacques Liotier	Maître de conférences (HDR), IMT Mines Alès
Rapporteur	M. Samir Allaoui	Professeur, Université de Reims
Examinatrice	Mme. Karine Gautier	Maître de conférences (HDR), LPMT, UHA
Directeur de thèse	M. Xavier LEGRAND	Professeur, ENSAIT
Co-directeur	M. Peng WANG	Professeur, Université Haute Alsace

Thèse préparée dans le Laboratoire GEMTEX
Ecole Doctorale SPI 072

University of Registration: Centrale Lille

Doctoral School: Doctoral school Sciences for the Engineer University Lille, North of France (ED 072)

Host Laboratory: GEMTEX (EA n°2461 ENSAIT Roubaix)

Period: 26/8/2018-25/08/2021

Financial Support: CSC (China Scholarship Council)

Acknowledgement

I acknowledge the generous financial support from the China Scholarship Council (CSC Grant Number: 201808070029).

I wish to express my deep gratitude to my supervisors Professor Xavier LEGRAND and Professor Peng WANG for their patience, support, guidance and advice throughout the whole research. Without their assistance and dedicated involvement, this paper would never be accomplished. Before the Ph.D. life, I have followed their class and was fortunate enough to participate in a project, their teaching style and expertise made a strong impression on me.

I am fortunate to have been a part of the MTC (Mechanics, Textile, Composites) group and I gratefully recognize the help of my research colleagues, Chan HUI, Hao SHEN, Shenglei XIAO, Liting Yao, Wenqian ZHAI, for all the discussions we had about work, all their help and extra hours they spent to promote my research.

Getting through my dissertation required more than academic support, I would express my appreciation to my friends Yan HONG and Cheng CHI, for their constant guidance and encouragement when I lost confidence.

Most importantly, I couldn't have lasted three years without my family. My parents offered their encouragement through phone calls every week. With her own brand of humor, my sister has been supportive of me. I am grateful for my family's unconditional, unequivocal, and loving support.

Contents

GENERAL INTRODUCTION	1
CHAPTER 1.STATE OF ART	6
1.1 Introduction.....	7
1.2 Natural fiber-reinforced composite materials (NFRC)	7
1.3 Sandwich structures	11
1.4 Optimization of sandwich structure with polymer foam core	16
1.4.1 Foam filled sandwich structure	16
1.4.2 Z-pinned sandwich structure	18
1.4.3 Stitched sandwich structure	21
1.4.4 Tufted sandwich structure	25
1.5 Resin infusion process	28
1.6 Conclusion	30
Reference.....	31
CHAPTER 2.MANUFACTURING PROCESS OF A TUFTED SANDWICH COMPOSITE WITH NONWOVEN CORE	42
2.1 Introduction.....	43
2.2 Design of the tufted sandwich structure with nonwoven core	44
2.3 Parameters of tufting process	45
2.3.1 Selection of tufting thread and preform layups	45
2.3.2 Tufting density.....	48
2.3.3 Tufting needle size	50
2.3.4 Preform fixation and support foam.....	52
2.3.5 Other parameters	55
2.4 Liquid resin infusion process	57

2.5	Ancillary adhesives	61
2.6	Conclusion	61
	Reference	62
CHAPTER 3. TOWARDS LAMINATE QUALITY AND MECHANICAL PERFORMANCE OF TUFTED SANDWICH COMPOSITES WITH CARBON FIBER NONWOVEN		
3.1	Introduction	65
3.2	Materials and methods	66
3.2.1	Manufacturing of tufted sandwich composite samples	66
3.2.2	Test methods	69
3.3	Results and discussion	72
3.3.1	Core shear test	72
3.3.2	Flatwise compression test	78
3.3.3	Three-point bending test	82
3.3.4	Charpy impact test	87
3.3.5	Specific properties	89
3.4	Conclusion	91
	Reference	92
CHAPTER 4. CHARACTERIZATION OF THE MECHANICAL BEHAVIOR OF TUFTED FLAX FIBER REINFORCED SANDWICH COMPOSITES		
4.1	Introduction	95
4.2	Materials and methods	95
4.2.1	Sandwich panel manufacture	95
4.2.2	Test methods	98
4.3	Results and discussion	99
4.3.1	Core shear test	99
4.3.2	Three-point bending test	103
4.3.3	Charpy impact test results	109

4.4	Conclusion	113
	Reference	114
CHAPTER 5. GENERAL CONCLUSION		117
5.1	Conclusions	118
5.2	Perspectives	119
RÉSUMÉ ÉTENDU		122
ABSTRACT		125
RÉSUMÉ		125

List of Figures

Figure 1.1 Automobile components made of natural fiber composites [12].	9
Figure 1.2 Schematics of (a) laminate composite and (b) sandwich composite [30].	12
Figure 1.3 Different core types of sandwich composite [31].	12
Figure 1.4 Cellular sandwich plates: (a) open-cell foam core and (b) closed-cell foam core [32].	13
Figure 1.5 Core structures of (a) octet-truss lattice [71], (b) pyramidal lattice truss [72] and (c) Kagome lattice grid [70].	16
Figure 1.6 Schematic illustrations of (a) 3D woven sandwich composite with foam core [76] and (b) sandwich panel with lattice foam core [77].	17
Figure 1.7 Paper honeycomb cores: (a) hollow core; (b) foam-filled core [78].	17
Figure 1.8 Schematic of the z-pin insertion process [84].	18
Figure 1.9 Cross-sectional views of X-cor and K-cor [85].	19
Figure 1.10 Comparison of load/normalized displacement curves for (a) different Z-pinning densities and (b) different Z-pin inclination angle [103].	21
Figure 1.11 Schematics of (a) chain stitch (b) lock stitch (c) modified lock stitch [106].	21
Figure 1.12 Modified-lock stitching process [111].	22
Figure 1.13 Typical results of (a) bending test, (b) flatwise compression and (c) core shear test [117].	24
Figure 1.14 Schematic diagrams of (a) lock stitching thread, (b) tufting thread.	26
Figure 1.15 Load/displacement curves of tufted and non-tufted polyurethane-core sandwich panels with (a) carbon fiber reinforcement and (b) E-glass fiber reinforcement under 3-point bending [150].	28
Figure 1.16 Schematics of process (a) RTM [158], (b) VARTM [159], (c) RFI [160] and (d) LRI.	29
Figure 2.1 Tufting machine and its function modules.	43
Figure 2.2 Carbon fiber tufted sandwich composite with a non-woven core.	45
Figure 2.3 Different tufting threads used in this work.	46
Figure 2.4 Sever bending thread during tufting process.	46

Figure 2.5 Removal of foam for hollow sandwich structure manufacture.....	48
Figure 2.6 Schematics of the (a) multi-row pattern and (b) circle spiral pattern [9].	49
Figure 2.7 Structures of preforms with (a) constant spacing between tufting points and (b) different tufting spacing.	50
Figure 2.8 (a) Solid tufting needle and (b) hollow tufting needle.....	51
Figure 2.9 Resin column formed during LRI.	52
Figure 2.10 Schematic of the tufting thread for position fixing.....	53
Figure 2.11 Compaction of preform during tufting process.....	54
Figure 2.12 Reused foam support.	54
Figure 2.13 (a) Damaged texture and (b) protected texture of bottom skin woven fabric.....	55
Figure 2.14 Schematic of tufting length.....	56
Figure 2.15 Removal of tufting loops before LRI.....	56
Figure 2.16 Schematic of tufting angle.	57
Figure 2.17 Liquid resin infusion process.	58
Figure 2.18 Stacking order for LRI process.....	59
Figure 2.19 Different through-the-thickness reinforcement of sandwich specimens tufted with and without yarn.....	60
Figure 3.1 Sandwich composite specimens containing non-woven core.....	66
Figure 3.2 Non-tufted sandwich structure with nonwoven core layer.	67
Figure 3.3 Micro-observation of the cross-section of the different samples.....	68
Figure 3.4 Core shear test set-up.....	69
Figure 3.5 Compressive test device.....	70
Figure 3.6 Bending test set-up.....	71
Figure 3.7 Charpy impact test schematization.	72
Figure 3.8 Shear stress vs. shear strain curves of the sandwich composite parts.....	73
Figure 3.9 Observation of the failure mode in core shear tests.....	75
Figure 3.10 The illustration of shear deformation (a) and shear load (b) in SW-3 sample.....	76
Figure 3.11 Micro-observation of tufting threads in SW-1 sample.	78
Figure 3.12 Observation of the extracted threads on rupture surface of SW-1 sample.	78
Figure 3.13 Flatwise compression stress-strain curves.	79
Figure 3.14 Schematic of the analytical calculation of SW-3 and SW-4 samples.....	82

Figure 3.15 Bending load vs. deflection curves of the tested sandwich composites.	83
Figure 3.16 (a) Structure failure during 3-point bending test and (b) Observation of the cross-section failures.....	84
Figure 3.17 Core shear ultimate strength of sandwich samples in bending test.	85
Figure 3.18 Impact energy absorbed during Charpy test.	88
Figure 3.19 Fractured specimens after Charpy impact test.	89
Figure 4.1 Schematic of a flax fiber reinforced sandwich panel.....	96
Figure 4.2 Experimental set-ups for different loadings.....	98
Figure 4.3 Typical stress-strain curves of core shear behavior of tufted sandwich panels.	99
Figure 4.4 Typical core shear stress-strain curves of SW-T0 and SW-T6.....	100
Figure 4.5 Fracture modes of tufted sandwich panels.....	101
Figure 4.6 Typical bending load-deflection curve plots for each tufting density.	104
Figure 4.7 Typical bending load-deflection curves of SW-T0 and SW-T6.....	104
Figure 4.8 Fracture modes of each group of sandwich panel.....	106
Figure 4.9 Impact behaviors of different sandwich panels.	109
Figure 4.10 Specific impact properties of each sandwich panels.	110
Figure 4.11 Typical ruptured sandwich panels by Charpy impact tests.....	111
Figure 4.12 Fracture modes: (a) fiber of nonwoven, (b) foam, (c) fiber of bottom skin, (d) delamination and (e) fiber of top skin.	112

List of Tables

Table 1.1 Benefits and drawbacks of natural fiber composites (NFCs) [6].	8
Table 1.2 Typical properties of commonly studied natural fibers and several synthetic fibers [11].	10
Table 1.3 Mechanical properties of stitched foam-core sandwich structure [121].	24
Table 2.1 Properties of tufting threads.	47
Table 2.2 Basic parameters of textile layups.	47
Table 3.1 Main properties of tufted sandwich composite samples.	67
Table 3.2 Mechanical properties of sandwich composites in the core shear tests.	74
Table 3.3 Comparison of the experimental and analytical results of the core shearing modulus.	77
Table 3.4 Compressive properties of sandwich composites.	80
Table 3.5 Main properties of the tested sandwich composites in 3-point bending tests.	83
Table 3.6 Comparison of the experimental and analytical results of the bending.	86
Table 3.7 Material mechanical and physical properties used in the analytical investigation.	87
Table 3.8 Specific mechanical properties of sandwich composites.	90
Table 3.9 Specific modulus of sandwich composites under different loadings.	91
Table 4.1 Parameters of sandwich raw materials.	96
Table 4.2 Relation between tufting density and tufting spacing.	97
Table 4.3 Mechanical properties of sandwich composites in the shear test.	100
Table 4.4 Core shear properties of flax fiber-reinforced and carbon fiber-reinforced sandwich panels.	102
Table 4.5 Experiment and prediction results of the core shear modulus.	102
Table 4.6 Flexural properties of each group of sandwich panel.	105
Table 4.7 Bending properties of tufted sandwich panels in carbon fiber and in flax fiber.	106
Table 4.8 Comparison of the results from experiments and analytical equations.	108
Table 4.9 Comparison of the results from experiments and analytical equations.	109

GENERAL INTRODUCTION

Sandwich composites are widely employed in many industrial areas such as aerospace, transportation, construction and shipbuilding due to their higher stiffness and strength per weight ratio than conventional laminate composites. Typical sandwich composites are manufactured by joining two thin but stiff outer skins to a light but thick internal core. As a structure developed from laminates, sandwich composite presents the same delamination problem which results in premature failure [1]. The main cause is that there are different mechanical properties across the interface between the core and the skin [2, 3]. The present solution is to insert reinforcement through the thickness of the sandwich structures. The sandwich composites with reinforcement in the Z-axis successfully ameliorate the ultimate stress and modulus regarding the principal mechanical tests such as bending and shear [4]. Several techniques have been developed such as Interlock 3D weaving [5–7], z-pinning [8–11] and stitching/tufting [12–18]. Nevertheless, Interlock weaving has a slow production rate and a limited capacity of the textile machine [19]. And the inserted z-pins are independent, thus there are no anchors or locks to the top and bottom skins. Z-pinning is less effective in preventing delamination. Compared to other processes, tufting is more efficient and less expensive [20]. The tufted dry sandwich preform needs to be impregnated by resin to obtain the desired composite parts. However, the low mechanical properties of common foam core usually lead to poor impact damage resistance. In addition to the delamination, the crack of foam core is another common failure mode of the sandwich composite. Foam is conducive to lightweight but the low mechanical properties limit its application.

Nowadays, increasing environmental concerns have encouraged researchers to adapt recyclable materials to replace traditional materials for sandwich composites manufacturing. The bio composite based on natural fibers is widely applied in automotive due to their low cost, low density, high specific strength, low energy consumption in fabrication, biodegradable characteristics and recyclability [21]. Among the natural fibers such as hemp, jute, and bamboo, flax fibers are increasingly being used in green composites because of their better mechanical properties [22][23].

This study aims to the development and optimization of the tufted sandwich structure by using nonwoven core materials and the analysis of the mechanical performance. And on this basis realize this novel sandwich structure by using bio-resources (flax fiber reinforcement and bio-resins).

A review of the fiber-reinforced sandwich composite is presented in the first chapter. The section introduces two aspects of fiber materials (glass fiber, carbon fiber, etc.) and structures (laminated and sandwich) along with the history of the composite development, and analyzes their strengths and disadvantages.

The design of a novel sandwich structure and its manufacturing process is presented in detail in chapter 2. All the sandwich composite panels in the present work are fabricated by the tufting and liquid resin infusion (LRI) processes. The setting of relevant parameters is introduced and the variables among them investigated in the following chapters are listed.

In chapter 3, the influence of nonwoven layer and tufting thread on the mechanical behavior of carbon fiber reinforced sandwich composite part is investigated. And the feasibility of using nonwoven instead of foam as the core layer of sandwich structure is initially verified according to the experimental results. Chapter 4 is dedicated to realizing a green sandwich composite in flax fiber with the structure validated in chapter 3. And the influence of tufting density and flax fiber nonwoven quantities is discussed.

Finally, the last chapter is the general conclusion and perspective of this thesis.

Reference

- [1] Sharma SC, Krishna M, Narasimha Murthy HN. Buckling response of stitched polyurethane foam composite sandwich structures. *J Reinf Plast Compos* 2004;23:1267–77. <https://doi.org/10.1177/0731684404037042>.
- [2] Langdon GS, von Klemperer CJ, Rowland BK, Nurick GN. The response of sandwich structures with composite face sheets and polymer foam cores to air-blast loading: Preliminary experiments. *Eng Struct* 2012;36:104–12. <https://doi.org/10.1016/j.engstruct.2011.11.023>.
- [3] Wang B, Wu L, Jin X, Du S, Sun Y, Ma L. Experimental investigation of 3D sandwich structure with core reinforced by composite columns. *Mater Des* 2010;31:158–65. <https://doi.org/10.1016/j.matdes.2009.06.039>.
- [4] Lascoup B, Aboura Z, Khellil K, Benzeggagh M. On the mechanical effect of stitch addition in sandwich panel. *Compos Sci Technol* 2006;66:1385–98. <https://doi.org/10.1016/j.compscitech.2005.09.005>.
- [5] Tekalur SA, Bogdanovich AE, Shukla A. Shock loading response of sandwich panels with 3-D woven E-glass composite skins and stitched foam core. *Compos Sci Technol* 2009;69:736–53. <https://doi.org/10.1016/j.compscitech.2008.03.017>.
- [6] Mouritz AP, Bannister MK, Falzon PJ, Leong KH. Review of applications for advanced three-dimensional fibre textile composites. *Compos Part A Appl Sci Manuf* 1999;30:1445–61. [https://doi.org/10.1016/S1359-835X\(99\)00034-2](https://doi.org/10.1016/S1359-835X(99)00034-2).

- [7] Gereke T, Cherif C. A review of numerical models for 3D woven composite reinforcements. *Compos Struct* 2019;209:60–6. <https://doi.org/10.1016/j.compstruct.2018.10.085>.
- [8] Du L, Jiao G. Indentation study of Z-pin reinforced polymer foam core sandwich structures. *Compos Part A Appl Sci Manuf* 2009;40:822–9. <https://doi.org/10.1016/j.compositesa.2009.04.004>.
- [9] Nanayakkara A, Feih S, Mouritz AP. Experimental impact damage study of a z-pinned foam core sandwich composite. *J Sandw Struct Mater* 2012;14:469–86. <https://doi.org/10.1177/1099636212443915>.
- [10] Kaya G, Selver E. Impact resistance of Z-pin-reinforced sandwich composites. *J Compos Mater* 2019;53:3681–99. <https://doi.org/10.1177/0021998319845428>.
- [11] M'membe B, Gannon S, Yasae M, Hallett SR, Partridge IK. Mode II delamination resistance of composites reinforced with inclined Z-pins. *Mater Des* 2016;94:565–72. <https://doi.org/10.1016/j.matdes.2016.01.051>.
- [12] Hao S, Wang P, Legrand X, Liu L, Soulat D. Influence of the tufting pattern on the formability of tufted multi-layered preforms. *Compos Struct* 2019;228. <https://doi.org/10.1016/j.compstruct.2019.111356>.
- [13] Liu LS, Zhang T, Wang P, Legrand X, Soulat D. Influence of the tufting yarns on formability of tufted 3-Dimensional composite reinforcement. *Compos Part A Appl Sci Manuf* 2015;78:403–11. <https://doi.org/10.1016/j.compositesa.2015.07.014>.
- [14] Dell'Anno G, Treiber JWG, Partridge IK. Manufacturing of composite parts reinforced through-thickness by tufting. *Robot Comput Integr Manuf* 2016;37:262–72. <https://doi.org/10.1016/j.rcim.2015.04.004>.
- [15] Hui C, Wang P, Legrand X. Improvement of tufting mechanism during the advanced 3-dimensional tufted composites manufacturing: To the optimisation of tufting threads degradation. *Compos Struct* 2019;220:423–30. <https://doi.org/10.1016/j.compstruct.2019.04.019>.
- [16] Hartley JW, Kratz J, Ward C, Partridge IK. Effects of Loop Length and of Multiple Tufts on the Crushing Behaviour of Tufted Sandwich Specimens 2017;112:1–13.
- [17] Zheng XT, Zhang JF, Yang F, Chai YN, Li Y. Experimental and analytical study on the mechanical behavior of stitched sandwich composite panel with a foam core. *Adv Mater Res* 2008;33–37 PART:477–82. <https://doi.org/10.4028/www.scientific.net/amr.33-37.477>.
- [18] Mouritz AP, Cox BN. A mechanistic interpretation of the comparative in-plane mechanical properties of 3D woven, stitched and pinned composites. *Compos Part A Appl Sci Manuf* 2010;41:709–28. <https://doi.org/10.1016/j.compositesa.2010.02.001>.
- [19] Aktas A, Potluri P, Porat I. Multi-needle stitched composites for improved damage tolerance. *ICCM Int. Conf. Compos. Mater.*, 2009.
- [20] Liu LS, Wang P, Legrand X, Soulat D. Investigation of mechanical properties of tufted composites: Influence of tuft length through the thickness reinforcement. *Compos Struct* 2017;172:221–8. <https://doi.org/10.1016/j.compstruct.2017.03.099>.
- [21] Rashid M, Chetehouna K, Cablé A, Gascoin N. Analysing Flammability Characteristics of Green Biocomposites: An Overview. *Fire Technol* 2021;57:31–67. <https://doi.org/10.1007/s10694-020-01001-0>.
- [22] Lascano D, Guillen-Pineda R, Quiles-Carrillo L, Ivorra-Martínez J, Balart R, Montanes N, et al. Manufacturing and characterization of highly environmentally friendly sandwich composites from polylactide cores and flax-polylactide faces. *Polymers (Basel)* 2021;13:1–14. <https://doi.org/10.3390/polym13030342>.

[23] Bourmaud A, Beaugrand J, Shah DU, Placet V, Baley C. Towards the design of high-performance plant fibre composites. *Prog Mater Sci* 2018;97:347–408. <https://doi.org/10.1016/j.pmatsci.2018.05.005>.

CHAPTER 1. STATE OF ART

1.1 Introduction

Since the invention of glass fiber composites in the 1940s, fiber-reinforced composites have been increasingly employed. Carbon fiber, boron fiber and aramid fiber composites have been developed one after another. They are mainly applied in aerospace, transportation, construction and mechanical engineering to replace metal materials. Compared with metals, the fiber-reinforced composites exhibit higher strength-to-weight and stiffness-to-weight ratios [1]. With their increasing applications, more types of fiber-reinforced composites have been developed to improve the mechanical properties of the composites and to address recycling issues.

In this chapter, the development of composite materials from both structure and raw materials aspects is introduced, especially the flax fiber-reinforced composite and the sandwich structure. Compared with the laminate structure, the sandwich structure presents several advantage but also some limits, which are listed in this section.

Then the current solutions to the delamination problem of the sandwich structure are reviewed and presented. Among these different techniques, tufting, as the selected process in this thesis, is mainly introduced.

1.2 Natural fiber-reinforced composite materials (NFRC)

In the last decades, due to environmental concerns and requests, the green composite based on natural fibers has been developed rapidly. The common fibers, such as kenaf, flax, jute, hemp, have been normally mixed with polymeric resins to form NFRC [2–4]. Moreover, they can be incorporated with bio plastics to produce a green composite [5]. The utilization of these composites as alternative materials to traditional composites attracts increasing attention due to their typical advantages (see Table 1.1).

Table 1.1 Benefits and drawbacks of natural fiber composites (NFCs) [6].

Benefits	Drawback
Very good sound, acoustic, and electrical insulating properties	Moisture absorption, causing fibers to swell
Reactivity-materials provide sites for water absorption and are also available for chemical modification	Restricted maximum processing temperature
Biodegradability: as a result of their tendency to absorb water, natural fibers will biodegrade under certain circumstances through the actions of fungi and/or bacteria	Lower durability, fiber treatments can improve this drawback
Combustibility: products can be disposed of through burning at the end of their useful service life, and energy can simultaneously be generated	Dimensional stability as a consequence of the hygroscopicity of fibers, products, and materials
Very good mechanical properties, especially tensile strength. Concerning their weight, the best fibers attain strength similar to Kevlar. The abrasive nature of natural fibers is much lower compared to glass fibers, which leads to advantages in regards to the technical aspects, material recycling, or processing of composites materials	Variability in quality, dependent on unpredictable variables such as weather Less fire retardance
Plant fibers are renewable raw materials and their availability is unlimited	Lower strength properties, particularly impact strength

NFRCs are mainly used in the transport industry [7]. Many NFRCs have experimented since the first environmentally friendly composite occurred in 1941 [8]. Various structural pieces such as roof, boot lid, bonnet, and doors (shown in Figure 1.1) have been successfully manufactured from a thermosetting phenolic resin and natural fiber [9]. Several automotive companies, such as

Daimler Chrysler, Mercedes Benz and Toyota, have employed NFRCs into their products and increasing its use proportion has been incorporated in the future plan [10][11].



Figure 1.1 Automobile components made of natural fiber composites [12].

The mechanical performance of NFRC depends on the fiber reinforcement. Therefore, investigation and understanding of natural fiber properties and forms are considered to realize improvement [13][14]. Table 1.2 tabulates the properties of several fibers. Of all natural fibers listed in the table, flax fiber has proven to be the best replacement for glass fiber [15–18]. In general, the mechanical properties of flax fiber are lower than those of glass fiber. Nevertheless, considering the lower density of flax fiber, then it is comparable to glass fiber in terms of specific strength and modulus. In addition, compared with other natural fibers, flax is an annual fiber plant, the consumption of water, fertilizers and pesticides is much lower. And the crop's requirements for soil and climate are lower. These make the production of flax much higher than most plant fibers, conducive to large-scale processing and application, but also fully justified their use as a reinforcement for bio composites [8,16,19,20].

Table 1.2 Typical properties of commonly studied natural fibers and several synthetic fibers [11].

Fiber type	Density (g/cm ³)	Tensile strength (MPa)	Tensile modulus (GPa)	Specific modulus	Elongation (%)
Coir	1.2-1.5	95–230	3–6	4	15–51
Cotton	1.5–1.6	287–800	6–13	6	3–10
Flax	1.53	745–1145	44–61	35	2.07
Hemp	1.48	690	70	47	1.6
Jute	1.3	393–773	27	21	1.5–1.8
Kenaf	1.4–1.5	223–930	15–53	24	1.5–2.7
Ramie	1.5	560	25	17	2.5
Sisal	1.3–1.5	363–700	9–38	17	2.0–7.0
Carbon fiber	1.8	4330	231	129	1.8
E-glass	2.5–2.6	2000–3500	70–76	29	1.8–4.8

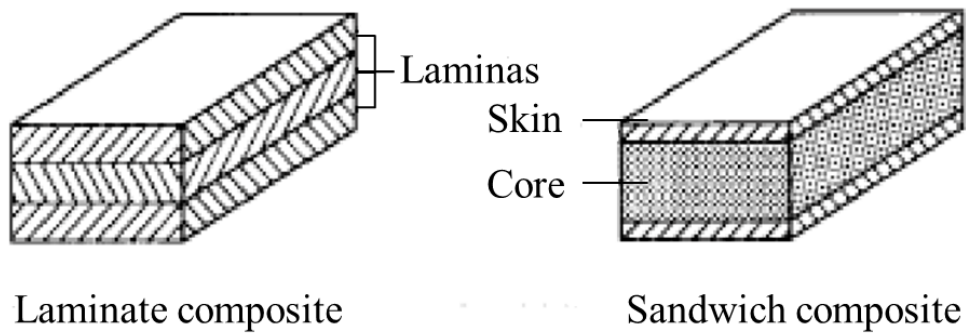
Chandrasekar et al. [21] fabricated hybrid composites with the flax as skin and sugar palm fiber (SPF) as core by hot press molding. Results analysis revealed that hybridization of flax into the SPF reinforced composites resulted in excellent mechanical strength and inter-laminar shear strength. Velmurugan et al. [22] investigated the mechanical characteristics of hemp and flax-based hybrid composites reinforced with epoxy resin at cryogenic and room temperatures. Cryogenic temperature had a significant effect on the flexural, tensile and impact behaviors of composites which vary depending on the amount of cryogenic treatment. N.Karthi et al. [23] studied the influence of weight fraction on the mechanical properties of flax and jute fibers reinforced hybrid composites. Five different fiber weight fractions were considered and the results showed that the maximum tensile strength, flexural strength, inter-laminar shear strength and impact strength were obtained only for a composite having 30% weight fraction flax fiber reinforcement. A research was conducted by Barkoula et al. [24] to study the effect of fiber content and manufacturing technique on the mechanical properties of randomly oriented flax fiber reinforced composites. They found that the stiffness of the composites increased with the fiber contents while the strength decreased slightly upon fiber content addition. And, no significant effect of processing methods on the tensile properties of the composites was observed.

Another study related to the fiber fraction was conducted by Charlet et al. [25], they investigated the effect of fiber volume fraction on the tensile properties of unidirectional flax

fiber/epoxy matrix composites. The tensile strength and modulus increased linearly with fiber volume fraction. There have been a large number of studies on unidirectional flax fiber composites. For instance, Oksman [26] compared the mechanical properties of traditionally retted unidirectional flax fiber composites to the pure resin. The results showed that flax/epoxy composite had a stiffness of about 40 GPa and tensile strength of 280 MPa compared to the stiffness in pure epoxy of 3.2 GPa and the tensile strength of 80 MPa. Goutianos et al. [27] reported that UD knitted flax fabric/epoxy composites cannot directly compete in terms of strength with glass fiber composites. However, they were able to compete with glass fiber in terms of stiffness/weight ratio. A modified theoretical model was developed by Madson and Lilholt [28] to predict unidirectional flax fiber composite tensile properties by integrating the parameters of composite porosity content and anisotropy of fiber properties. Frederic et al. [29] proposed a model to predict the mechanical properties of flax fiber reinforced polymer composites. Different damage laws were identified calibrated and many stacking sequences were validated. This model can also be used to reproduce the crack locations and buckling zones and under tension and three points bending loadings.

1.3 Sandwich structures

There are two common types of composite structures: laminated composites and sandwich composites. The former consists of several textile laminas in different orientations (shown in Figure 1.2). Sandwich composites are developed based on the laminates, the purpose of which is to further reduce the weight of the material. The core material of the sandwich composite is responsible for connecting the upper and lower face sheets, improving the bending bearing capacity of the structure, transferring shear stress between two face sheets, and not bearing the main structural load. Therefore, materials with lower density are often used for the core to ensure that the structure is sufficiently lightweight.



(a)

(b)

Figure 1.2 Schematics of (a) laminate composite and (b) sandwich composite [30].

Common core materials include corrugated core, honeycombs, foam cores, and lattice cores (see Figure 1.3).

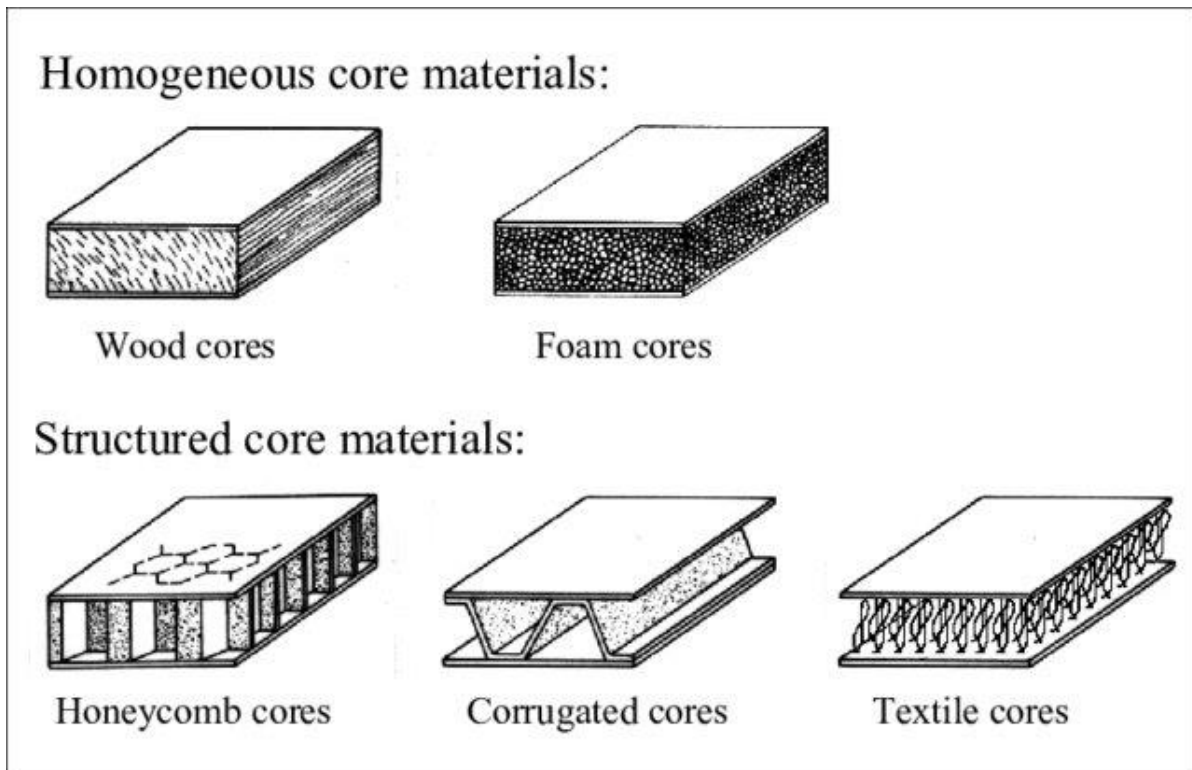


Figure 1.3 Different core types of sandwich composite [31].

Different from the core constructions which make use of voids to decrease mass (such as the honeycomb core and integrated woven core), the foam core is adopted because of its low density.

Because of the large thickness of the foam core, face sheets can develop very high bending stresses. The mechanical properties of the foam are relatively weaker compared to the face sheet of sandwich composite. When the damage of the face sheet/core interface appears, the initial cracks easily extend to the core material, which in turn triggers the deformation and damage of the foam. Thus the fracture damage behavior and characteristics of the foam need to be considered. The foam is divided into open-cell foam and closed-cell foam (see Figure 1.4), both of which have different mechanical properties; energy absorption, sound insulation and heat insulation. It is possible to select the appropriate foam according to different material processing demands [32].

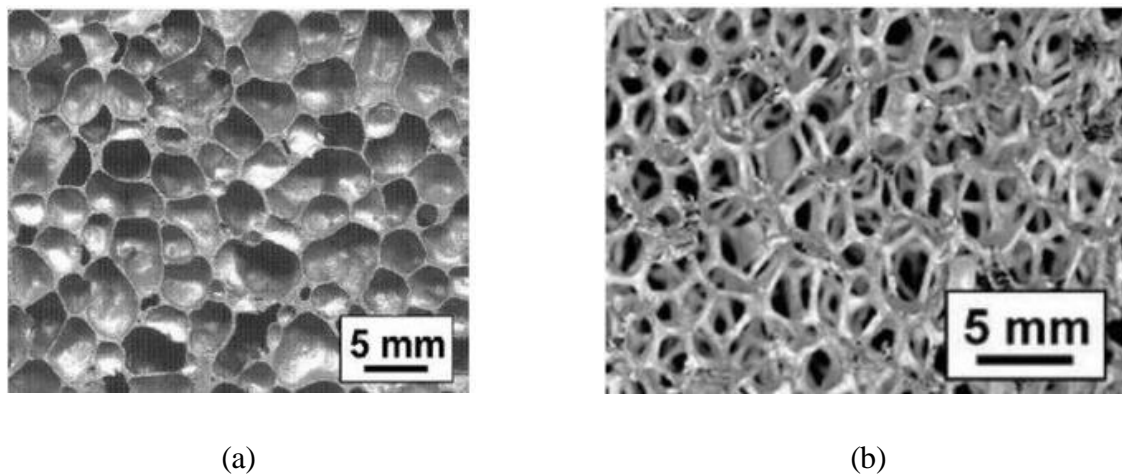


Figure 1.4 Cellular sandwich plates: (a) open-cell foam core and (b) closed-cell foam core [32].

Yun et al. [33] investigated the effects of elevated temperature on mode II interfacial fracture of foam core sandwich composites. Results showed that the strain energy release rate decreased under the same crack length as the temperature increased. Moreover, an analytical model was proposed and verified to accurately predict the interfacial strain energy release rate. Kulkarni et al. [34] investigated the fatigue crack growth of foam core sandwich beams loaded in flexure. A model based on local damage in the low-density foam core was developed and validated. The first damage was a core–skin debond which propagated into the core as a shear crack resulting in total specimen collapse. The initial failure of in-plane compression can take the form of global Euler buckling, shear buckling of the core, wrinkling, face sheet or fracture Core fracture [35]. Xingyuan et al. [36] developed a sandwich structure with foam core slits filled with resin. Results showed that the sandwich composite with resin-filled slits presented better fracture resistance

than those with intact foam. Belingardi et al. [37] fabricated a sandwich structure made of glass fiber epoxy face sheets with a polymeric foam core, as the front shield of a high-speed train. Then static and dynamic impact tests were then performed and the results showed that the structural response of the sandwich depends primarily on the strength properties of the foam core material. Aniber et al. [38] investigated and assessed the effect of foam density on flexural behavior of foam-core sandwich panels with three different foam densities (60 kg/m³, 80 kg/m³ and 100 kg/m³). The results showed that the sandwich structure with higher foam density withstood a higher bending load and higher shear strength. A parametric study on impact damage resistance of sandwich panels with carbon fiber-vinyl ester faces and PVC foam core was conducted by Peter et al. [39]. They developed a plastic micro buckling approach to predict the residual strength of carbon fiber sandwich structures. Two different groups of sandwich panels (1. thin faces and an intermediate density core; 2. thick faces and high-density core) were tested by both spherical impactor and pyramid impactor. The experimental values were close to the predictions and validated the prediction method.

Honeycomb cores are usually hexagonal cellular solids and are manufactured by expansion and corrugation techniques [40–42]. The core materials can be selected among metallic and non-metallic materials such as aluminum alloy, stainless steel, Nomex, Kraft paper and glass fiber [43–54]. Much works have investigated the mechanical behavior of honeycomb core and many numerical models were developed to characterize and optimize the structure. Gpoichand et al. [55] fabricated sandwiches with copper core and stainless steel facing. Three-point bending test was conducted to compare the theoretical load and the deflection values with experimental and simulation results. It was found that the gradient of deflection curve was higher for lower core height. Yicheng et al. [56] evaluated the effects of honeycomb core height and cell size on the flexural properties of the lab-made sandwich panels with bio fiber reinforced polymer composite skins and a commercial resin-impregnated aramid paper honeycomb core. They concluded that these lab-made sandwich panels had higher specific bending rigidity and flexural load bearing capability compared to the commercial products. Choon et al. [57] used the fundamental mechanical properties of the Nomex paper for the finite element modeling and analysis of Nomex honeycomb structures. They compared with numerical analyses for static tension and compression and concluded that the young's modulus of the honeycomb was dependent on the size of the specimen. Giglio et al. [45] conducted several numerical simulations of the

mechanical behavior of a Nomex honeycomb core in a flatwise compressive test, and then validated them by reproducing all features, properties and failure modes of the components. Abbadi et al. [40] adopted a general kinematic model for the simulation of honeycomb sandwich panel submitted to the four-point bending test. Meifeng [58] found that the satisfying weight of the honeycomb core was 50–66.7% of the whole sandwich panel weight by theoretical analysis. The honeycomb sandwich panels were designed based on this theory and the results were verified by further experiments. Xingyu et al. [59] developed analytical models based on the failure modes (including shear macro-buckling, intracellular dimpling, face wrinkling, face fracture and debonding) to investigate the in-plane compressive characteristics of all-composite honeycomb sandwich columns. The experimental results agree well with the models.

The structure of corrugated cores is characterized by the formation of open channels in one direction. Several studies on the mechanical properties of corrugated cores have been conducted [60–62]. For example, Côté et al. [63] analyzed the out-of-plane compressive, transverse shear and longitudinal shear responses of the corrugated cores and the results showed that this core was conducive to the longitudinal shear strength but was weaker on compression and transverse shear performance than the square-honeycomb core. Rejab and Cantwell [64] investigated the failure mode of axial compression in corrugated-core sandwich panels based on an aluminum alloy, a glass fiber reinforced plastic and a carbon fiber reinforced plastic. Buckling of the cell walls was found to be initial failure mode. Recently, several novel designs of corrugated core were developed such as the hierarchical corrugated cores, two-way corrugated cores and integrated woven corrugated cores [65–68].

Recent researches have shown the high mechanical properties/weight ratio of lattice structures [69]. The lattice core can be designed in different geometric patterns depending on the load to be carried (as shown in Figure 1.5). Fan et al. [70] manufactured a carbon fiber reinforced kagome lattice sandwich panel and investigated its mechanical behaviors by out-of-plane compression, in-plane compression and three-point bending. It showed that buckling and debonding were the major failure modes of sandwich panels. Deshpande et al. [71] investigated the properties of the octet-truss lattice material. The effective mechanical properties were obtained both experimentally and theoretically and a good agreement was found between them. It showed that the strength and stiffness of the octet-truss material compared favorably with the metallic foams.

Douglas et al. [72] developed a pyramidal lattice structures with hollow metallic trusses and explored the out-of-plane compression properties. The results indicated that the compressive strength of a hollow lattice was approximately twice that of a similar lattice made with the solid trusses.

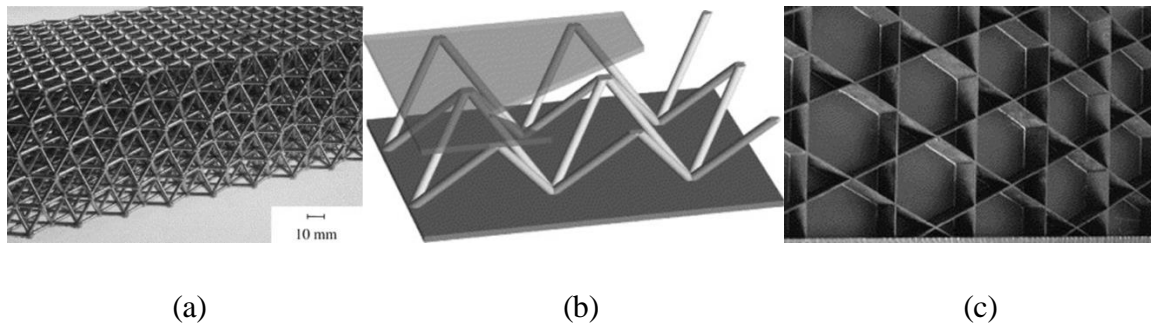


Figure 1.5 Core structures of (a) octet-truss lattice [71], (b) pyramidal lattice truss [72] and (c) Kagome lattice grid [70].

1.4 Optimization of sandwich structure with polymer foam core

The polymer foam core materials normally have low transverse shear resistance but can provide high flexural stiffness and strength-to-weight ratio because of their larger thickness. However, the weak interface between the face sheet and the core results in delamination, which is also one of the main failure modes. Two major solutions have been proposed to improve the properties of the interface. One is to use foam to fill the voids based on the structure of the existing connection or reinforcement between the top and bottom skins (such as the lattice or truss core) [73][74]. Another is the inserting of through-the-thickness reinforcement to link the skins and foam, including the z-pinning, stitching and tufting.

1.4.1 Foam filled sandwich structure

All sandwich composites with voids or channels in the core can be added by foam to enhance the mechanical properties. Taghipoor et al. [73] studied the energy absorption and collapse behaviors of a polyurethane foam-filled sandwich beam. It was obtained that the polyurethane foam could increase the energy absorption of the sandwich beam by up to 80%. Sensen and Hualin [74] filled pultruded sandwich panels with expanded polystyrene foamed concrete to improve mechanical performances. The results showed that the shear modulus increased by 144 times and the flexural rigidity increased by 33 times. The flexural failure mode changed from

core shear failure to skin fracture. Judawisastra et al. [75] developed a 3D weaving sandwich composite with a foam core which was injected into the hollow core, and the fatigue performance was mainly investigated. The mixed failure mode was observed instead of the pure core shear failure in the 3-point bending test. A finite-element model was conducted by Vuure et al. [76] to simulate the mechanical performance of a 3D woven sandwich with foam core (the structure is shown in Figure 1.6a). And it presented an accurate prediction of flexural shear and flat compressive behavior. Liu et al. [77] designed and manufactured a novel glass fiber reinforced composite lattice sandwich panel (see Figure 1.6b). The core consisted of orthogonal corrugated composites truss and foam cubes.

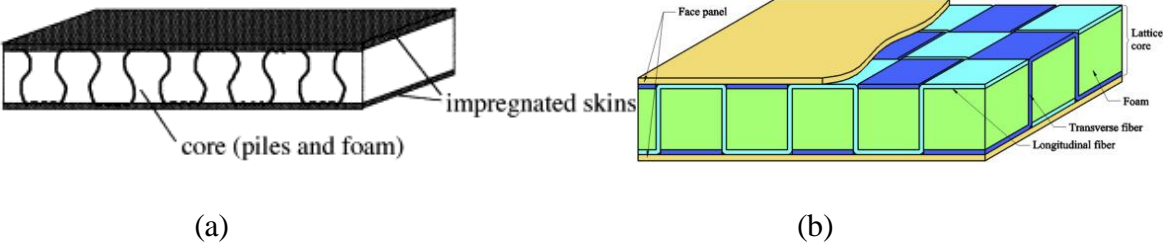


Figure 1.6 Schematic illustrations of (a) 3D woven sandwich composite with foam core [76] and (b) sandwich panel with lattice foam core [77].

Furthermore, Fu et al. [78] have studied the mechanical behavior of hollow honeycomb core and foam-filled honeycomb core (see Figure 1.7), where they obtained the foam had a positive effect on load capacity but almost no influence on the bending stiffness.

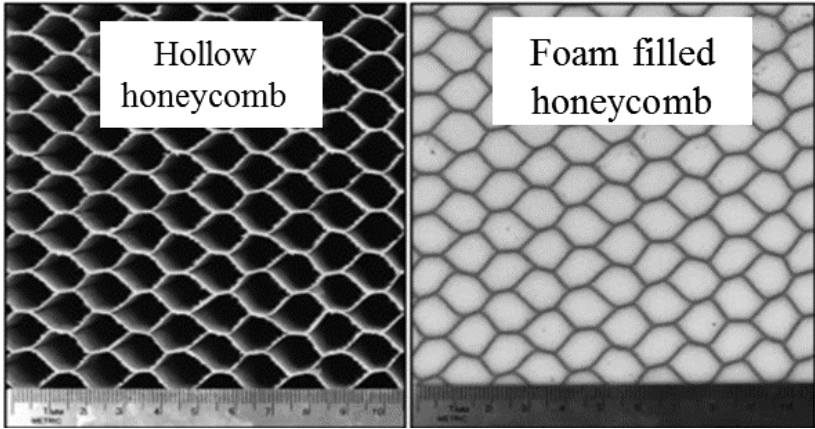


Figure 1.7 Paper honeycomb cores: (a) hollow core; (b) foam-filled core [78].

1.4.2 Z-pinned sandwich structure

Z-pinning is a technique to insert reinforcements along the Z-direction of fiber reinforced sandwich composites. As a through-the-thickness reinforcement technology, the pins most commonly used can be divided into two types: metal rods and unidirectional fiber/polymer rods. The latter can be manufactured using any type of fibrous tow with high mechanical properties (e.g. carbon/aramid) [79–82]. Typically, these fibers are impregnated with liquid polymer and then cured and inserted into composites. Z-pins can be fabricated into cylinders, rectangular rods or other suitable shapes conducive to the process and properties [83].

The most common method for inserting z-pins is using ultrasonic. During this process, an ultrasonic gun compresses the foam which encases the z-pins and forces the pins from foam into the material. The pins are pre-distributed evenly in the foam at a specific density. The high-frequency vibrations of the pins can heat and soften the resin and thus, the pins are introduced into the preform. Finally, remove the excess z-pins that remained into the foam (see Figure 1.8).

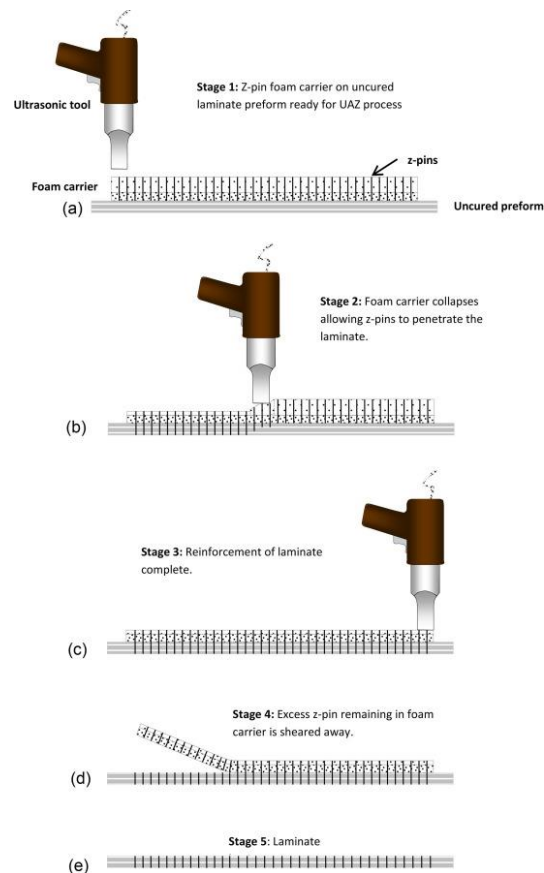


Figure 1.8 Schematic of the z-pin insertion process [84].

Z-pins can be arranged into a sandwich composite in the perpendicular direction to the thickness or at an inclined angle. The z-pins inclined at 45° can significantly provide high shear resistance. The former includes the pins inserted in the face sheet of the sandwich, which can enhance the interfacial properties. While the pins in the latter are flush with the interface between the foam core and the face sheet (see Figure 1.9).

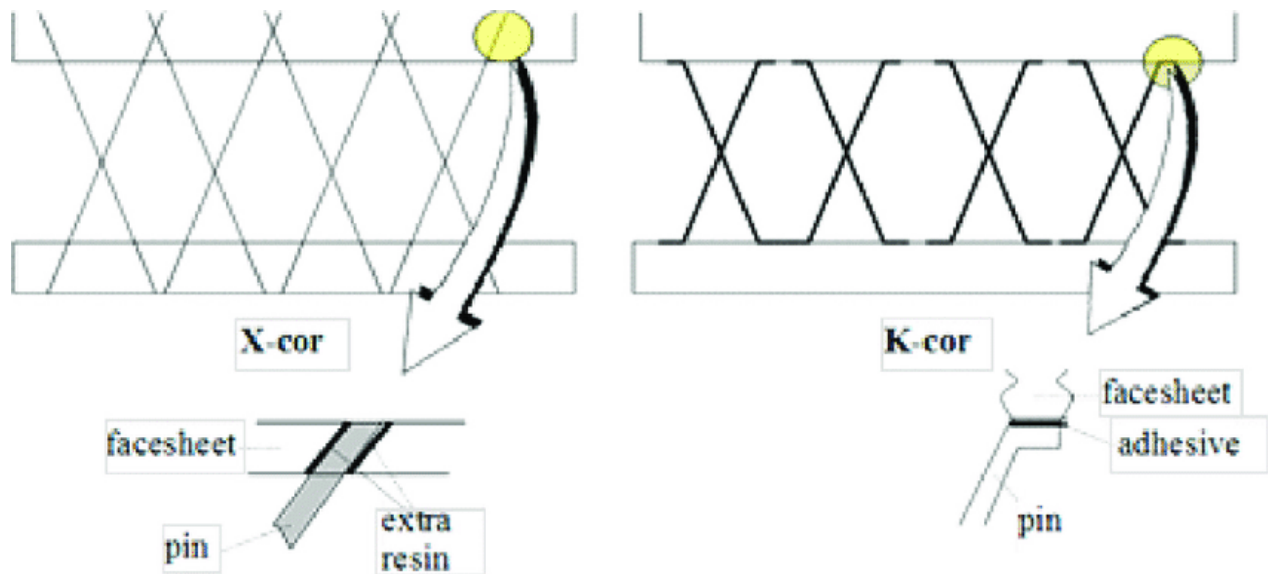


Figure 1.9 Cross-sectional views of X-cor and K-cor [85].

There have been extensive works indicating that Z-pinning dramatically improves the resistance to delamination. Andrea et al. [86] investigated the out-of-plane tension, shear and compression properties of novel X-Cor and K-Cor flat sandwich panels. The novel Z-pinned cores were found to exhibit higher specific stiffness than conventional sandwich cores. The main failure modes were pin pull-out (in X-Cor), pin end debond (K-Cor). Tao et al. [87] developed a micromechanics-based model to predict the plastic collapse strength of pin-reinforced sandwich beam under 3-point bending. The results demonstrated that the weaker the foam is, the better the optimizing effect of the pin-reinforced foam core is. Xu Dan et al. [88] proposed a model to simulate the types and propagation path of the failure and the failure mechanisms of X-cor sandwich under shear loading. The finite element analysis showed the resin regions failed firstly and then followed with Z-pin pull-out, Z-pin shear off and Z-pin buckling. The error range between the model results and experimental results was -10.4%~7.4%. J. Hao et al. [89] investigated the effects of Z-pin inserting angle, inserting density and inserting direction on

compression and shear properties. Results showed that the compression properties were improved by the increase of Z-pin inserting angle and density. On the contrary, the shear properties decreased. Virakthi et al. [90] compared various models to estimate the out-of-plane compressive stiffness and strengths of sandwich panels with K-Cor core. The first model captured the dependence of pin angle, cell spacing and core thickness on compressive stiffness and strength. The second was a finite element model that did not incorporate pin-facesheet interactions. Model 3 incorporated the effect of pin-facesheet interactions on the specimen compressive modulus, which turned out to match reasonably well with experimental values.

The flatwise compression and flexural behaviors of foam core sandwich and polymer pin-reinforced foam core sandwich panels were experimentally explored by Abdi et al. [91]. It was found that the flatwise compression and flexural properties of sandwich panels were enhanced significantly by adding the polymer pins. There are plenty of other studies on the flatwise compression properties of sandwich composites with z-pins perpendicular to thickness [92–98]. This property is sensitive to the volume fraction of z-pin [96]. Virtually all the results presented that the z-pins can offer an obvious improvement on the compression performance. In addition to the angle and volume content, the improvement can also be controlled by the material type and diameter of the z-pins.

Many studies showed that z-pins are also conducive to improving the shear and bending performance of sandwich composites [99–101]. Long et al. [102] investigated the influence of the orientation of z-pins on the core shear properties. The z-pins were aligned along or opposite to the shear loading direction. Experimental results indicated that these two kinds of pins had almost the same effect on the shear properties. Then they studied the effects of pinning density on the load-indentation response and the resulting damage modes [103]. It showed that the effect of the inclination angle of pins was not obvious compared with that of Z-pinning density. And the structure failed mainly because of the pin buckling (see Figure 1.10).

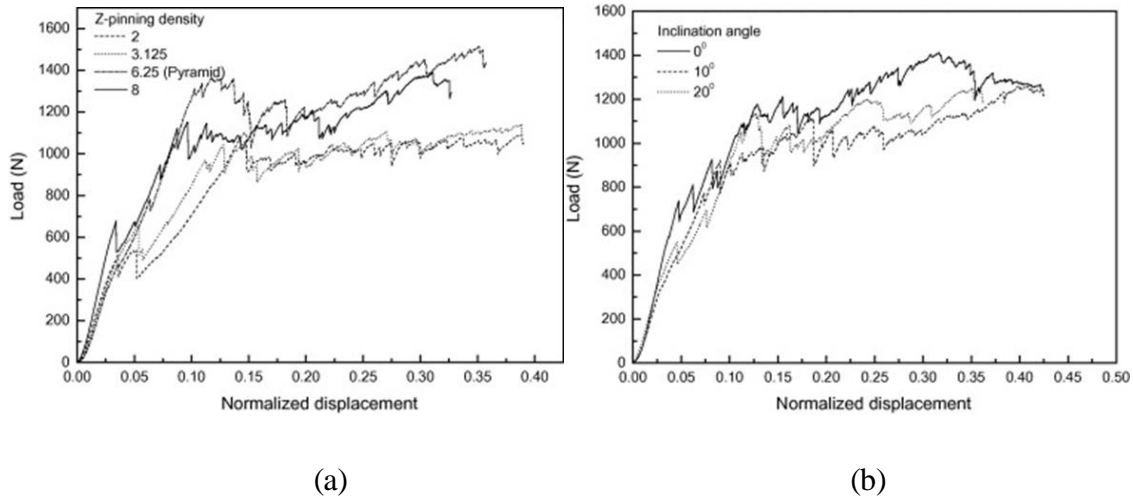


Figure 1.10 Comparison of load/normalized displacement curves for (a) different Z-pinning densities and (b) different Z-pin inclination angle [103].

Vaidya et al. [104] reinforced the sandwich constructions by way of three-dimensional Z-pins embedded into foam, honeycomb cells filled with foam. The results validated that z-pin reinforcement of the core suppressed core crushed effectively under the high strain rate impact loading. Mouritz [105] reviewed the recent researches about z-pinned sandwich composites. The progress of z-pins influence on the impact damage resistance and in-plane mechanical properties of sandwich composites materials were summarized.

1.4.3 Stitched sandwich structure

The stitching process introduces the thread with high performance (such as carbon, glass and Kevlar) through the thickness of a dry preform by a sewing machine. It can provide a significant improvement in interlaminar fracture toughness, fatigue resistance and impact resistance [106–108]. Common stitching methods include the modified lock stitch, lock stitch, and chain stitch (as shown in Figure 1.11).

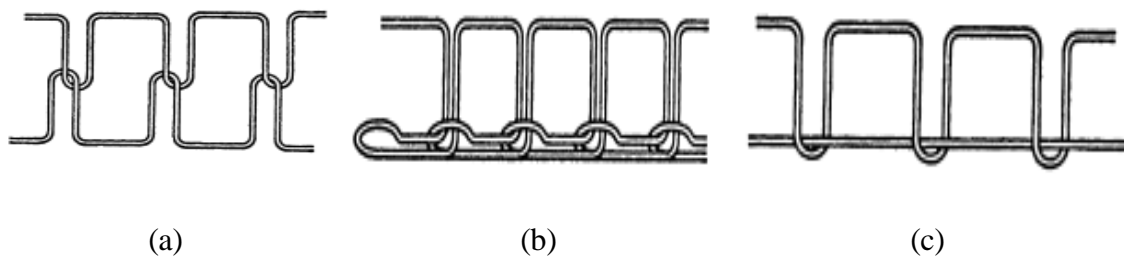


Figure 1.11 Schematics of (a) chain stitch (b) lock stitch (c) modified lock stitch [106].

During the process, a dual-threading system (bobbin & needle threads) makes the seam by forming loops and knots through laminates (shown in Figure 1.12) [109]. Stitches are periodically spaced and characterized by the stitch pitch P (distance between two adjacent stitches along the same stitch seam and the stitch spacing) and spacing S (distance between two adjacent seams of stitching) [110].

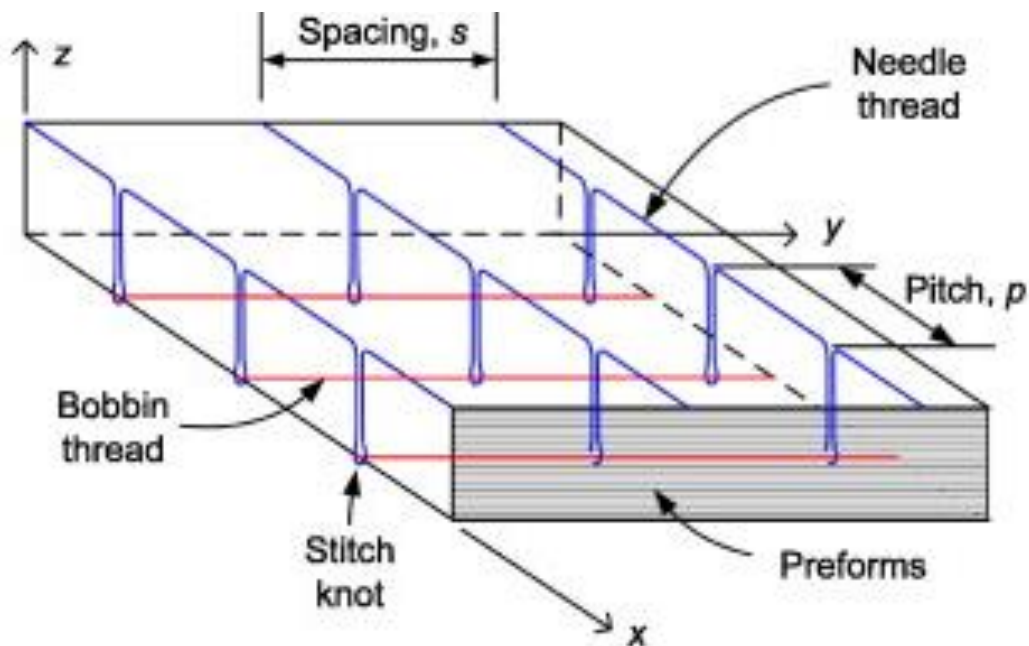


Figure 1.12 Modified-lock stitching process [111].

A large number of works have been done to enhance the foam cores by stitching process. Daniel et al. [112] performed single cantilevered beam tests to characterize the facesheet-core debonding within the stitched sandwich composites, and also adopted a discrete cohesive zone modeling approach to simulate the separation of the facesheet from the core. Good agreement between prediction and experimental measurements was obtained. Kim et al. [113] investigated the static and fatigue characteristics of polyurethane foam-cored sandwich structures. The results showed that the bending strength of the stitched specimen was increased by 50% compared to the non-stitched sandwich. Multi mechanical tests were conducted to characterize the behavior of stitched foam core sandwich under bending, compression, core shear and impact conditions [114][115]. All the results showed the same conclusion: stitching of sandwich panels significantly increases the maximum failure loads. Raju et al. [116] investigated the energy absorption characteristics of sandwich panels with through-the-thickness stitches under edgewise

compression. The results indicated that the average sustained crush load increases with reduced stitch row spacing.

Lascoup et al. [117] studied the influence of the macro-structural parameters of the stitches (step and angle) on the mechanical behavior of the sandwich structure. By comparing with the sandwich without stitches, it was found that the gain brought by the stitches was obvious for the moduli and maximum stresses of core shear, flatwise compression and 4-point bending tests (as shown in Figure 1.13). However, many stitches also increased the weight of the sandwich and a compromise between the mechanical performance and the mass must be found. Another similar work about the investigation of flexural properties of stitched sandwich composites was conducted by Potluri et al. [118]. Different series of sandwich panels were fabricated by modifying the stitch density and stitch orientation (orthogonal and bias). It showed that the bending stiffness and strength increased with bias stitching and slightly reduced with orthogonal stitching. They also compared the effect of stitch thread on debonding resistance by quasi-static indentation tests. It was obtained that the orthogonal stitches were better than bias stitches in preventing the debonding and debonding area decreased with an increase in stitch density. The researchers further advanced their work on the bending characterization of sandwich structures with stitches in 2008 [119]. An original model was proposed to predict the elastic in-plane behavior of such stitched sandwich structures. The results determined the optimal angle and step combination. After 4 years, a model to represent the performances of these structures under out-of-plane shearing and compressive stress was developed [120].

Another novel model to calculate the flexural rigidity of stitched foam-core sandwich structure was proposed by Peiyan et al [121]. Several stitched foam core sandwich beam specimens with different stitching densities were employed in the three-point bending tests. The results showed that bending strength increased with the increase of stitching density, but the flexural rigidity decreased (shown in Table 1.3).

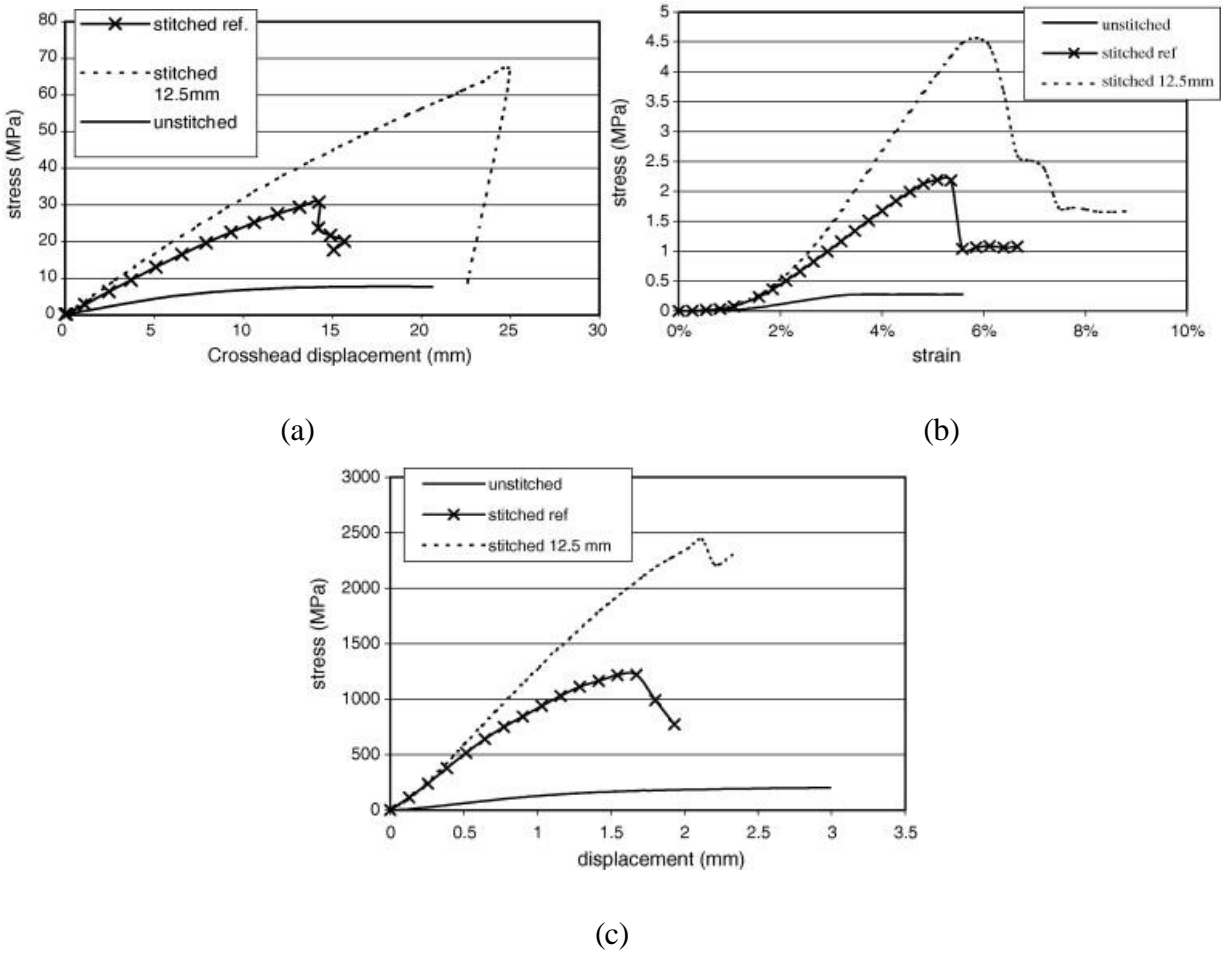


Figure 1.13 Typical results of (a) bending test, (b) flatwise compression and (c) core shear test [117].

Table 1.3 Mechanical properties of stitched foam-core sandwich structure [121].

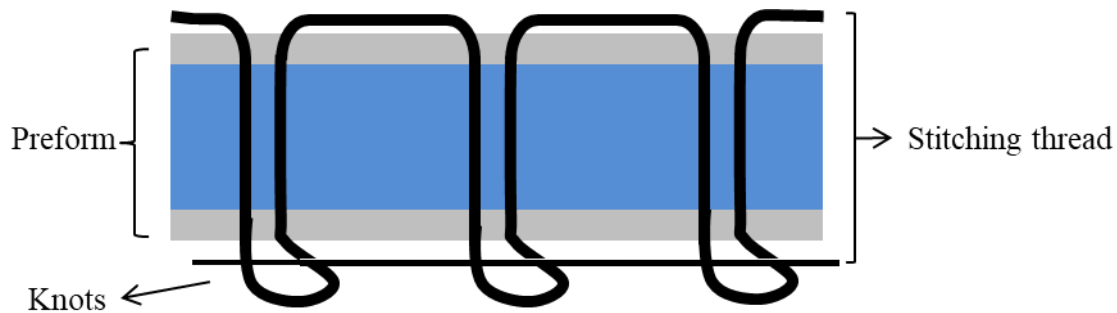
Stitching density (mm)	Failure load		Flexural rigidity		Shear rigidity	
	Ave. (N)	COV (%)	Ave. (N mm ²)	COV (%)	Ave. (N)	COV (%)
–	440.61	1.23	46,102,680	2.92	6889.4	4.45
5 × 5	1583.24	4.93	47,973,960	2.46	9277.2	5.73
6.5 × 6.5	1109.62	5.50	51,440,040	2.47	14950.6	2.29
8 × 8	869.19	2.14	52,411,590	2.26	16575.9	2.46

The compression behavior of the integrated 3D composite sandwich structure was investigated by Wu et al. [122]. The results showed that the out-of-plane compressive properties of the integrated 3D composite sandwich structures were better than those of the traditional foam core because the composite columns and the foam support each other. Sharma et al. [123] conducted the edgewise compression (buckling) tests of unstitched and stitched sandwich specimens. Ultimate load carrying capacity and failure modes were determined.

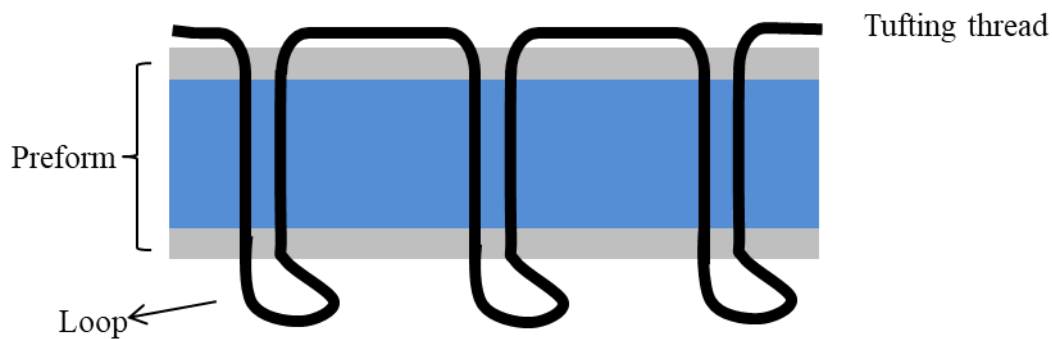
The studies about impact performances of stitched foam core sandwich composites were conducted by many researchers. The impact damages of unstitched and stitched foam core sandwich composites were compared and analyzed by Xia and Wu. Compare to the unstitched samples, the damage angle of stitched samples increase by 48% [124]. Similar studies were conducted by Santhanakrishnan et al. [125]. It was found that the introduction of stitches improved the impact performance. Vaidya et al. [126] investigated the impact damages of stitched sandwich cores with and without foams. The results showed that buckling of the cores and the rupture of the face sheets mainly appeared in specimens without foam. The foam increased the strength of the sandwich structure by preventing buckling of core piles. The low-velocity impact performances of a stitched foam core sandwich composite were investigated experimentally and numerically [127]. Potluri et al. [128] prepared stitched sandwich samples with different stitching densities for impact tests. Results obtained showed that the failure loads of skin and the stiffness of the sandwich panel increased with an increase in density.

1.4.4 Tufted sandwich structure

Similar to the stitching, the tufting process can connect the reinforcement layers by inserting the yarn through the thickness of the dry preform. The difference is that the thread carried by the tufting needle is tension-free and it only needs to insert from one side of the preform. The tufting technique is more economical and flexible because the tufting thread forms loops at the bottom of the preform rather than knots as stitching (see Figure 1.14) [129].



(a)



(b)

Figure 1.14 Schematic diagrams of (a) lock stitching thread, (b) tufting thread.

This technology was originally used in the production of carpets but is now being used extensively in the field of composite materials [130]. As a process developed from stitching, the principle and operation mechanism of tufting are similar to stitching. And the novelty is that the tufting is one-side stitching and the thread inserted into the preform is tension-free. The thread can be retained into preform by the friction between yarn and fabric or between yarn and foam. Tufting is simple than stitching, but in another hand, the binding of layers is weaker because it has no locks of thread at the bottom of the preform. The tufting thread through the thickness can provide significant resistance against delamination. Gnaba et al. [109] presented an excellent review of tufted reinforcement for composite.

Since tufting was developed late in these z-directional reinforcement technologies, most of the current research was focused on laminates or dry preforms. Dell'Anno et al. published a series of papers on tufted composites, involving design, manufacturing process and characterization of

their mechanical properties. They firstly investigated the mechanical performance of carbon fiber reinforced composite tufted with glass fiber thread by tensile test, compression-after-impact tests and double-cantilever beam test. The benefits of tensile strength and the delamination crack growth resistance brought by the glass thread were validated [131]. Then a practical guideline was provided for the manufacture of tufted composite parts. They analyzed the effects of the process parameters on the preform fiber architecture and on the mesostructure of the reinforced component such as the equipment configuration and setup, latest advances in tooling, thread selection, preform supporting systems and choice of ancillary materials [130]. Subsequent studies concentrated on the delamination resistance and mechanism of composite [132–134]. And they also continued to improve the tufting process [135]. More research on anti-delamination of tufting was also available in the works of Pappas et al., they first studied the effect of tuft geometry or tufting pattern on Mode I interlaminar fracture in a glass fiber reinforced composite [136], and then developed a model based on experimental results [137]. Both model values and experimental results indicated that tuft's failure mechanism is strongly affected by the tufting pattern. Besides, the Mode II fracture of the tufted composite was also explored and analyzed by some researchers [138][139]. Other basic mechanical tests such as in-plane tensile [140], compression [141], and bending [142] and impact test [143][144] have also been conducted and investigated. The tensile properties of tufting thread were studied in the works of Hui [145] and Liu [146]. The former focused on the effect of tufting density on the dry tufting threads degradation and the latter investigated the influence of the tuft length on the tensile performance of tufting threads through the thickness of composites. The formability of the tufted preforms is important to the manufacturing process. Some works have been performed to study the out-of-plane deformability of tufted preforms by stamping test. The effects of tufting thread orientations, superposing layup orientations [147] and tufting pattern [148][149] were respectively analyzed.

Given the significant improvement in delamination identified in all studies, tufting has also been used in recent years to reinforce the foam-core sandwich structure. In terms of the mechanical properties of the tufted sandwich composite, several studies have been carried out to characterize the mechanical performance. Henao et al. [150] focused on the influence of tufting thread on compression and bending properties of sandwich structures. The sandwich panels with carbon fiber reinforcement and E-glass fiber reinforcement were respectively tested. The experimental results showed that the improvement of edgewise compression strength is modest,

while the increase of 3-point bending strength is significant (see Figure 1.15). Hartley et al. [151] [154][155] studied the effect of tufting density and loop length on the crushing behavior of tufted sandwich composite. An increase of the crushing performance by 25% brought by the tufts was observed. Nevertheless, the loop size appeared to have a negligible effect on the loading response. A new test method was proposed and developed to test the contribution of the tuft drift mechanism observed under crushing loads. It showed that the load increased with increasing numbers of tufts. Icardi et al. [152] adopted a hierarchic model to study the influence of stitches and tufts on stress and displacement fields. Numerical results showed that the insertion of thread through the thickness of the sandwich can considerably reduce the transverse shear stress as well as the transverse displacements. Blok et al. [153] improved the in-plane crushing response of sandwich structures by adding aramid tufting thread. It can be obtained that tufting improved the specific energy absorption from 11.5 kJ/kg to 20.5 kJ/kg and the crushing force efficiency from 0.22 to 0.55.

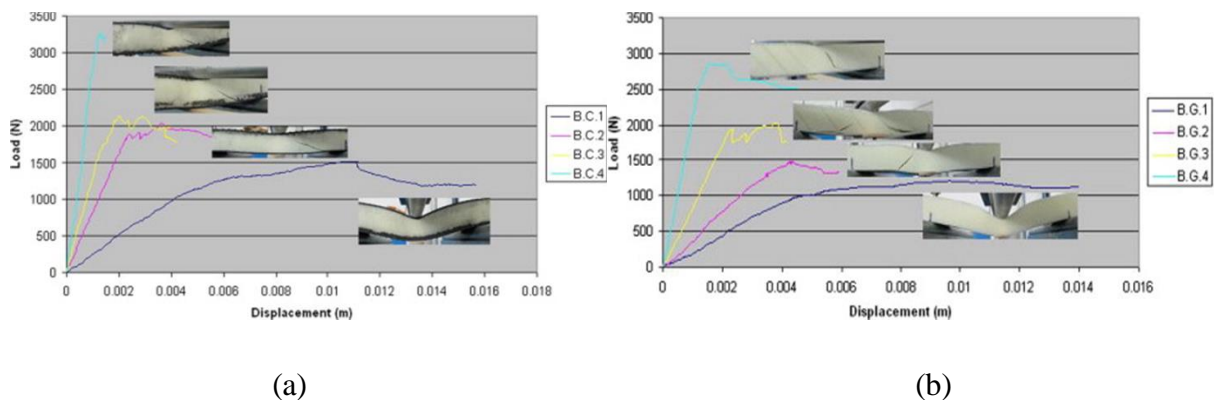


Figure 1.15 Load/displacement curves of tufted and non-tufted polyurethane-core sandwich panels with (a) carbon fiber reinforcement and (b) E-glass fiber reinforcement under 3-point bending [150].

1.5 Resin infusion process

Liquid Composite Molding (LCM) has been significantly developed such as the Resin Transfer Molding (RTM), Vacuum Assisted RTM (VARTM), Resin Film Infusion (RFI), and Liquid Resin Infusion (LRI). These technologies have been widely employed in advanced fields of automotive, aeronautics, shipbuilding and wind power generators [156]. The LCM process is a two-step process in general. First, the resin is injected and fills the stack of the preform, then transforms the resin from liquid state to the solid state.

Resin transfer molding (RTM) is a closed-mold process developed in the 1990s [157]. The mold is usually fabricated by rigid metal and the preform is placed into it. The resin is then injected into the dry fibrous preform and cured. This process allows the obtained composite parts to have complex shapes and smooth surfaces. And the volume fractions of resin and fiber are well controlled. Whereas the matched metal molds increase the cost. VARTM is developed based on the RTM. Different from RTM, resin flow is introduced into a fiber layup by a vacuum, which is more cost-effective and facilitates the manufacture of large size parts. However, the vacuum bag only allows the molded part to have one smooth side.

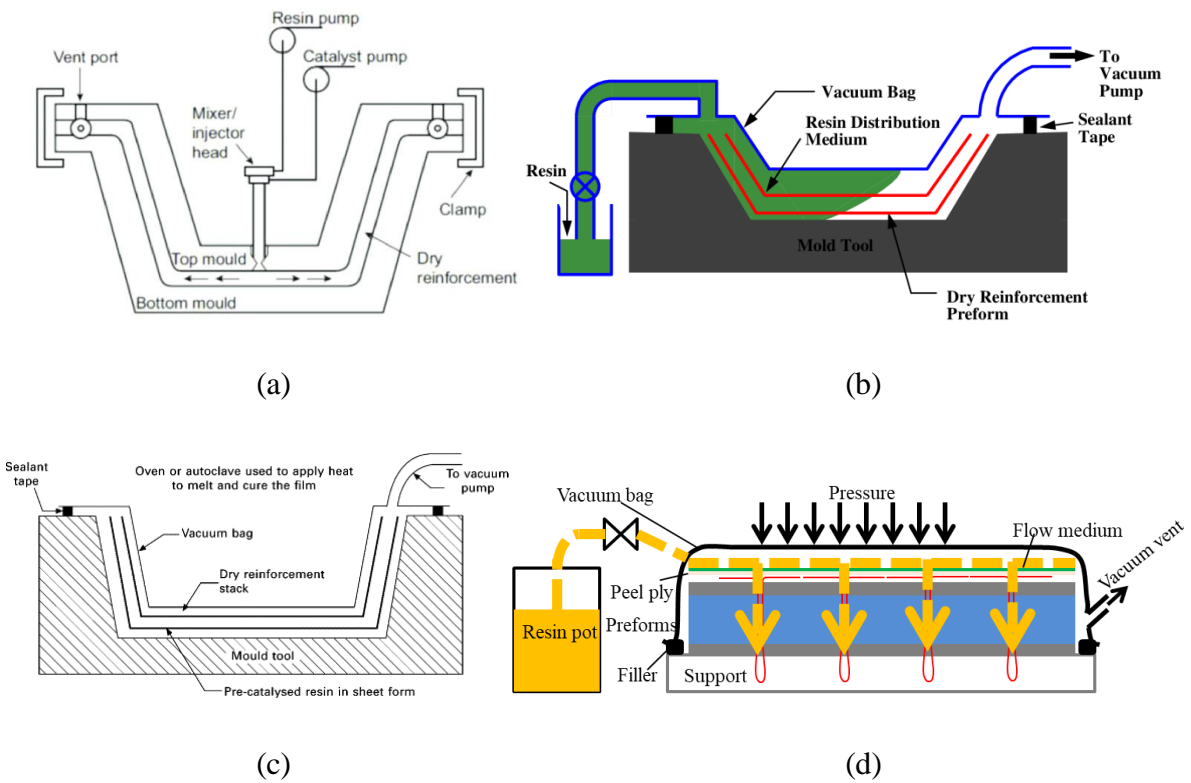


Figure 1.16 Schematics of process (a) RTM [158], (b) VARTM [159], (c) RFI [160] and (d) LRI.

The principle of the RFI process is presented in Figure 1.13c [160–162]. The preform is placed onto a layer of solid resin. And a metal plate is placed on the stacking layers to ensure a flat upper surface of the final part. Various non-stick plastic films are used to isolate the composite from the equipment and in particular to place it together on a vacuum. Then, with the application of the temperature cycle by autoclave, the viscosity of the resin decreases. This drop in viscosity and the action of the pressure cycle (vacuum pump) allow the resin to infuse through the thickness of the

preform. A thermo-hardening phase will be carried out by the temperature and pressure cycle after filling with the resin.

Unlike RFI, the LRI uses liquid resin rather than a solid resin film. During the process, a dry preform is placed inside a vacuum bag and then the liquid resin enters into the preform by vacuum (see Figure 1.13d). This process has low cost and high production efficiency because of its straightforward technique [163]. Setting parameters of LRI is related to the preform size and request fiber volume fraction. And the mechanical characterization of composite parts fabricated by LRI has been investigated [164–166].

1.6 Conclusion

Sandwich structure composites with two composite skins and a low-density core are widely used in aerospace, automobile, building and consumer industries due to their excellent mechanical properties, such as superior bending stiffness, low weight, outstanding thermal insulation and acoustic damping. The primary drawbacks of the traditional polymer foam core, however, are the delamination and its weak mechanical properties. In decades, several innovations have been advanced to overcome the shortcoming of delamination. The major method involves the insertion of through-the-thickness reinforcement in a sandwich structure such as z-pin, stitching and tufting.

This study focuses mainly on the tufted sandwich composite because of the low cost, high efficiency and fewer limits than others. Developed from stitching, tufting also calls for an introduction of yarn into the sandwich preform. The difference, however, is that tufting is similar to one-sided stitching in that the tufting thread is not locked by a second thread after passing through the preform. Therefore it needs to be fixed by friction between the thread and the preform or between the thread and the support foam, and the selection of thread and needle is more stringent.

Nevertheless, the low mechanical properties of foam core have rarely solutions presently. In this study, a new sandwich structure design is proposed and realized by adding a nonwoven core, which aims to improve the mechanical performance of foam core and limit the increase of weight meanwhile. The density and mechanical properties of nonwovens are intermediate between those

of fabrics and foams, making it advantageous to find a compromise between improved mechanical properties and weight reduction.

This sandwich structure was firstly applied in the carbon fiber reinforced sandwich and the manufacturing process is introduced in the following chapters. And the mechanical behavior under different loadings is investigated and discussed in chapter 3. To validate the feasibility and further optimize the structure, the effects of nonwoven, tufting thread and foam are respectively analyzed.

With increasingly stringent environmental requirements, flax fiber-reinforced sandwich composites are more and more used in transport and construction fields due to the high mechanical properties of the natural fibers. To develop a green sandwich composite with the novel sandwich structure, the flax fiber reinforcement and bio-based epoxy resin are selected. Afterward, the analysis of its mechanical behavior under core shear load and 3-point bending load was focused.

Reference

- [1] Dodun O, Slatineanu L, Nagit G, Mares M, Hrituc A, Coteata M, et al. Mechanical properties of composites reinforced with textile. *Mater Plast* 2020;57:21–7. <https://doi.org/10.37358/MP.20.1.5308>.
- [2] Zuhri MYM, Guan ZW, Cantwell WJ. The mechanical properties of natural fibre based honeycomb core materials. *Compos Part B Eng* 2014;58:1–9. <https://doi.org/10.1016/j.compositesb.2013.10.016>.
- [3] Alix S, Marais S, Morvan C, Lebrun L. Biocomposite materials from flax plants: Preparation and properties. *Compos Part A Appl Sci Manuf* 2008;39:1793–801. <https://doi.org/10.1016/j.compositesa.2008.08.008>.
- [4] Hepworth DG, Hobson RN, Bruce DM, Farrent JW. Use of unretted hemp fibre in composite manufacture. *Compos Part A Appl Sci Manuf* 2000;31:1279–83. [https://doi.org/10.1016/S1359-835X\(00\)00098-1](https://doi.org/10.1016/S1359-835X(00)00098-1).
- [5] Jumaidin R, Khiruddin MAA, Asyul Sutan Saidi Z, Salit MS, Ilyas RA. Effect of cogon grass fibre on the thermal, mechanical and biodegradation properties of thermoplastic cassava starch biocomposite. *Int J Biol Macromol* 2020;146:746–55. <https://doi.org/10.1016/j.ijbiomac.2019.11.011>.
- [6] Alsubari S, Zuhri MYM, Sapuan SM, Ishak MR, Ilyas RA, Asyraf MRM. Potential of natural fiber reinforced polymer composites in sandwich structures: A review on its mechanical properties. *Polymers (Basel)* 2021;13:1–20. <https://doi.org/10.3390/polym13030423>.
- [7] Adekomaya O. Adaption of green composite in automotive part replacements: discussions on material modification and future patronage. *Environ Sci Pollut Res* 2020;27:8807–13. <https://doi.org/10.1007/s11356-019-07557-x>.

- [8] Baley C, Bourmaud A, Davies P. Eighty years of composites reinforced by flax fibres: A historical review. *Compos Part A Appl Sci Manuf* 2021;144. <https://doi.org/10.1016/j.compositesa.2021.106333>.
- [9] Akampumuza O, Wambua PM, Ahmed A, Li W, Qin XH. Review of the applications of biocomposites in the automotive industry. *Polym Compos* 2017;38:2553–69. <https://doi.org/10.1002/pc.23847>.
- [10] Holbery J, Houston D. Natural-fiber-reinforced polymer composites in automotive applications. *JOM* 2006;58:80–6. <https://doi.org/10.1007/s11837-006-0234-2>.
- [11] Li M, Pu Y, Thomas VM, Yoo CG, Ozcan S, Deng Y, et al. Recent advancements of plant-based natural fiber-reinforced composites and their applications. *Compos Part B Eng* 2020;200. <https://doi.org/10.1016/j.compositesb.2020.108254>.
- [12] Monteiro SN, Satyanarayana KG, Ferreira AS, Nascimento DCO, Lopes FPD, Silva ILA, et al. Selection of high strength natural fibers. *Rev Mater* 2010;15:488–505. <https://doi.org/10.1590/S1517-70762010000400002>.
- [13] Shah DU. Developing plant fibre composites for structural applications by optimising composite parameters: A critical review. *J Mater Sci* 2013;48:6083–107. <https://doi.org/10.1007/s10853-013-7458-7>.
- [14] Abrial H, Arikxa J, Mahardika M, Handayani D, Aminah I, Sandrawati N, et al. Highly transparent and antimicrobial PVA based bionanocomposites reinforced by ginger nanofiber. *Polym Test* 2020;81. <https://doi.org/10.1016/j.polymertesting.2019.106186>.
- [15] Mahboob Z, Bougherara H. Fatigue of flax-epoxy and other plant fibre composites: Critical review and analysis. *Compos Part A Appl Sci Manuf* 2018;109:440–62. <https://doi.org/10.1016/j.compositesa.2018.03.034>.
- [16] Shah DU. Natural fibre composites: Comprehensive Ashby-type materials selection charts. *Mater Des* 2014;62:21–31. <https://doi.org/10.1016/j.matdes.2014.05.002>.
- [17] El-Sabbagh A, Steuernagel L, Ziegmann G, Meiners D, Toepfer O. Processing parameters and characterisation of flax fibre reinforced engineering plastic composites with flame retardant fillers. *Compos Part B Eng* 2014;62:12–8. <https://doi.org/10.1016/j.compositesb.2014.02.009>.
- [18] Yan L, Chouw N, Jayaraman K. Flax fibre and its composites - A review. *Compos Part B Eng* 2014;56:296–317. <https://doi.org/10.1016/j.compositesb.2013.08.014>.
- [19] Joshi S V., Drzal LT, Mohanty AK, Arora S. Are natural fiber composites environmentally superior to glass fiber reinforced composites? *Compos. Part A Appl. Sci. Manuf.*, vol. 35, 2004, p. 371–6. <https://doi.org/10.1016/j.compositesa.2003.09.016>.
- [20] Dittenber DB, Gangarao HVS. Critical review of recent publications on use of natural composites in infrastructure. *Compos Part A Appl Sci Manuf* 2012;43:1419–29. <https://doi.org/10.1016/j.compositesa.2011.11.019>.
- [21] Chandrasekar M, Shahroze RM, Ishak MR, Saba N, Jawaid M, Senthilkumar K, et al. Flax and sugar palm reinforced epoxy composites: Effect of hybridization on physical, mechanical, morphological and dynamic mechanical properties. *Mater Res Express* 2019;6. <https://doi.org/10.1088/2053-1591/ab382c>.
- [22] Velmurugan G, Shaafi T, Bhagavathi MS, V SS. Evaluate the tensile, flexural and impact strength of hemp and flax based hybrid composites under cryogenic environment. *Mater Today Proc* 2021. <https://doi.org/10.1016/j.matpr.2021.08.244>.
- [23] Karthi N, Kumaresan K, Sathish S, Prabhu L, Gokulkumar S, Balaji D, et al. Effect of weight fraction on the mechanical properties of flax and jute fibers reinforced epoxy hybrid composites. *Mater. Today Proc.*, vol. 45, 2021, p. 8006–10. <https://doi.org/10.1016/j.matpr.2020.12.1060>.

- [24] Barkoula NM, Garkhail SK, Peijs T. Biodegradable composites based on flax/polyhydroxybutyrate and its copolymer with hydroxyvalerate. *Ind Crops Prod* 2010;31:34–42. <https://doi.org/10.1016/j.indcrop.2009.08.005>.
- [25] Charlet K, Baley C, Morvan C, Jernot JP, Gomina M, Bréard J. Characteristics of Hermès flax fibres as a function of their location in the stem and properties of the derived unidirectional composites. *Compos Part A Appl Sci Manuf* 2007;38:1912–21. <https://doi.org/10.1016/j.compositesa.2007.03.006>.
- [26] Oksman K. High quality flax fibre composites manufactured by the resin transfer moulding process. *J Reinf Plast Compos* 2001;20:621–7. <https://doi.org/10.1106/CA5A-6FAX-VJRB-80P0>.
- [27] Goutianos S, Peijs T, Nystrom B, Skrifvars M. Development of flax fibre based textile reinforcements for composite applications. *Appl Compos Mater* 2006;13:199–215. <https://doi.org/10.1007/s10443-006-9010-2>.
- [28] Madsen B, Lillholt H. Physical and mechanical properties of unidirectional plant fibre composites-an evaluation of the influence of porosity. *Compos Sci Technol* 2003;63:1265–72. [https://doi.org/10.1016/S0266-3538\(03\)00097-6](https://doi.org/10.1016/S0266-3538(03)00097-6).
- [29] Lachaud F, Boutin M, Espinosa C, Hardy D. Failure prediction of a new sandwich panels based on flax fibres reinforced epoxy bio-composites. *Compos Struct* 2021;257. <https://doi.org/10.1016/j.compstruct.2020.113361>.
- [30] Jha AK. Free vibration analysis of sandwich panel. 2007.
- [31] Pflug J, Fan XY, Vangrimde B, Verpoest I, Bratfisch P, Vanderpitte D. Development of a sandwich material with polypropylene/natural fiber skins and paper honeycomb core. *Proc 10th Eur Conf Compos Mater* 2002:331.
- [32] NAKAMURA M. Structural Health Monitoring in Building Structures. *J Soc Instrum Control Eng* 2002;41:819–24. <https://doi.org/10.11499/sicej11962.41.819>.
- [33] Zhang Y, Liu W, Yin C, Ma Y, Wang L. Mode II interfacial fracture characterization of foam core sandwich materials at elevated temperatures: the effects of frictional stresses between the crack edges. *Int J Solids Struct* 2020;193–194:28–38. <https://doi.org/10.1016/j.ijsolstr.2020.02.001>.
- [34] Kulkarni N, Mahfuz H, Jeelani S, Carlsson LA. Fatigue Failure Mechanism and Crack Growth in Foam Core Sandwich Composites under Flexural Loading. *J Reinf Plast Compos* 2004;23:83–94. <https://doi.org/10.1177/0731684404029347>.
- [35] Lindström A, Hallström S. In-plane compression of sandwich panels with debonds. *Compos Struct* 2010;92:532–40. <https://doi.org/10.1016/j.compstruct.2009.08.039>.
- [36] Miao XY, Lu R, Chen X. Fracture behaviour of foam core sandwich structures with manufacturing defects using phase-field modelling. *Compos Struct* 2021;274. <https://doi.org/10.1016/j.compstruct.2021.114294>.
- [37] Belingardi G, Cavatorta MP, Duella R. Material characterization of a composite-foam sandwich for the front structure of a high speed train. *Compos Struct* 2003;61:13–25. [https://doi.org/10.1016/S0263-8223\(03\)00028-X](https://doi.org/10.1016/S0263-8223(03)00028-X).
- [38] Thomas AB. MD. Estimation of Flexural Strength and Shear Strength of Sandwich Panel by Varying Foam Density. *Int J Sci Res* 2014;3:389–90.
- [39] Bull PH, Edgren F. Compressive strength after impact of CFRP-foam core sandwich panels in marine applications. *Compos Part B Eng* 2004;35:535–41. <https://doi.org/10.1016/j.compositesb.2003.11.007>.

- [40] Abbadi A, Koutsawa Y, Carmasol A, Belouettar S, Azari Z. Experimental and numerical characterization of honeycomb sandwich composite panels. *Simul Model Pract Theory* 2009;17:1533–47. <https://doi.org/10.1016/j.simpat.2009.05.008>.
- [41] Hexcel Composites. *HexWeb Honeycomb Attributes and Properties*. 1999.
- [42] Keshavanarayana SR, Shahverdi H, Kothare A, Yang C, Bingenheimer J. The effect of node bond adhesive fillet on uniaxial in-plane responses of hexagonal honeycomb core. *Compos Struct* 2017;175:111–22. <https://doi.org/10.1016/j.compstruct.2017.05.010>.
- [43] Ratcliffe JG, Czabaj MW, Jackson WC. A model for simulating the response of aluminum honeycomb structure to transverse loading. 27th Annu. Tech. Conf. Am. Soc. Compos. 2012, Held Jointly with 15th Jt. US-Japan Conf. Compos. Mater. ASTM-D30 Meet., 2012, p. 38–53.
- [44] Heimbs S. Virtual testing of sandwich core structures using dynamic finite element simulations. *Comput Mater Sci* 2009;45:205–16. <https://doi.org/10.1016/j.commatsci.2008.09.017>.
- [45] Giglio M, Manes A, Gilioli A. Investigations on sandwich core properties through an experimental- numerical approach. *Compos Part B Eng* 2012;43:361–74. <https://doi.org/10.1016/j.compositesb.2011.08.016>.
- [46] Yang X, Sun Y, Yang J, Pan Q. Out-of-plane crashworthiness analysis of bio-inspired aluminum honeycomb patterned with horseshoe mesostructure. *Thin-Walled Struct* 2018;125:1–11. <https://doi.org/10.1016/j.tws.2018.01.014>.
- [47] Hong ST, Pan J, Tyan T, Prasad P. Quasi-static crush behavior of aluminum honeycomb specimens under non-proportional compression-dominant combined loads. *Int J Plast* 2006;22:1062–88. <https://doi.org/10.1016/j.ijplas.2005.07.003>.
- [48] Dharmasena KP, Wadley HNG, Xue Z, Hutchinson JW. Mechanical response of metallic honeycomb sandwich panel structures to high-intensity dynamic loading. *Int J Impact Eng* 2008;35:1063–74. <https://doi.org/10.1016/j.ijimpeng.2007.06.008>.
- [49] Rodriguez-Ramirez J de D, Castanie B, Bouvet C. Experimental and numerical analysis of the shear nonlinear behaviour of Nomex honeycomb core: Application to insert sizing. *Compos Struct* 2018;193:121–39. <https://doi.org/10.1016/j.compstruct.2018.03.076>.
- [50] Kim G, Sterkenburg R, Tsutsui W. Investigating the effects of fluid intrusion on Nomex® honeycomb sandwich structures with carbon fiber facesheets. *Compos Struct* 2018;206:535–49. <https://doi.org/10.1016/j.compstruct.2018.08.054>.
- [51] Abd Kadir N, Aminanda Y, Ibrahim MS, Mokhtar H. Experimental study of low-velocity impact on foam-filled Kraft paper honeycomb structure. *IOP Conf. Ser. Mater. Sci. Eng.*, vol. 290, 2018. <https://doi.org/10.1088/1757-899X/290/1/012082>.
- [52] Chen Z, Yan N. Investigation of elastic moduli of Kraft paper honeycomb core sandwich panels. *Compos Part B Eng* 2012;43:2107–14. <https://doi.org/10.1016/j.compositesb.2012.03.008>.
- [53] Toribio MG, Spearing SM. Compressive response of notched glass-fiber epoxy/honeycomb sandwich panels. *Compos - Part A Appl Sci Manuf* 2001;32:859–70. [https://doi.org/10.1016/S1359-835X\(00\)00150-0](https://doi.org/10.1016/S1359-835X(00)00150-0).
- [54] Shahdin A, Mezeix L, Bouvet C, Morlier J, Gourinat Y. Fabrication and mechanical testing of glass fiber entangled sandwich beams: A comparison with honeycomb and foam sandwich beams. *Compos Struct* 2009;90:404–12. <https://doi.org/10.1016/j.compstruct.2009.04.003>.
- [55] Gpoichand A, Mohanrao R, Sankar NVS, Balaji GR, Kumar PS. Design and Analysis of Copper Honeycomb Sandwich Structure. *Int J Eng Adv Technol* 2013;2:635–8.

- [56] Du Y, Yan N, Kortschot MT. Light-weight honeycomb core sandwich panels containing biofiber-reinforced thermoset polymer composite skins: Fabrication and evaluation. *Compos Part B Eng* 2012;43:2875–82. <https://doi.org/10.1016/j.compositesb.2012.04.052>.
- [57] Foo CC, Chai GB, Seah LK. Mechanical properties of Nomex material and Nomex honeycomb structure. *Compos Struct* 2007;80:588–94. <https://doi.org/10.1016/j.compstruct.2006.07.010>.
- [58] He M, Hu W. A study on composite honeycomb sandwich panel structure. *Mater Des* 2008;29:709–13. <https://doi.org/10.1016/j.matdes.2007.03.003>.
- [59] Wei X, Wu Q, Gao Y, Qiang Yang, Xiong J. Composite honeycomb sandwich columns under in-plane compression: Optimal geometrical design and three-dimensional failure mechanism maps. *Eur J Mech - A/Solids* 2021;91:104415. <https://doi.org/10.1016/j.euromechsol.2021.104415>.
- [60] Kazemahvazi S, Tanner D, Zenkert D. Corrugated all-composite sandwich structures. Part 2: Failure mechanisms and experimental programme. *Compos Sci Technol* 2009;69:920–5. <https://doi.org/10.1016/j.compscitech.2008.11.035>.
- [61] Kazemahvazi S, Zenkert D. Corrugated all-composite sandwich structures. Part 1: Modeling. *Compos Sci Technol* 2009;69:913–9. <https://doi.org/10.1016/j.compscitech.2008.11.030>.
- [62] Chang WS, Ventsel E, Krauthammer T, John J. Bending behavior of corrugated-core sandwich plates. *Compos Struct* 2005;70:81–9. <https://doi.org/10.1016/j.compstruct.2004.08.014>.
- [63] Côté F, Deshpande VS, Fleck NA, Evans AG. The compressive and shear responses of corrugated and diamond lattice materials. *Int J Solids Struct* 2006;43:6220–42. <https://doi.org/10.1016/j.ijsolstr.2005.07.045>.
- [64] Rejab MRM, Cantwell WJ. The mechanical behaviour of corrugated-core sandwich panels. *Compos Part B Eng* 2013;47:267–77. <https://doi.org/10.1016/j.compositesb.2012.10.031>.
- [65] Jin F, Chen H, Zhao L, Fan H, Cai C, Kuang N. Failure mechanisms of sandwich composites with orthotropic integrated woven corrugated cores: Experiments. *Compos Struct* 2013;98:53–8. <https://doi.org/10.1016/j.compstruct.2012.09.056>.
- [66] Kooistra GW, Deshpande V, Wadley HNG. Hierarchical corrugated core sandwich panel concepts. *J Appl Mech Trans ASME* 2007;74:259–68. <https://doi.org/10.1115/1.2198243>.
- [67] Kılıçaslan C, Odacı İK, Güden M. Single- and double-layer aluminum corrugated core sandwiches under quasi-static and dynamic loadings. *J Sandw Struct Mater* 2016;18:667–92. <https://doi.org/10.1177/1099636215603692>.
- [68] Seong DY, Jung CG, Yang DY, Moon KJ, Ahn DG. Quasi-isotropic bending responses of metallic sandwich plates with bi-directionally corrugated cores. *Mater Des* 2010;31:2804–12. <https://doi.org/10.1016/j.matdes.2010.01.009>.
- [69] Wallach JC, Gibson LJ. Mechanical behavior of a three-dimensional truss material. *Int J Solids Struct* 2001;38:7181–96. [https://doi.org/10.1016/S0020-7683\(00\)00400-5](https://doi.org/10.1016/S0020-7683(00)00400-5).
- [70] Fan HL, Meng FH, Yang W. Sandwich panels with Kagome lattice cores reinforced by carbon fibers. *Compos Struct* 2007;81:533–9. <https://doi.org/10.1016/j.compstruct.2006.09.011>.
- [71] Deshpande VS, Fleck NA, Ashby MF. Effective properties of the octet-truss lattice material. *J Mech Phys Solids* 2001;49:1747–69. [https://doi.org/10.1016/S0022-5096\(01\)00010-2](https://doi.org/10.1016/S0022-5096(01)00010-2).
- [72] Queheillalt DT, Wadley HNG. Pyramidal lattice truss structures with hollow trusses. *Mater Sci Eng A* 2005;397:132–7. <https://doi.org/10.1016/j.msea.2005.02.048>.
- [73] Taghipoor H, Eyvazian A, Musharavati F, Sebaey TA, Ghiaskar A. Experimental investigation of the three-point bending properties of sandwich beams with polyurethane foam-filled lattice cores. *Structures* 2020;28:424–32. <https://doi.org/10.1016/j.istruc.2020.08.082>.

- [74] Li S, Fan H. Flexural behaviors and local failure analyses of EPS foam-filled GFRC truss-core sandwich panels. *Case Stud Constr Mater* 2021;15:e00688. <https://doi.org/10.1016/j.cscm.2021.e00688>.
- [75] Judawisastra H, Ivens J, Verpoest I. The fatigue behaviour and damage development of 3D woven sandwich composites. *Compos Struct* 1998;43:35–45. [https://doi.org/10.1016/S0263-8223\(98\)00093-2](https://doi.org/10.1016/S0263-8223(98)00093-2).
- [76] Van Vuure AW, Pflug J, Ivens JA, Verpoest I. Modelling the core properties of composite panels based on woven sandwich-fabric preforms. *Compos Sci Technol* 2000;60:1263–76. [https://doi.org/10.1016/s0266-3538\(00\)00070-1](https://doi.org/10.1016/s0266-3538(00)00070-1).
- [77] Liu Y, Zhou C, Cen B, Zeng Z, Lu X, Zhu X. Compression property of a novel lattice sandwich structure. *Compos Part B Eng* 2017;117:130–7. <https://doi.org/10.1016/j.compositesb.2017.02.036>.
- [78] Fu Y, Sadeghian P. Flexural and shear characteristics of bio-based sandwich beams made of hollow and foam-filled paper honeycomb cores and flax fiber composite skins. *Thin-Walled Struct* 2020;153. <https://doi.org/10.1016/j.tws.2020.106834>.
- [79] Wang XX, Chen L. Manufacture and characteristics of fibrous composite Z-pins. *Appl. Mech. Mater.*, vol. 33, 2010, p. 110–3. <https://doi.org/10.4028/www.scientific.net/AMM.33.110>.
- [80] Cartié DDR, Troulis M, Partridge IK. Delamination of Z-pinned carbon fibre reinforced laminates. *Compos Sci Technol* 2006;66:855–61. <https://doi.org/10.1016/j.compscitech.2004.12.018>.
- [81] Che Z, Wang H, Wang S, Gu Y, Li M. Delamination properties and in situ damage monitoring of z-pinned carbon fiber/epoxy composites. *Sci Eng Compos Mater* 2021;28:415–25. <https://doi.org/10.1515/secm-2021-0041>.
- [82] Liao B, Zhou J, Zheng J, Tao R, Xi L, Zhao T, et al. Effect of Z-pin inclined angle on the impact damage suppression effectiveness for cross-ply composite laminates. *Compos Part A Appl Sci Manuf* 2021;142. <https://doi.org/10.1016/j.compositesa.2020.106264>.
- [83] Knaupp M, Scharr G. Manufacturing process and performance of dry carbon fabrics reinforced with rectangular and circular z-pins. *J Compos Mater* 2014;48:2163–72. <https://doi.org/10.1177/0021998313495070>.
- [84] Chang P, Mouritz AP, Cox BN. Properties and failure mechanisms of z-pinned laminates in monotonic and cyclic tension. *Compos Part A Appl Sci Manuf* 2006;37:1501–13. <https://doi.org/10.1016/j.compositesa.2005.11.013>.
- [85] Haldar S, Caputo D, Buesking K, Bruck HA. Flexural behavior of singly curved X-Cor® sandwich composite structures: Experiment and finite element modeling. *Compos Struct* 2015;129:70–9. <https://doi.org/10.1016/j.compstruct.2015.03.043>.
- [86] Marasco AI, Cartié DDR, Partridge IK, Rezai A. Mechanical properties balance in novel Z-pinned sandwich panels: Out-of-plane properties. *Compos Part A Appl Sci Manuf* 2006;37:295–302. <https://doi.org/10.1016/j.compositesa.2005.03.029>.
- [87] Liu T, Deng ZC, Lu TJ. Analytical modeling and finite element simulation of the plastic collapse of sandwich beams with pin-reinforced foam cores. *Int J Solids Struct* 2008;45:5127–51. <https://doi.org/10.1016/j.ijsolstr.2008.05.028>.
- [88] Dang X, Shi S, Guo Y, Xiao J. A new method for analyzing X-cor sandwich's shear strength. *Adv. Mater. Res.*, vol. 510, 2012, p. 356–61. <https://doi.org/10.4028/www.scientific.net/AMR.510.356>.
- [89] Hao J, Zhang Z, Zhang L, Li M, Sun Z. Effects of Z-pin inserting parameters on X-cor sandwich mechanical property. *Hangkong Xuebao/Acta Aeronaut Astronaut Sin* 2008;29:763–8.

- [90] Virakthi A, Lee S, Haldar S, Bruck H, Rahman A. Modeling of pin-facesheet interactions in K-Cor sandwich structures under out-of-plane compressive loading. *Collect. Tech. Pap. - AIAA/ASME/ASCE/AHS/ASC Struct. Struct. Dyn. Mater. Conf.*, 2013.
- [91] Abdi B, Azwan S, Abdullah MR, Ayob A, Yahya Y, Xin L. Flatwise compression and flexural behavior of foam core and polymer pin-reinforced foam core composite sandwich panels. *Int J Mech Sci* 2014;88:138–44. <https://doi.org/10.1016/j.ijmecsci.2014.08.004>.
- [92] Jayaram RS, Nagarajan VA, Vinod Kumar KP. Compression and low velocity impact response of sandwich panels with polyester pin-reinforced foam filled honeycomb core. *J Sandw Struct Mater* 2019;21:2014–30. <https://doi.org/10.1177/1099636218792675>.
- [93] Virakthi A, Kwon S, Lee SW. A viable model for out-of-plane compressive and shear properties of Z-pin reinforced composite sandwich panels. *J Compos Mater* 2018;52:3961–72. <https://doi.org/10.1177/0021998318772159>.
- [94] Abdi B, Azwan S, Abdullah MR, Ayob A, Yahya Y. Comparison of foam core sandwich panel and through-thickness polymer pin-reinforced foam core sandwich panel subject to indentation and flatwise compression loadings. *Polym Compos* 2016;37:612–9. <https://doi.org/10.1002/pc.23218>.
- [95] Haldar S, Bruck HA. A New Methodology for Scaling the Mechanics of Pin-reinforcement in Composite Sandwich Structures under Compression using Digital Image Correlation. *Exp Mech* 2015;55:27–40. <https://doi.org/10.1007/s11340-014-9932-9>.
- [96] Nanayakkara A, Feih S, Mouritz AP. Experimental analysis of the through-thickness compression properties of z-pinned sandwich composites. *Compos Part A Appl Sci Manuf* 2011;42:1673–80. <https://doi.org/10.1016/j.compositesa.2011.07.020>.
- [97] Mouritz AP. Compression properties of z-pinned sandwich composites. *J Mater Sci* 2006;41:5771–4. <https://doi.org/10.1007/s10853-006-0114-8>.
- [98] Cartié DD, Fleck NA. The effect of pin reinforcement upon the through-thickness compressive strength of foam-cored sandwich panels. *Compos Sci Technol* 2003;63:2401–9. [https://doi.org/10.1016/S0266-3538\(03\)00273-2](https://doi.org/10.1016/S0266-3538(03)00273-2).
- [99] Goettner W, Reimerdes HG. Bending strength of sandwich panels with different cores after impact. *Fract. Nano Eng. Mater. Struct. - Proc. 16th Eur. Conf. Fract.*, 2006, p. 1261–2. https://doi.org/10.1007/1-4020-4972-2_626.
- [100] Jayaram RS, Nagarajan VA, Vinod Kumar KP. Polyester pinning effect on flexural and vibrational characteristics of foam filled honeycomb sandwich panels. *Lat Am J Solids Struct* 2017;14:1314–26. <https://doi.org/10.1590/1679-78253688>.
- [101] Selver E, Kaya G. Flexural properties of sandwich composite laminates reinforced with glass and carbon Z-pins. *J Compos Mater* 2019;53:1347–59. <https://doi.org/10.1177/0021998318800146>.
- [102] Du L, Guiqiong J, Tao H. Z-pin reinforcement on the core shear properties of polymer foam sandwich composites. *J Compos Mater* 2009;43:289–300. <https://doi.org/10.1177/0021998308099223>.
- [103] Du L, Jiao G. Indentation study of Z-pin reinforced polymer foam core sandwich structures. *Compos Part A Appl Sci Manuf* 2009;40:822–9. <https://doi.org/10.1016/j.compositesa.2009.04.004>.
- [104] Vaidya UK, Nelson S, Sinn B, Mathew B. Processing and high strain rate impact response of multi-functional sandwich composites. *Compos Struct* 2001;52:429–40. [https://doi.org/10.1016/S0263-8223\(01\)00033-2](https://doi.org/10.1016/S0263-8223(01)00033-2).
- [105] Mouritz AP. Review of z-pinned laminates and sandwich composites. *Compos Part A Appl Sci Manuf* 2020;139. <https://doi.org/10.1016/j.compositesa.2020.106128>.

- [106] Mouritz AP, Cox BN. Mechanistic approach to the properties of stitched laminates. *Compos Part A Appl Sci Manuf* 2000;31:1–27. [https://doi.org/10.1016/S1359-835X\(99\)00056-1](https://doi.org/10.1016/S1359-835X(99)00056-1).
- [107] Tan KT, Watanabe N, Iwahori Y. Stitch fiber comparison for improvement of interlaminar fracture toughness in stitched composites. *J Reinf Plast Compos* 2011;30:99–109. <https://doi.org/10.1177/0731684410383065>.
- [108] Aymerich F, Priolo P, Sun CT. Static and fatigue behaviour of stitched graphite/epoxy composite laminates. *Compos Sci Technol* 2003;63:907–17. [https://doi.org/10.1016/S0266-3538\(02\)00314-7](https://doi.org/10.1016/S0266-3538(02)00314-7).
- [109] Gnaba I, Legrand X, Wang P, Soulat D. Literature review of tufted reinforcement for composite structures. *IOP Conf Ser Mater Sci Eng* 2017;254. <https://doi.org/10.1088/1757-899X/254/4/042011>.
- [110] Drake DA, Sullivan RW, Lovejoy AE, Clay SB, Jegley DC. Influence of stitching on the out-of-plane behavior of composite materials – A mechanistic review. *J Compos Mater* 2021. <https://doi.org/10.1177/00219983211009290>.
- [111] Yudhanto A, Watanabe N, Iwahori Y, Hoshi H. Compression properties and damage mechanisms of stitched carbon/epoxy composites. *Compos Sci Technol* 2013;86:52–60. <https://doi.org/10.1016/j.compscitech.2013.07.002>.
- [112] Drake DA, Sullivan RW, Clay S. On the use of a trilinear traction-separation law to represent stitch failure in stitched sandwich composites. *J Sandw Struct Mater* 2021. <https://doi.org/10.1177/10996362211042929>.
- [113] Kim JH, Lee YS, Park BJ, Kim DH. Evaluation of durability and strength of stitched foam-cored sandwich structures. *Compos. Struct.*, vol. 47, 1999, p. 543–50. [https://doi.org/10.1016/S0263-8223\(00\)00019-2](https://doi.org/10.1016/S0263-8223(00)00019-2).
- [114] Chen A, Davalos JF. Development of facesheet for honeycomb FRP sandwich panels. *J Compos Mater* 2012;46:3277–95. <https://doi.org/10.1177/0021998312437432>.
- [115] Yalkin HE, Icten BM, Alpyildiz T. Enhanced mechanical performance of foam core sandwich composites with through the thickness reinforced core. *Compos Part B Eng* 2015;79:383–91. <https://doi.org/10.1016/j.compositesb.2015.04.055>.
- [116] Raju KS, Tomblin JS. Energy absorption characteristics of stitched composite sandwich panels. *J Compos Mater* 1999;33:712–28. <https://doi.org/10.1177/002199839903300804>.
- [117] Lascoup B, Aboura Z, Khellil K, Benzeggagh M. On the mechanical effect of stitch addition in sandwich panel. *Compos Sci Technol* 2006;66:1385–98. <https://doi.org/10.1016/j.compscitech.2005.09.005>.
- [118] Potluri P, Kusak E, Cumellas AJ. Structural performance of orthogonal and bias stitched sandwich structures with rigid close-cellular foams. *Collect Tech Pap - AIAA/ASME/ASCE/AHS/ASC Struct Struct Dyn Mater Conf* 2003;7:4991–7. <https://doi.org/10.2514/6.2003-1949>.
- [119] Lascoup B, Aboura Z, Khellil K, Benzeggagh M. Homogenization of the core layer in stitched sandwich structures. *Compos Sci Technol* 2010;70:350–5. <https://doi.org/10.1016/j.compscitech.2009.11.006>.
- [120] Lascoup B, Aboura Z, Khellil K, Benzeggagh M. Prediction of out-of-plane behavior of stitched sandwich structure. *Compos Part B Eng* 2012;43:2915–20. <https://doi.org/10.1016/j.compositesb.2012.07.002>.
- [121] Wang P, Lei Y, Yue Z. Experimental and numerical evaluation of the flexural properties of stitched foam core sandwich structure. *Compos Struct* 2013;100:243–8. <https://doi.org/10.1016/j.compstruct.2012.12.040>.

- [122] Wu Z, Xiao J, Zeng J, Liu J. Compression performance of integrated 3D composite sandwich structures. *J Sandw Struct Mater* 2014;16:5–21. <https://doi.org/10.1177/1099636213501927>.
- [123] Sharma SC, Krishna M, Narasimha Murthy HN. Buckling response of stitched polyurethane foam composite sandwich structures. *J Reinf Plast Compos* 2004;23:1267–77. <https://doi.org/10.1177/0731684404037042>.
- [124] Xia F, Wu X qing. Study on impact properties of through-thickness stitched foam sandwich composites. *Compos Struct* 2010;92:412–21. <https://doi.org/10.1016/j.compstruct.2009.08.016>.
- [125] Santhanakrishnan R, Samlal S, Joseph Stanley A, Jayalatha J. Impact study on sandwich panels with and without stitching. *Adv Compos Mater* 2018;27:163–82. <https://doi.org/10.1080/09243046.2017.1410376>.
- [126] Vaidya AS, Vaidya UK, Uddin N. Impact response of three-dimensional multifunctional sandwich composite. *Mater Sci Eng A* 2008;472:52–8. <https://doi.org/10.1016/j.msea.2007.03.064>.
- [127] Han F, Yan Y, Ma J. Experimental study and progressive failure analysis of stitched foam-core sandwich composites subjected to low-velocity impact. *Polym Compos* 2018;39:624–35. <https://doi.org/10.1002/pc.23976>.
- [128] Potluri P, Kusak E, Reddy TY. Novel stitch-bonded sandwich composite structures. *Compos Struct* 2003;59:251–9. [https://doi.org/10.1016/S0263-8223\(02\)00087-9](https://doi.org/10.1016/S0263-8223(02)00087-9).
- [129] Sun X, Liu HY, Yan W, Tong L, Mai YW. Modelling composite reinforcement by stitching and z-pinning. *Multi-Scale Model Compos Mater Syst Art Predict Damage Model* 2005:319–55. <https://doi.org/10.1533/9781845690847.319>.
- [130] Dell’Anno G, Treiber JWG, Partridge IK. Manufacturing of composite parts reinforced through-thickness by tufting. *Robot Comput Integr Manuf* 2016;37:262–72. <https://doi.org/10.1016/j.rcim.2015.04.004>.
- [131] Dell’Anno G, Cartié DD, Partridge IK, Rezai A. Exploring mechanical property balance in tufted carbon fabric/epoxy composites. *Compos Part A Appl Sci Manuf* 2007;38:2366–73. <https://doi.org/10.1016/j.compositesa.2007.06.004>.
- [132] Scott M, Dell’Anno G, Clegg H. Effect of Process Parameters on the Geometry of Composite Parts Reinforced by Through-the-Thickness Tufting. *Appl Compos Mater* 2018;25:785–96. <https://doi.org/10.1007/s10443-018-9710-4>.
- [133] Clegg HM, Dell’Anno G, Partridge IK. Creating damage tolerant intersections in composite structures using tufting and 3D woven connectors. *Adv Aircr Spacecr Sci* 2019;6:145–56. <https://doi.org/10.12989/aas.2019.6.2.145>.
- [134] Green SD, Dell’Anno G. Impact resistance of carbon/epoxy L-sections reinforced through-the-thickness by tufting. *ICCM Int. Conf. Compos. Mater.*, vol. 2017–August, 2017.
- [135] Clegg HM, Centre NC, Centre NC, Scott M, Centre NC, Partridge IK. Twenty-Second International Conference on Composite Materials (Iccm22) Suppressing Delamination in Composite Intersections With Tufting and Z-Pinning Suppressing Delamination in Composite Intersections With Tufting and Z-Pinning 2019.
- [136] Pappas G, Joncas S, Michaud V, Botsis J. The influence of through-thickness reinforcement geometry and pattern on delamination of fiber-reinforced composites: Part I – Experimental results. *Compos Struct* 2018;184:924–34. <https://doi.org/10.1016/j.compstruct.2017.09.091>.

- [137] Pappas G, Joncas S, Michaud V, Botsis J. The influence of through-thickness reinforcement geometry and pattern on delamination of fiber-reinforced composites: Part II – Modeling. *Compos Struct* 2017;181:379–90. <https://doi.org/10.1016/j.compstruct.2017.08.096>.
- [138] Verdier MC De, Pickett AK, Skordos AA, Witzel V. Effect of Tufting on the Response of Non-Crimp Fabric 2007:12–4.
- [139] Colin de Verdier M, Pickett AK, Skordos AA, Witzel V. Evaluation of the mechanical and damage behaviour of tufted non crimped fabric composites using full field measurements. *Compos Sci Technol* 2009;69:131–8. <https://doi.org/10.1016/j.compscitech.2008.08.025>.
- [140] Masa SK, Mallya AB, Dhanapal K, Ramachandra RV, Kishore. Post-failure Analysis and Fractography of In-plane Tension-Tested Tufted Carbon Fabric-Reinforced Epoxy Composite Laminates. *J Mater Eng Perform* 2015;24:1581–6. <https://doi.org/10.1007/s11665-015-1411-7>.
- [141] Rashid M, Hanus JL, Chetehouna K, Khellil K, Aboura Z, Gascoin N. Investigation of the effect of tufts contribution on the in-plane mechanical properties of flax fibre reinforced green biocomposite. *Funct Compos Mater* 2021;2. <https://doi.org/10.1186/s42252-021-00019-z>.
- [142] Clegg HM, Kratz J, Partridge I, Dell’Anno G. Evaluation of the effects of tufting on performance of composite T-joints. *ECCM 2016 - Proceeding 17th Eur. Conf. Compos. Mater.*, 2016.
- [143] Verma KK, Viswarupachari CH, Gaddikeri KM, Ramesh S, Kumar S, Bose S. Unfolding the effects of tuft density on compression after impact properties in unidirectional carbon/epoxy composite laminates. *Compos Struct* 2021;258. <https://doi.org/10.1016/j.compstruct.2020.113378>.
- [144] Martins AT, Aboura Z, Harizi W, Laksimi A, Khellil K. Analysis of the impact and compression after impact behavior of tufted laminated composites. *Compos Struct* 2018;184:352–61. <https://doi.org/10.1016/j.compstruct.2017.09.096>.
- [145] Hui C, Wang P, Legrand X. Improvement of tufting mechanism during the advanced 3-dimensional tufted composites manufacturing: To the optimisation of tufting threads degradation. *Compos Struct* 2019;220:423–30. <https://doi.org/10.1016/j.compstruct.2019.04.019>.
- [146] Liu LS, Wang P, Legrand X, Soulat D. Investigation of mechanical properties of tufted composites: Influence of tuft length through the thickness reinforcement. *Compos Struct* 2017;172:221–8. <https://doi.org/10.1016/j.compstruct.2017.03.099>.
- [147] Gnaba I, Soulat D, Legrand X, Wang P. Investigation of the formability behaviour during stamping of tufted and un-tufted carbon preforms: towards localized reinforcement technologies. *Int J Mater Form* 2021. <https://doi.org/10.1007/s12289-020-01606-4>.
- [148] Hao S, Wang P, Legrand X, Liu L, Soulat D. Influence of the tufting pattern on the formability of tufted multi-layered preforms. *Compos Struct* 2019;228. <https://doi.org/10.1016/j.compstruct.2019.111356>.
- [149] Shen H, Wang P, Legrand X, Liu L. Characterisation and optimisation of wrinkling during the forming of tufted three-dimensional composite preforms. *Compos Part A Appl Sci Manuf* 2019;127. <https://doi.org/10.1016/j.compositesa.2019.105651>.
- [150] Henao A, Carrera M, Miravete A, Castejón L. Mechanical performance of through-thickness tufted sandwich structures. *Compos Struct* 2010;92:2052–9. <https://doi.org/10.1016/j.compstruct.2009.11.005>.
- [151] Hartley JW, Kratz J, Ward C, Partridge IK. Effect of tufting density and loop length on the crushing behaviour of tufted sandwich specimens. *Compos Part B Eng* 2017;112:49–56. <https://doi.org/10.1016/j.compositesb.2016.12.037>.
- [152] Icardi U, Sola F. Recovering critical stresses in sandwiches using through-the-thickness reinforcement. *Compos Part B Eng* 2013;54:269–77. <https://doi.org/10.1016/j.compositesb.2013.05.027>.

- [153] Blok LG, Kratz J, Lukaszewicz D, Hesse S, Ward C, Kassapoglou C. Improvement of the in-plane crushing response of CFRP sandwich panels by through-thickness reinforcements. *Compos Struct* 2017;161:15–22. <https://doi.org/10.1016/j.compstruct.2016.11.034>.
- [154] Hartley JW, Dyson M, Ward C. Improving the performance of tufted composite sandwich structures. *ICCM Int. Conf. Compos. Mater.*, vol. 2017–August, 2017.
- [155] Hartley J, Ward C. Improving the understanding of tufted energy absorbing sandwich structures. 32nd Tech Conf Am Soc Compos 2017 2017;3:2260–73. <https://doi.org/10.12783/asc2017/15347>.
- [156] Celle P, Etienne DS-, Etienne MDS-, Batoz J, Vautrin A, Bergheau J, et al. Couplages fluide / milieu poreux en grandes déformations pour la modélisation des procédés d'élaboration par infusion 2012.
- [157] Trofimov A, Le-Pavic J, Ravey C, Albouy W, Therriault D, Lévesque M. Multi-scale modeling of distortion in the non-flat 3D woven composite part manufactured using resin transfer molding. *Compos Part A Appl Sci Manuf* 2021;140. <https://doi.org/10.1016/j.compositesa.2020.106145>.
- [158] Nawaz A, Islam B, Khattak MS, Ali L, Saleem U, Ullah A, et al. Polyester Usage in Manufacturing of Electrical and Mechanical Products and Assemblies. *Polyest. - Prod. Charact. Innov. Appl.*, 2018. <https://doi.org/10.5772/intechopen.74368>.
- [159] Song X. Vacuum Assisted Resin Transfer Molding (VARTM): Model Development and Verification. Dr Thesis 2003:161.
- [160] Manufacturing of fibre–polymer composite materials. *Introd. to Aerosp. Mater.*, 2012, p. 303–37. <https://doi.org/10.1533/9780857095152.303>.
- [161] Antonucci V, Giordano M, Nicolais L, Calabrò A, Cusano A, Cutolo A, et al. Resin flow monitoring in resin film infusion process. *J. Mater. Process. Technol.*, vol. 143–144, 2003, p. 687–92. [https://doi.org/10.1016/S0924-0136\(03\)00338-8](https://doi.org/10.1016/S0924-0136(03)00338-8).
- [162] Han NL, Suh SS, Yang JM, Hahn HT. Resin film infusion of stitched stiffened composite panels. *Compos Part A Appl Sci Manuf* 2003;34:227–36. [https://doi.org/10.1016/S1359-835X\(03\)00002-2](https://doi.org/10.1016/S1359-835X(03)00002-2).
- [163] Bouchak M, Harasani W. Assessment of liquid resin infusion impregnation quality using scanning electron microscopy. *Adv Compos Lett* 2015;24:6–11. <https://doi.org/10.1177/096369351502400102>.
- [164] Kadiyala AK, Portela A, Devlin K, Lee S, O'Carroll A, Jones D, et al. Mechanical evaluation and failure analysis of composite laminates manufactured using automated dry fibre tape placement followed by liquid resin infusion. *Compos Sci Technol* 2021;201. <https://doi.org/10.1016/j.compscitech.2020.108512>.
- [165] Allagui S, Mahi A El, Rebiere JL, Beyaoui M, Bouguecha A, Haddar M. Effect of recycling cycles on the mechanical and damping properties of flax fibre reinforced elium composite: Experimental and numerical studies. *J Renew Mater* 2021;9:695–721. <https://doi.org/10.32604/jrm.2021.013586>.
- [166] Cicala G, Pergolizzi E, Piscopo F, Carbone D, Recca G. Hybrid composites manufactured by resin infusion with a fully recyclable bioepoxy resin. *Compos Part B Eng* 2018;132:69–76. <https://doi.org/10.1016/j.compositesb.2017.08.015>.

**CHAPTER 2. MANUFACTURING
PROCESS OF A TUFTED
SANDWICH COMPOSITE WITH
NONWOVEN CORE**

2.1 Introduction

The conventional sandwich structure has only fiber reinforcement in X/Y directions, which leads to the delamination between the layers. In recent years, the tufting process has been increasingly adopted to insert the reinforcement in the Z-axial direction because of its high efficiency and low cost [1–3]. During the tufting process, a layered preform was placed on support foam which can guarantee the needle to puncture thoroughly the thickness. Then the thread forms loops and is left by the friction between fiber and foam when the needle retracts. Some different tufting equipment were invented and designed to realize the process [4][5]. The tufting machine in this work (as shown in Figure 2.1) consists of 4 function modules: the tufting system, the feeding system, the presser foot and the frame. The tufting system includes a needle connected to a pneumatic cylinder which allows the penetration of the preform at a given height and angle. The feeding device supplies the tufting thread stably with a certain length and pre-tension. The presser foot is also linked with a pneumatic jack to fix the preform when the needle penetrates. Thus the layers can be tightened and provide friction to remain the tufting thread. The pressure of the tufting needle and presser foot can be modified according to the different types of the preform and tufting yarn. The optimum needle inserting and retreating speed for our experiments is 60 mm/s and the maximum needle stroke is 50 mm. Other initial setup and more details of this automated tufting machine such as the codes of the application have been presented in previous publications [1]. Except the constant parameters, the relevant variable parameters are introduced in the following contents.

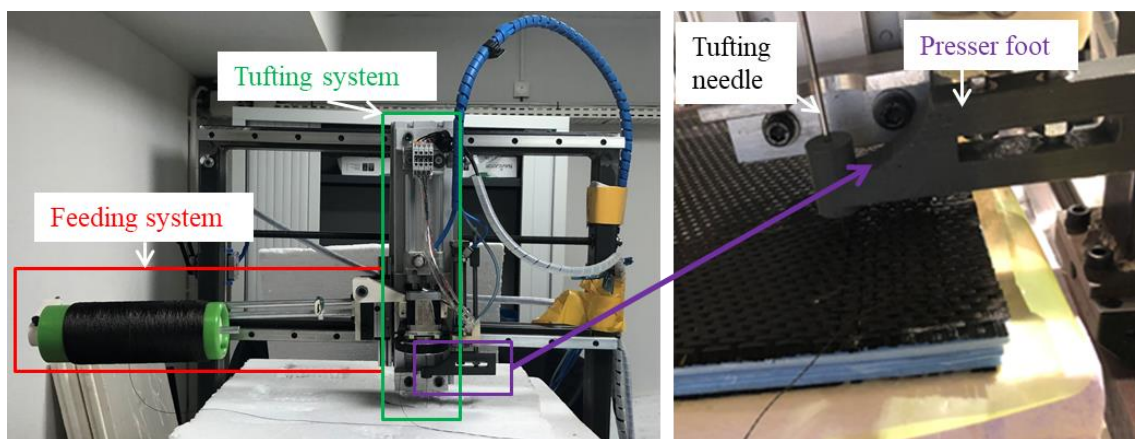


Figure 2.1 Tufting machine and its function modules.

After the tufting process, the dry sandwich preform was impregnated with resin to manufacture the final composite panel. The tufted sandwich composite part was lightweight and had the through-the-thickness reinforcement to prevent delamination. However, some foam is not environmentally friendly and have poor mechanical properties, which may cause pollution and limit their applications. This section details development and improvements in the tufting process, which were made in the course of this work, along with identified critical parameters for high-quality tufting. A summary of required auxiliary materials and equipment for the tufting process is given.

2.2 Design of the tufted sandwich structure with nonwoven core

The novelty of tufted sandwich composite specimens in this work is the use of nonwoven fabric to replace part or all of the foam (as shown in Figure 2.2). The objective is to improve the low mechanical properties of pure foam. Moreover, the nonwoven mat can provide a larger thickness than normal woven tissue because of its low density. The non-woven layer is impregnated with resin and finally formed a fiber-reinforced composite layer, which is located in the middle of the sandwich structure. This composite layer can increase the structural stiffness and prevent the crack from expanding along the thickness direction when cracks occur in the foam, avoiding structural failure due to core fracture through the entire thickness. This expected effect will be discussed in Chapters 3 and 4. Two series of the sandwich composite were designed and manufactured: the carbon fiber reinforced sandwich composite and the flax fiber-reinforced sandwich composite. The latter is eco-friendly and less expensive. Tufting threads are made of the same fibers as the fabric reinforcement.

The structure in Figure 2.2 consists of three principal parts: the carbon fabric skin, the carbon non-woven core and the carbon fiber tufting yarns in Z-axial direction. The resin was also enriched around the tufting threads to form thread/resin composite columns. This carbon-reinforced sandwich composite preliminarily determines the feasibility of replacing the foam core with nonwoven fabric.

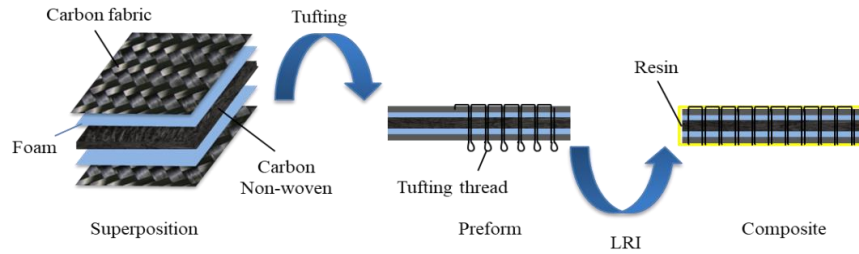


Figure 2.2 Carbon fiber tufted sandwich composite with a non-woven core.

2.3 Parameters of tufting process

Tufting process can effectively enhance the shear and delamination resistance. The profit is related to the status and properties of the tufting thread which can be controlled by various parameters, such as the areal tufting density, the tufting loop length, the diameter of the tufting thread and the needle size. These parameters directly affect the structure, thickness and porosity of dry preform which affect the following infusion process. Accordingly, when the conditions permit, in addition to the influence of various parameters on the mechanical properties of composites, the interaction between the process parameters should also be considered.

2.3.1 Selection of tufting thread and preform layups

2.3.1.1 Tufting thread

The influence of tufting thread on the mechanical performance of sandwich panels is investigated in the following chapter by comparing the sandwich tufted with and without thread.

The improved mechanical performance of a tufted sandwich depends in large part on the properties of the tufting thread itself. Moreover, the tufting thread has to be selected to meet the requirements of the tufting process (e.g. with high tensile strength, suitable diameter, etc.). Commonly tufted yarns include carbon fiber, glass fiber and other high strength and high modulus chemical fiber yarns, but as environmental requirements become more stringent, some natural fibers with good tensile properties (e.g. flax fiber) are also considered as suitable alternatives (see Figure 2.3).

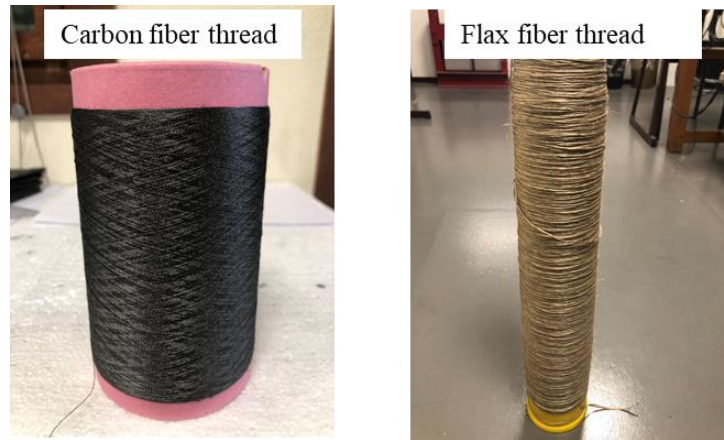


Figure 2.3 Different tufting threads used in this work.

The brittle nature of the carbon fiber makes the carbon thread susceptible to local splitting under severe bending especially if used in closely packed layups (see Figure 2.4). This damage leads to complete failure of the tufting thread and has detrimental effects on the mechanical performance of the tufting thread. After several testing, the carbon fiber yarn with linear density 2×67 Tex performs the highest in the tufting process, it is protected and presents almost no complete breakage due to its special reverse twist and a slight PU coating. The yarn without the coating often breaks during the process because of the large friction. Therefore, this yarn is adopted as the tufting yarn in the preparation of carbon fiber reinforced sandwich composite. In the selection of the thread, a compromise must be found between suitability for the tufting process and mechanical properties. For the same reason, the selection of flax tufting thread is shown in Table 2.1. However, though the tufting process is guaranteed to run smoothly, it is still challenging to avoid the loss of mechanical properties of the yarn with the existing machines [6].

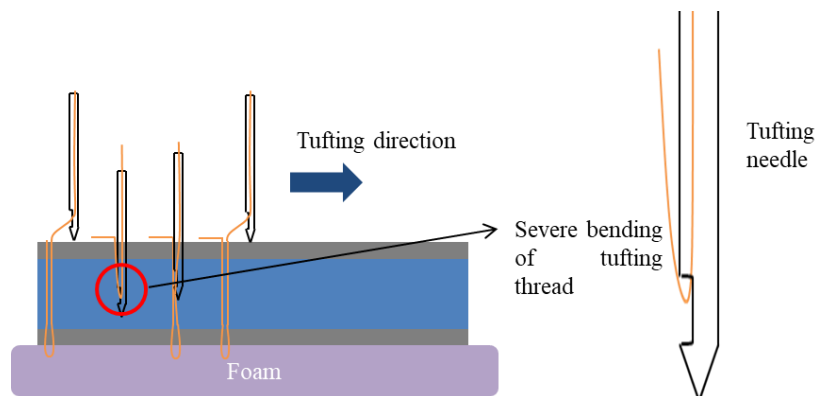


Figure 2.4 Sever bending thread during tufting process.

Table 2.1 Properties of tufting threads.

Tufting thread	Linear density (Tex)	Tensile strength (MPa)	Tensile modulus (GPa)
Carbon fiber	2×67	1585.07	41.23
Flax fiber	500	204.33	4.23

2.3.1.2 Sandwich preform layups

Both carbon twill fabrics (warp and weft yarn count $3.5 \times 3.5/\text{cm}^2$, 400 Tex) and plain flax plain fabrics (warp and weft yarn count $20 \times 20/\text{cm}^2$, Ne:17S) appear to be perfectly suitable for tufting of preforms between 3 and 10 mm thickness with little resistance to the needle penetration. Their pick counts and yarn density can provide enough voids between the yarns of both two fabrics to ensure the smooth puncture of needle and also to avoid the rupture of tufting thread caused by large friction. This is related to the porosity of the fabric. The greater the warp and weft density, the thicker the yarn, the tighter its structure and the higher its mechanical properties, but it is not conducive to tufting needle for puncture. The damage of texture brought by needle penetration is less and thus the loss of mechanical properties is smaller. On the contrary, the textile with smaller warp and weft densities and thinner yarn can remain the basic shape and structure during the process which maximizes the retention of the mechanical properties. Considering this contradiction, the tufting process should be ensured as a priority and therefore the woven fabrics in Table 2.2 are chosen. In the beginning, the nonwoven is designed to replace the foam and therefore it should have a low density. However, after the experiments in Chapter 3, it is found that a smaller density implies that the looser its structure and the higher the porosity, the more the preforms are compressed in the thickness direction during both tufting and LRI processes, resulting in its inability to provide sufficient thickness. Consequently, nonwoven fabric with a higher density is selected for the preparation of the flax fiber-reinforced sandwich structure (as shown in Table 2.2).

Table 2.2 Basic parameters of textile layups.

Layup (dry textiles)	Fiber	Area density (g/m^2)	Young's modulus (MPa)
Weaving fabric (Twill 2×2)	Carbon	285	25.7×10^3
Nonwoven		210	20.5×10^3
Weaving fabric (Plain)	Flax	189	98.42
Nonwoven		354	23.45
Foam (in Chapter 3)	Polystyrene	138	16.00

In the next chapter, a hollow sandwich structure with only tufting thread/resin columns in the core is fabricated. The preform core layups of this structure are foam layers that are dissolved by acetone after LRI (see Figure 2.5).

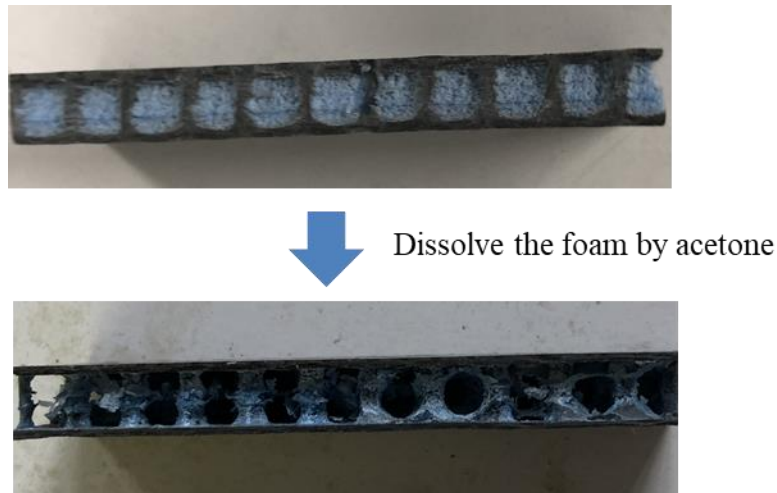


Figure 2.5 Removal of foam for hollow sandwich structure manufacture.

To avoid errors caused by external conditions (e.g. storage temperature, type of testing machine, etc.), the mechanical properties of all the above materials were measured at room temperature by our laboratory's MTS machine.

2.3.2 Tufting density

Tufting density is defined as the total number of tufting points per unit area of the preform. It depends on the tufting pattern and the space between tufting points. The former has been studied by several researchers and it shows that the tufting pattern has an impact on the formability [7] and the permeability values [8] of the tufted preform. Since the specimens used for testing in this study are all rectangular specimens, the tufting pattern is selected as a multi-row linear arrangement (as shown in Figure 2.6a). The tufting pattern can be drawn in advance by Solidworks and then converted to Python code and input the control program of the tufting machine. The program determines the position of tufting points according to Cartesian coordinates, thus the preform is fixed in a specific position: its length and width are oriented parallel to the x and y axes.

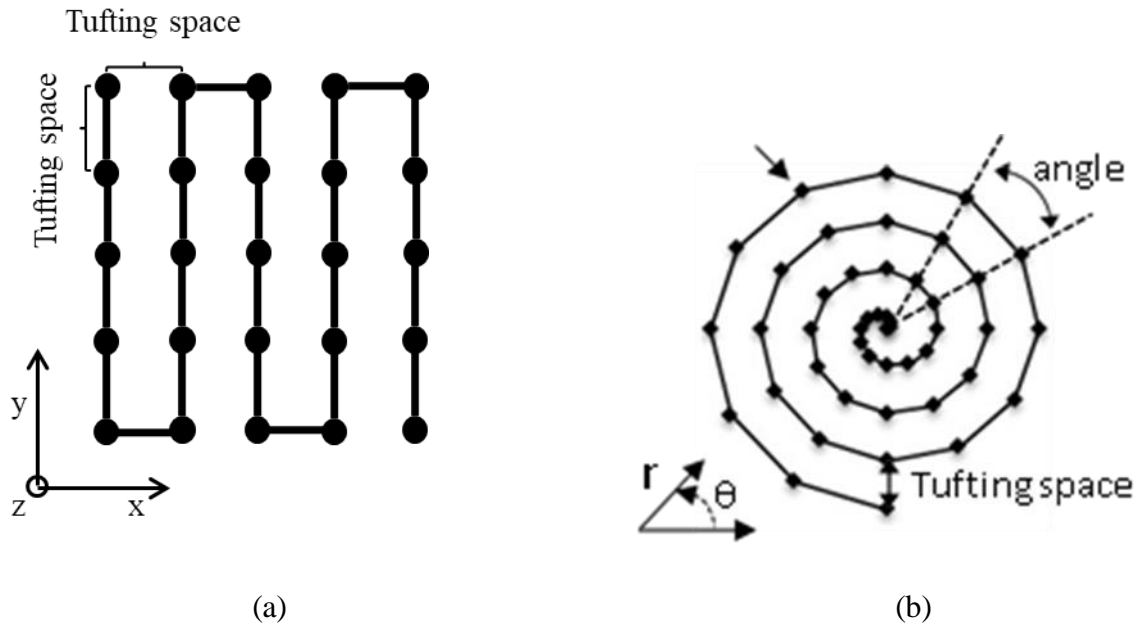
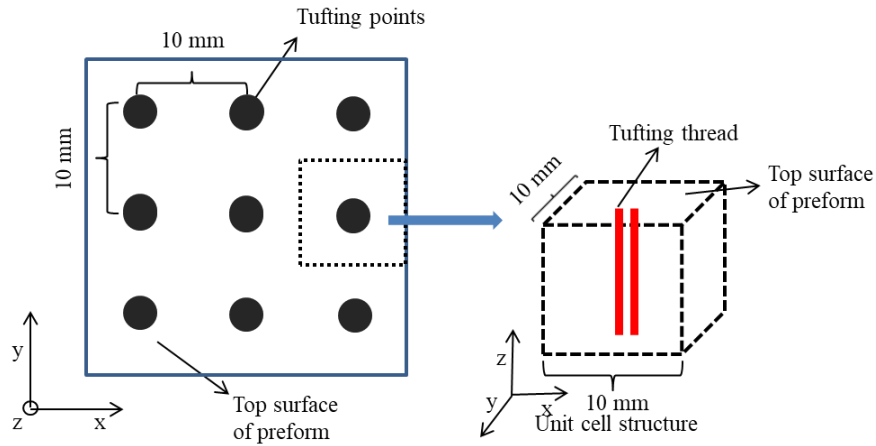
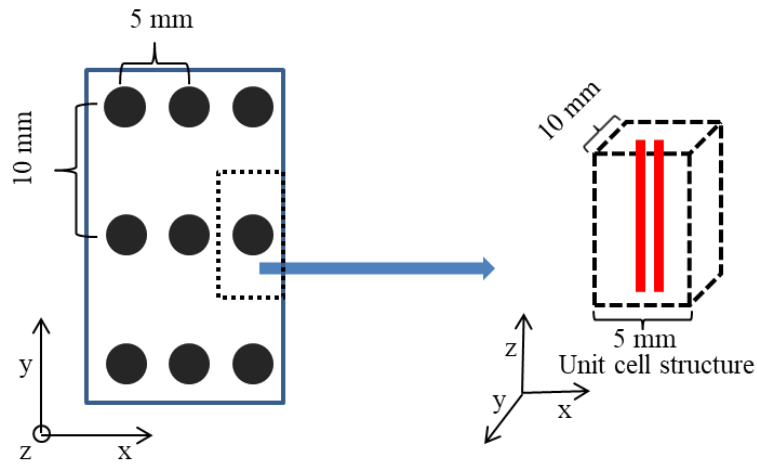


Figure 2.6 Schematics of the (a) multi-row pattern and (b) circle spiral pattern [9].

In general, the spacing of any two adjacent tufting points in both length and width direction is set to be constant to ensure that the tufting thread is uniformly distributed in the preform, its unit cell is basic (see Figure 2.7a). However, occasionally the spacing is not the same due to preform dimension or other requirements; its unit-cell structure needs to contain at least one repeatable structure (see Figure 2.7b). Some works showed that a high tufting density can effectively improve the mechanical properties of a tufted sample [10–14]. Whereas, on the other hand, the tufting thread damages the original texture of the fabric reinforcement layer. The higher the tufting density, the more holes punctured on the layers by the tufting needle and the greater the resulting loss of mechanical properties of the fabric layers. Tufting thread has both advantages and disadvantages. Besides, the increase in tufting thread leads to an increase in the mass of the sample because the resin fills the holes left after the preform is tufted. Consequently, a compromise between the mechanical properties of layers and the weight of the sample must be found. The tufting density is also limited by the tufting needle diameter. The minimum tufting spacing for a needle diameter of 2 mm is tested to be 3 mm. Despite all measures introduced to increase the accuracy of tuft insertion, it was found that the rotation of the tufting needle caused an offset of tufts, especially for small tuft spacing. Therefore, it is better not to set the tufting density as the minimum value. All the tufting spacing chosen in this work is greater than 3 mm. The effect of tufting density is discussed in chapter 4.



(a)



(b)

Figure 2.7 Structures of preforms with (a) constant spacing between tufting points and (b) different tufting spacing.

2.3.3 Tufting needle size

An important element of successful tuft insertion is the tufting needle. Commonly used tufting needles are divided into two categories, one is a full needle with a small hole near the tip for the tufting thread to pass through, and the other is a hollow needle with the tufting thread passing through the hollow cavity (see Figure 2.8). The latter is suitable for some brittle tufting threads with small diameters such as carbon fiber yarn to avoid breaking. As the needle isolates the tufting threads and layups during the penetration, the contact between them is reduced, thus

diminishing excessive friction. Hence, the hollow needle was selected for the flax fiber thread. This minimizes the degradation and mechanical damage of the tufting thread.

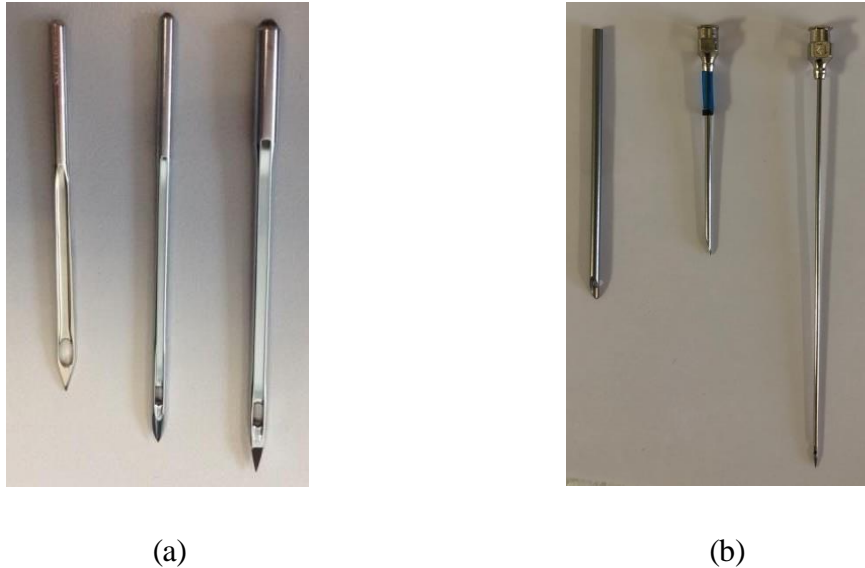


Figure 2.8 (a) Solid tufting needle and (b) hollow tufting needle.

The needle diameter limits the maximum linear density of the tufting thread. In general, the diameter of the thread should be smaller than the inner diameter of the hollow needle. In addition to this, the matching of tufting needles and tufting threads is also related to the roughness of the thread. Other parameters being equal, a rougher thread requires a larger inner-diameter hollow needle to avoid much abrasion.

The selection of the tufting needle size is also related to the thickness of the sandwich preform, texture and material of the textile layups. The preforms are too thick, the structure is too dense, and the porosity is low, all of which can cause the tufting needles with a small diameter to bend or be broken.

Some holes are formed through the thickness of the preform by needle puncture, and these holes will be filled with liquid resin during the resin infusion process, eventually forming solid resin columns (see Figure 2.9) with a similar shape to the holes. Resin columns of different shapes and sizes exhibit different mechanical properties under the same load. This is related to the size of the tufting needles, as well as the properties of reinforcement materials in the dry preforms. A tufting needle with a large diameter will cause greater damage to the layup structure because of forming the holes, and also make the tufting thread lean or bend in the holes. The

needle diameter too small will lead to greater friction between thread and needle, increasing the degradation and breaking risk of thread, which is not conducive to tufting stability (e.g. the needle with an inner diameter less than 1 mm is too small for 500 Tex flax yarn). Hence, it is essential to select the suitable tufting needle according to the fineness and material of the tufting thread. Taking all the above factors into consideration, the diameter of the selected needle is 2 mm for the tufting process of this study.

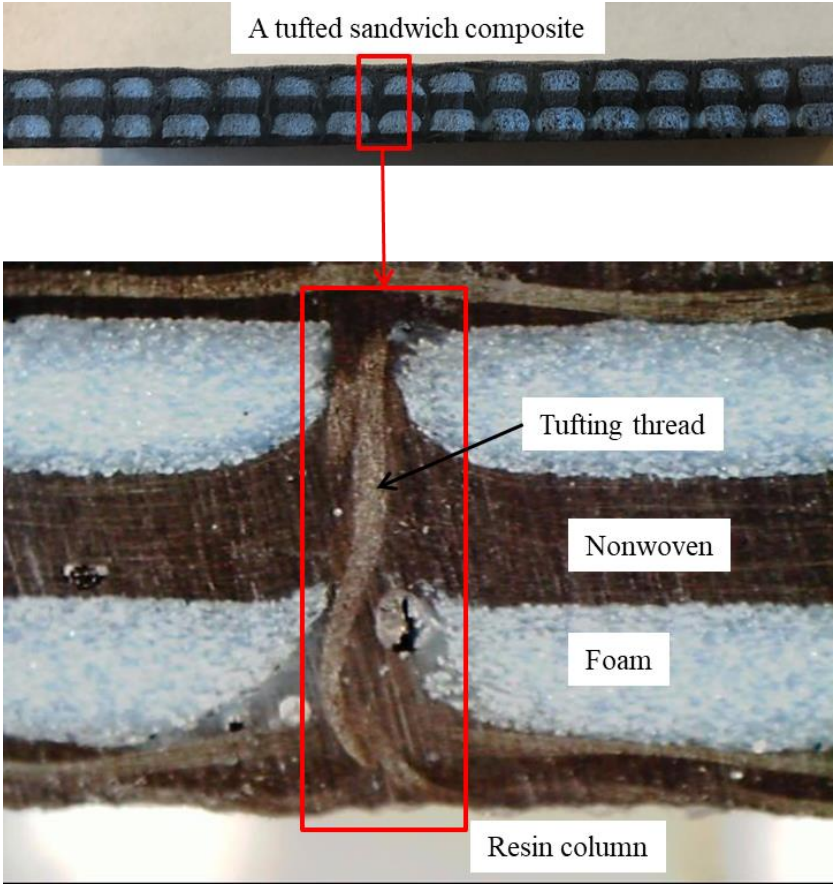


Figure 2.9 Resin column formed during LRI.

2.3.4 Preform fixation and support foam

Due to the lack of locking in the thickness direction, slippage may occur between the layers during the tufting process. Therefore, before starting tufting, 1 or 2 tufting circles (depending on the size of preform) are made around all four sides of the preform so that each layer can be locked in that location (as shown in Figure 2.10).

The presser foot compresses during needle penetration and extraction, increasing the pressure of the foot base onto the preform. This allows two functions: on one hand, the presser foot compresses the preform close to its net-shape thickness (the thickness after vacuuming during LRI). This is essential because the low compaction of the sandwich preform during the tufting process can result in winding tufting thread when compressed during LRI (as shown in Figure 2.9). On the other hand, the presser foot prevents the unexpected extraction of previous tuft loops during insertion of the next tufting loop by fixing the thread on the top surface of the preform.

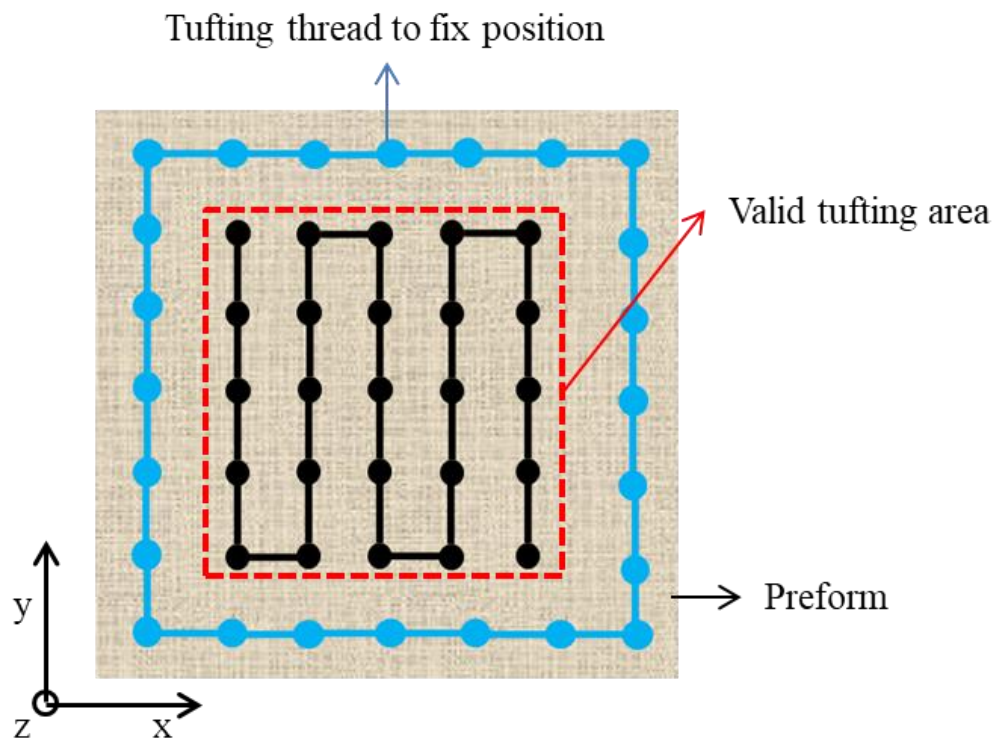


Figure 2.10 Schematic of the tufting thread for position fixing.

After several tufting rows, the fabric compaction by presser foot and then a lock of thickness by tufting thread were found to cause uneven thicknesses of the preform, especially nonwoven has a significant bulkiness which results in a large space for compression (see Figure 2.11). Hence, the surface between the tufted area and non-tufted area is no longer flat and this pronounced slope causes the final tufted thread to be unevenly aligned on the surface. In other words, the tufting space is partially changed. To inhibit the change of thickness, a heavy metal block is placed on the surface of the non-tufted area to play the role of the presser.

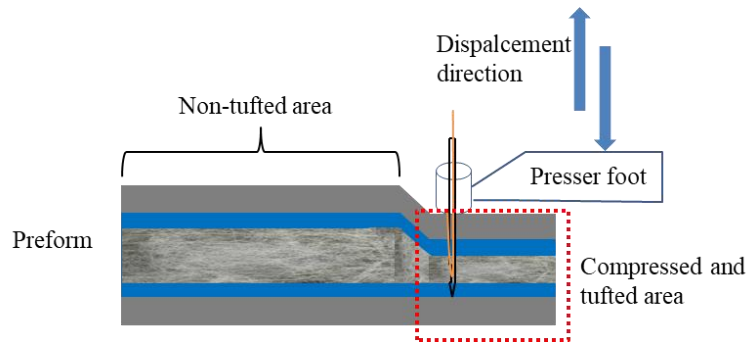


Figure 2.11 Compaction of preform during tufting process.

The foam support under the sandwich preform has to withstand the applied pressure of the presser foot and penetrating needle, and has to allow the needle to pass beyond the bottom surface of the preform. In literature, several support materials have been considered such as metal support [15] and stiff wooden support [16] with local grooves along the tuft path, support consisting of closely spaced standing plastic tubes (similar to a brush) [17] and closed-cell foam or rubber layers [18][19].

In this work, polymer foam is adopted as the support material due to its low cost and the fact that it can enhance significantly the uniformity of the inserted tuft loops [16]. Repeated use of several tufting cycles reduces the amount of necessary auxiliary materials for the tufting process (as seen in Figure 2.12). The foam needs to be selected according to the pressure force, needle type and the tufting thread, which are all designed to allow the tufting needle to pass totally through the preform and leave tufting loops in the foam. Therefore, comprehensive consideration of foam stiffness, low resistance to the penetrating needle and enhancement of the frictional contact to the tufting thread is required.

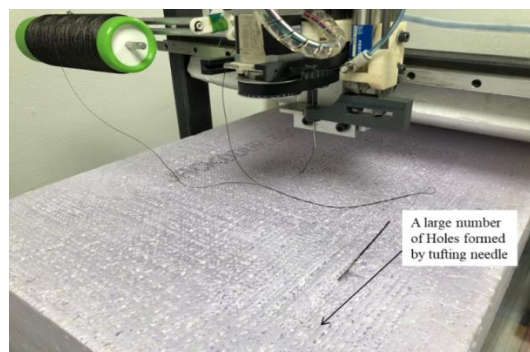


Figure 2.12 Reused foam support.

When the tufting needle penetrates, the yarn in the bottom skin fabric is drawn out (see Figure 2.13a). This damage weakened the mechanical properties of the weaving skin. Hence a plastic film was needed between the preform and support foam to prevent the fabric texture from being damaged. The sandwich preforms need to be removed manually after the tufting operation. Since the process has no conventional interlocking between thread loops, the pull-out of tufts should be avoided. The plastic film also facilitates distortion-free separation of preform and foam after the tufting process.

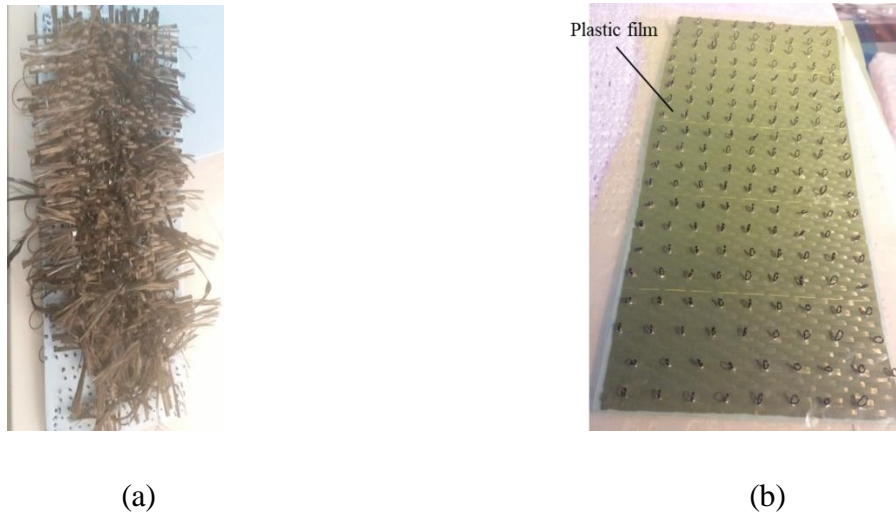


Figure 2.13 (a) Damaged texture and (b) protected texture of bottom skin woven fabric.

2.3.5 Other parameters

Other common parameters are the tufting length and tufting angle. For a preform completely penetrated through the thickness by the tufting thread, the tufting length can be divided into two parts: the length of thread into the preform and the loop length (see Figure 2.14). Given the current tufting machine and needle design, the maximum needle stroke is limited to 50 mm. The penetration depth can be varied by adjusting the height of the needle rod concerning the presser foot. Liu et al. studied the influence of tuft length on the characterizations of tufted composites and indicated a minimum tufting length exists to ensure that the multilayered composite panel can be well reinforced [20]. Due to the bending of the yarn and to avoid confusion between tufting thread length and tufting length, the tufting length is also referred to as tufting depth, which is related to the penetration depth of the tufting needle and not to the tufting thread.

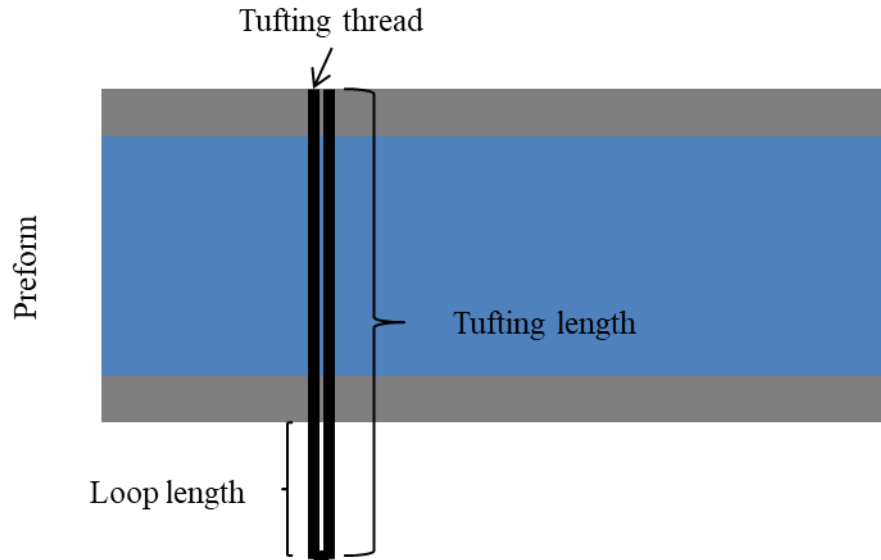


Figure 2.14 Schematic of tufting length.

Usually, the loops cause an increase in the thickness of the bottom skin of the sandwich due to a larger length than the thread on the top skin surface (see Figure 2.15). A large number of thread loops that are too concentrated can wrinkle the skin and cause errors when the skin tensile modulus needs to be brought into the calculation. Also, the voids formed by the wrinkles are filled in by resin during LRI, increasing the weight of the final part. According to the research of Jamie et al. [13], the length of the tuft has a negligible effect on the mechanical performance with no clear trend between loop size and the energy absorbed. Because of this, all loops are cut off after tufting to obtain a flatter bottom skin surface. The tufting threads are loosened at the bottom skin surface when the loops are removed, it is important to avoid tufting threads being pulled out from the top skin surface.

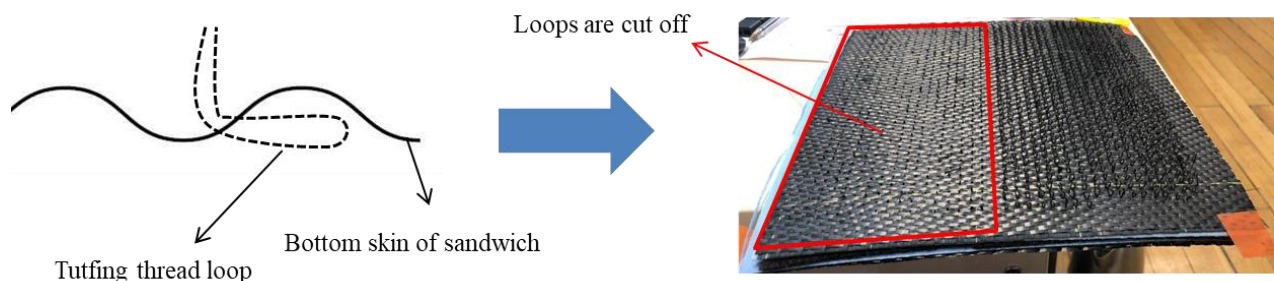


Figure 2.15 Removal of tufting loops before LRI.

Tufting angle is defined as the angle between the tufting needle and the normal of the preform top surface (shown in Figure 2.16). Variation of tufting angle will have different effects on the shear, bending, and compression properties of the material [21]. These two parameters are set constants in the study (Tufting depth 25 mm and tufting angle 0°).

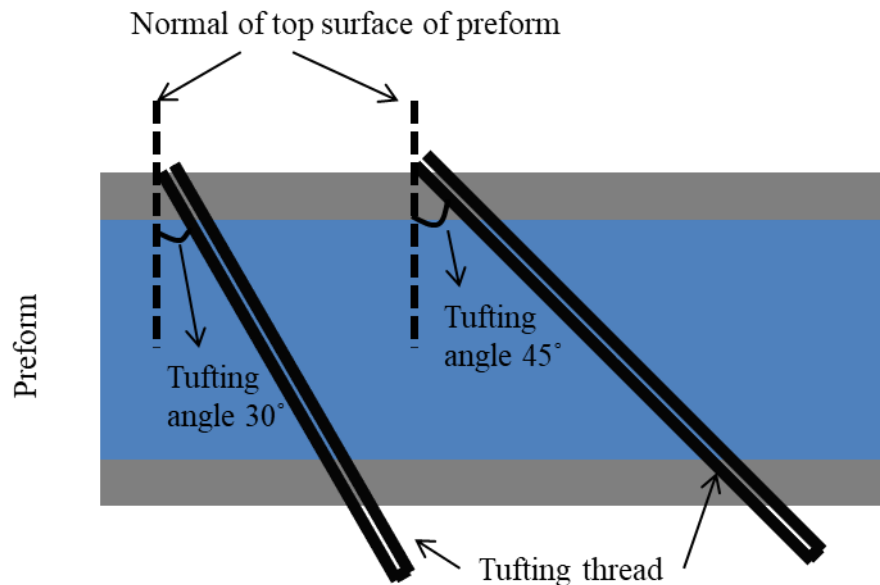


Figure 2.16 Schematic of tufting angle.

2.4 Liquid resin infusion process

The mechanical properties of the sandwich composite are strongly linked to the resin infusion process adopted. As a technique conducive to manufacturing large or complex parts by flowing liquid resin through the thickness of a fibrous reinforcement, the LRI process is particularly suitable for small businesses and laboratories because of its low investment and basic procedure. The resin used for carbon fiber reinforced sandwich composite is SR8200 epoxy resin and the resin hardener is SD7203 (mixing ratio by weight is 100: 37) which comes out of SICOMIN. The advantage of this product is that it contains the reactivity suitable for press contact lamination, or small parts under vacuum, the curing rate is fast for laminates in an ambient temperature of 20 to 30°C . Bio based epoxy resin SR InFuGreen 810 and the hardener SD 8825.2 (mixing ratio 100: 22) from the same enterprise are selected for the flax fiber reinforced sandwich preform. The mixing ratio by weight is 100: 22. The most valuable reason for using this resin is that it is

produced with about 38 % of carbon from plant origin and has a lower environmental impact than standard Epoxy systems.

The schematic of the LRI process is illustrated in the previous chapter (see Figure 1.13d). The stacking preform is put on a plate metal mold and a layer of release film is inserted between them. Then lay up another release film and a flow distribution mesh on the preform. Two tubes were connected respectively to the pump and resin pots as the entrance of resin and the vent hole. Finally, enclose all these materials in a vacuum bag. Seal up the entrance of resin and turn on the pump to vacuum the bag, next open the resin tube (see Figure 2.17). Once the whole preform is well wetted, the two tubes are closed and the preform is left in suitable curing conditions. The curing conditions of the two resins are different. Preforms impregnated by the epoxy resin were placed at temperature for at least 24h. And the bio resin needed to be heated to 80°C and left for 8 hours in a circulating oven.

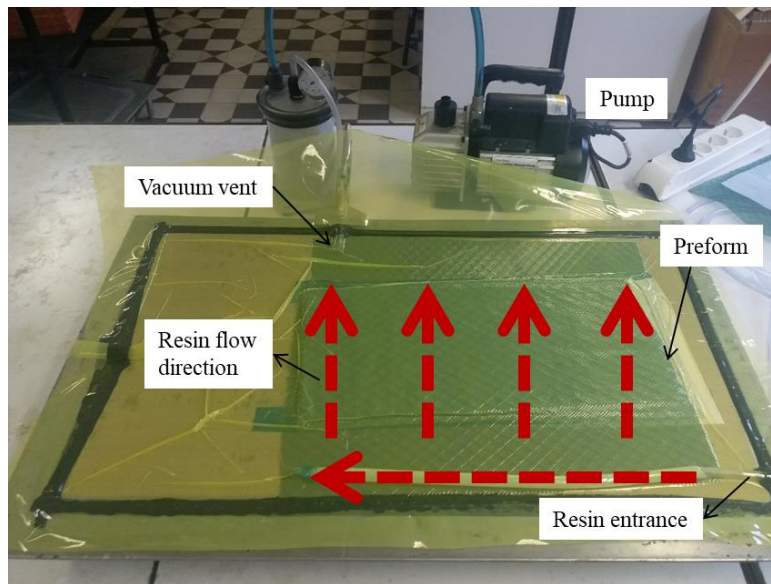


Figure 2.17 Liquid resin infusion process.

The procedure has been validated adaptable for manufacturing composite parts with small and medium size. Nevertheless, the problems appear during infusion according to the original LRI process. Controlling the fiber volume fraction becomes more difficult as the absorption of resin cannot be calculated in advance. Actually, if the amount of resin required is calculated in advance based on the expected target fiber volume fraction, it is found that this amount of resin is too little

to complete the infusion. Excessive resin is absorbed by the inserted nonwoven mat due to its higher porosity. For one thing, since the resin penetrates from the top of the preform downward, when the impregnation is incomplete, there are parts of the bottom that remain dry, which is not accepted. For another, the resin can be introduced into the core layer from the four sides of the preform, resulting in a large amount of resin absorption by the nonwoven and an increase in the weight of the final composite part.

Not well-distributed resin is not conducive to both lightweight design and resin infusion quality. To decrease the flow of resin into the nonwoven, a layer of foam is retained on each side of the top and bottom of the nonwoven when designing the core architecture (as shown in Figure 2.2). The resin can also be introduced into the nonwoven layer from the four sides of the preform, resulting in a large amount of resin absorption. The solution is closing the four sides of the preform by tape or other potential material which can isolate the resin. Thus the resin flow can only enter the nonwoven mat through the channels formed by tufting. Excessive absorption of resin is limited. To solve the incomplete resin impregnation at the bottom of the preform, another flow distribution layer and a release film are inserted under the bottom skin of the preform to accelerate the resin flow (see Figure 2.18). In this way, the liquid resin flows at the top and bottom at the same time, which ensures the bonding between skin and core. By all the above operations, the resin uptake in the intermediate position nonwoven is reduced while ensuring complete resin impregnation.

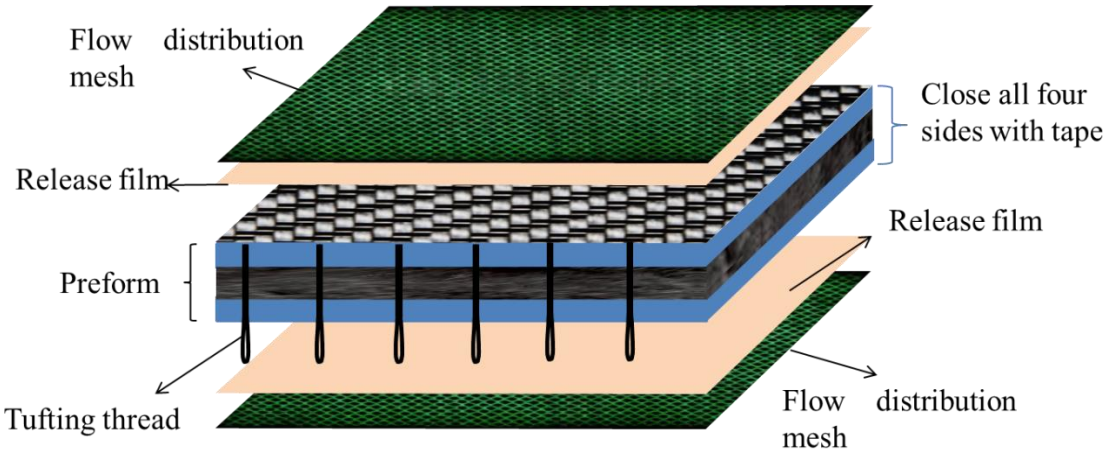


Figure 2.18 Stacking order for LRI process.

The carbon fiber reinforced sandwich specimens tufted with and without yarns are prepared and compared to investigate the influence of tufting thread on mechanical behavior. Many holes through-the-thickness formed by needle penetration facilitate the inflow of liquid resin. The resin fills these holes and forms the thread/resin composite columns. Even without the presence of tufting threads, the filled resin forms a pure resin column connecting the skins after curing (see Figure 2.19). These through-the-thickness channels are essential for resin infusion, which will be explained in the next chapter.

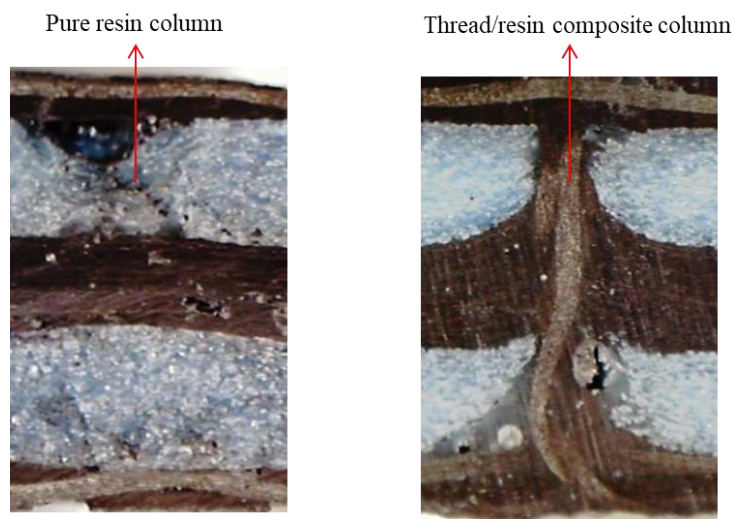


Figure 2.19 Different through-the-thickness reinforcement of sandwich specimens tufted with and without yarn.

The volume of absorbed resin is associated with the fabric structure of preform and the hygroscopicity of fibers themselves, which might lead to an inaccurate prediction. Since flax fiber is hydrophilic, it will absorb more resin during infusion, which needs to be considered when estimating its resin consumption [22]. Moreover, the moisture rate of flax fiber is sensitive to environmental changes, so the preform needs to stand in constant temperature and humidity conditions for at least 24h. Therefore, it is reasonable to prepare a slight excess of resin to avoid incomplete impregnation of the preform. LRI has also shown other defects such as controlling the thickness of the final piece and the poor resin impregnation caused by high void content [23–28]. The sandwich preform is compressed twice before resin infusion: the first is performed by the presser foot of the tufting machine and the second time by evacuation. The thickness of the tufted preform can be predicted by setting the same pressure for both, thus determining the quantity of

each layup. However, this can only roughly control the sample thickness and cannot be predicted accurately. Bubbles in the liquid resin can be reduced by resting them in a vacuum pot in advance. This improves the quality of the final composite part and reduces the void defects within it.

2.5 Ancillary adhesives

The core shear test requires that both sides of the sandwich specimen be bonded to two metal plates. The adhesive is subjected to the same shear force as the specimen and to avoid sample detachment, the adhesive needs to have high shear strength. The two-component epoxy adhesive EC-9323 B/A, supplied by 3M, is adopted due to its extremely high shear and peel strength over a wide temperature range once cured. It has excellent adhesion to a wide variety of substrates such as metals, glass, ceramics and plastics.

White resin component B and red hardener component A are mixed in a weight ratio of 100:27 by weight, applied and cured for 2 hours at 65°C to achieve the full shear strength of 28 MPa, as stated by the manufacturer. To achieve a uniform thickness of the adhesive layer, the two metal plates are fixed by inserting the screws in the opposite holes. The test specimens could be debonded easily from the metal plate with a metal blade after testing by heating the samples to 150°C for 20 minutes.

2.6 Conclusion

In this chapter, the process of manufacturing a tufted sandwich composite panel is presented in detail. Among the several techniques for adding through-the-thickness reinforcement, tufting was selected because of its low cost. The tufted sandwich preform was impregnated by the LRI process. In addition to preform size and fiber hygroscopicity, the amount of resin absorbed during infusion depends also on the tufting needle diameter and tufting density. Too high of two parameters can lead to increased voids inside and at the bottom of the preform, causing additional resin absorption. These effects eventually feed back into the thickness and fiber volume fraction of the final composite part, which influences its mechanical behavior.

The final sandwich composite part had three types of fiber reinforcement: the skin fabric, the nonwoven core and the through-the-thickness thread. All of them formed a composite by being impregnated with resin: composite skin, composite core and composite columns in Z direction. The composite skin was thin and rigid and was mainly loaded in tension or compression. And the

composite core was mainly loaded in compression and shear. The composite columns were mainly subjected to shear and tensile loads. Hence both the nonwoven layer and the tufting thread can improve the delamination under shear loading. It is essential to investigate the gains brought from the nonwoven and tufting thread and also to optimize the sandwich structure, which is presented in the following chapters.

Reference

- [1] Liu L. Development and optimization of the tufting process for textile composite reinforcement 2017.
- [2] Scott M, Dell'Anno G, Clegg H. Effect of Process Parameters on the Geometry of Composite Parts Reinforced by Through-the-Thickness Tufting. *Appl Compos Mater* 2018;25:785–96. <https://doi.org/10.1007/s10443-018-9710-4>.
- [3] Bortoluzzi DB, Gomes GF, Hirayama D, Ancelotti AC. Development of a 3D reinforcement by tufting in carbon fiber/epoxy composites. *Int J Adv Manuf Technol* 2019;100:1593–605. <https://doi.org/10.1007/s00170-018-2764-5>.
- [4] Chehura E, Dell'Anno G, Huet T, Staines S, James SW, Partridge IK, et al. On-line monitoring of multi-component strain development in a tufting needle using optical fibre Bragg grating sensors. *Smart Mater Struct* 2014;23. <https://doi.org/10.1088/0964-1726/23/7/075001>.
- [5] Henao A, Carrera M, Miravete A, Castejón L. Mechanical performance of through-thickness tufted sandwich structures. *Compos Struct* 2010;92:2052–9. <https://doi.org/10.1016/j.compstruct.2009.11.005>.
- [6] Hui C, Wang P, Legrand X. Improvement of tufting mechanism during the advanced 3-dimensional tufted composites manufacturing: To the optimisation of tufting threads degradation. *Compos Struct* 2019;220:423–30. <https://doi.org/10.1016/j.compstruct.2019.04.019>.
- [7] Hao S, Wang P, Legrand X, Liu L, Soulat D. Influence of the tufting pattern on the formability of tufted multi-layered preforms. *Compos Struct* 2019;228. <https://doi.org/10.1016/j.compstruct.2019.111356>.
- [8] Bodaghi M, Gnaba I, Legrand X, Soulat D, Wang P, Deléglise-Lagardère M, et al. In-plane permeability changes of plain weave glass fabric induced by tufting. *Adv Compos Mater* 2020. <https://doi.org/10.1080/09243046.2020.1840687>.
- [9] Hao S, Wang P, Legrand X, Liu L, Soulat D. Influence of the tufting pattern on the formability of tufted multi-layered preforms. *Compos Struct* 2019;228. <https://doi.org/10.1016/j.compstruct.2019.111356>.
- [10] Henao A, Guzmán De Villoria R, Cuartero J, Carrera M, Picón J, Miravete A. Enhanced impact energy absorption characteristics of sandwich composites through tufting. *Mech Adv Mater Struct* 2015;22:1016–23. <https://doi.org/10.1080/15376494.2014.918221>.
- [11] Wittig J. Recent development in the robotic stitching technology for textile structural composites. *J Text Apparel, Technol Manag* 2001;2.
- [12] Martins AT, Aboura Z, Harizi W, Laksimi A, Khellil K. Analysis of the impact and compression after impact behavior of tufted laminated composites. *Compos Struct* 2018;184:352–61. <https://doi.org/10.1016/j.compstruct.2017.09.096>.

- [13] Hartley JW, Kratz J, Ward C, Partridge IK. Effect of tufting density and loop length on the crushing behaviour of tufted sandwich specimens. *Compos Part B Eng* 2017;112:49–56. <https://doi.org/10.1016/j.compositesb.2016.12.037>.
- [14] Verma KK, Viswamurthy SR, Gaddikeri KM, Ramesh S, Kumar S, Bose S. Tufting thread and density controls the mode-I fracture toughness in carbon/epoxy composite. *Compos Struct* 2021;261. <https://doi.org/10.1016/j.compstruct.2020.113272>.
- [15] Thurm T. Applications of one-sided stitching techniques for resin infusion preforms and structures. *SAMPE J* 2005;41:64–7.
- [16] Treiber JWG. Performance of tufted carbon fibre / epoxy composites. Thesis 2011.
- [17] Koissin V, Ruopp A, Lomov S V., Verpoest I, Witzel V, Drechsler K. On-surface fibre-free zones and irregularity of piercing pattern in structurally stitched NCF preforms. *Adv Compos Lett* 2006;15:81–8. <https://doi.org/10.1177/096369350601500302>.
- [18] Dell’Anno G, Cartié DD, Partridge IK, Rezaei A. Exploring mechanical property balance in tufted carbon fabric/epoxy composites. *Compos Part A Appl Sci Manuf* 2007;38:2366–73. <https://doi.org/10.1016/j.compositesa.2007.06.004>.
- [19] Wittig J. In-mold-reinforcement of preforms by 3-dimensional tufting. *Int. SAMPE Symp. Exhib.*, vol. 47 II, 2002, p. 1043–51.
- [20] Liu LS, Wang P, Legrand X, Soulat D. Investigation of mechanical properties of tufted composites: Influence of tuft length through the thickness reinforcement. *Compos Struct* 2017;172:221–8. <https://doi.org/10.1016/j.compstruct.2017.03.099>.
- [21] Dell’Anno G, Treiber JWG, Partridge IK. Manufacturing of composite parts reinforced through-thickness by tufting. *Robot Comput Integr Manuf* 2016;37:262–72. <https://doi.org/10.1016/j.rcim.2015.04.004>.
- [22] Sawsen C, Fouzia K, Mohamed B, Moussa G. Optimizing the formulation of flax fiber-reinforced cement composites. *Constr Build Mater* 2014;54:659–64. <https://doi.org/10.1016/j.conbuildmat.2013.12.038>.
- [23] Sevostianov IB, Verijenko VE, Von Klemperer CJ, Chevallereau B. Mathematical model of stress formation during vacuum resin infusion process. *Compos Part B Eng* 1999;30:513–21. [https://doi.org/10.1016/S1359-8368\(99\)00012-8](https://doi.org/10.1016/S1359-8368(99)00012-8).
- [24] Celle P, Drapier S, Bergheau JM. Numerical modelling of liquid infusion into fibrous media undergoing compaction. *Eur J Mech A/Solids* 2008;27:647–61. <https://doi.org/10.1016/j.euromechsol.2007.11.002>.
- [25] Crivelli Visconti I, Durante M, Langella A, Morano U. Flow Front Analysis In Resin Infusion Process. *Intell. Prod. Mach. Syst. - 2nd I*PROMS Virtual Int. Conf.* 3-14 July 2006, 2006, p. 223–8. <https://doi.org/10.1016/B978-008045157-2/50043-2>.
- [26] Wang P, Drapier S, Molimard J, Vautrin A, Minni JC. Numerical and experimental analyses of resin infusion manufacturing processes of composite materials. *J Compos Mater* 2012;46:1617–31. <https://doi.org/10.1177/0021998311421990>.
- [27] Govignon Q, Bickerton S, Kelly PA. Simulation of the reinforcement compaction and resin flow during the complete resin infusion process. *Compos Part A Appl Sci Manuf* 2010;41:45–57. <https://doi.org/10.1016/j.compositesa.2009.07.007>.
- [28] Bourchak M, Harasani W. Assessment of liquid resin infusion impregnation quality using scanning electron microscopy. *Adv Compos Lett* 2015;24:6–11. <https://doi.org/10.1177/096369351502400102>.

**CHAPTER 3. TOWARDS LAMINATE
QUALITY AND MECHANICAL
PERFORMANCE OF TUTED
SANDWICH COMPOSITES WITH
CARBON FIBER NONWOVEN**

3.1 Introduction

Sandwich structure is widely employed in the design and manufacturing of composite materials due to their high bending stiffness per weight ratio. However, due to the weakness of the core material, the sandwich composite presents low mechanical properties in the through-the-thickness (TT) direction, such as poor impact damage resistance and strength [1].

As presented in Chapter 2, delamination is the major problem sandwich construction and tufting process is adopted to insert TT reinforcement for sandwich manufacturing. This chapter is dedicated to the influence of different core structures on the mechanical properties of tufted sandwich composites, especially the effect of nonwoven layers and tufting thread. Various studies have been carried out on the damage and failure behavior of composite sandwich panels. One of the most recognized researches of 3D sandwich structures is developed by Reis and Rizkalla, who summarized the findings of an experimental program to determine various parameters believed to affect the material characteristics [2]. Che et al. compared the compression performance of an octahedral stitched sandwich composite with the sandwich having cellular core materials [3]. The mechanical properties of foam core with perforation and stitching are investigated by Yalkin et al. [4], and they found that newly proposed stitched core specimens with relatively insignificant weight increase have superior mechanical performances than plain core specimens. Xi Tao et al. [5] quantified the effect of structural through-thickness reinforcement in foam core sandwich composite panels. Sharma et al. [6] investigated the characteristics of the specimens with through-thickness stitches and the influence of strain rate on buckling. The influence of the panel thickness, TT fiber configuration and density, and other parameters on the tension, compression, and flexion and shear behavior are studied by Long et al. [7]. Nishi et al. [8] investigate the Charpy impact property of sandwiches with polycarbonate core. Srivastava analyzed the impact behaviors of sandwiches with foam core and E-glass fiber face sheets by Charpy impact test, Izod impact test, and weight drop test [9]. The foam core with stitching or z-pin is characterized and corresponding models are created [4,10–12].

The present study aims to determine the feasibility of inserting the polystyrene foam core with nonwoven material in the tufting and LRI (liquid resin infusion) process. Although foam cores with stitches or z-pin reinforcement have been investigated in the other works [3,4,7,10,11,13], they do not involve the core composed with different layers, which meant additional processing

and characterization. Thus, an experimental investigation is conducted under different loadings to study the influence on mechanical performances of sandwich panels caused by these tufting threads and the non-woven core.

3.2 Materials and methods

3.2.1 Manufacturing of tufted sandwich composite samples

Figure 3.1 shows the principal sandwich structure used in the present study. It consists of three main parts: the carbon fabric skins, the foam and non-woven core layer and the through-the-thickness tufting yarns. The two foam layers between the skins and the non-woven aim to prevent the non-woven from absorbing excessive resin, which can reduce the mass of the final composite part.

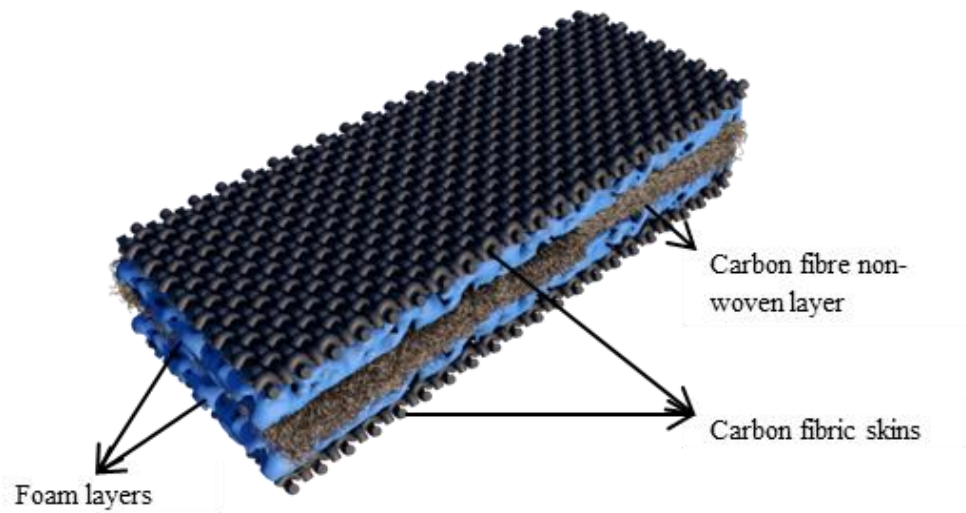


Figure 3.1 Sandwich composite specimens containing non-woven core.

During the tufting process, a hollow needle carried the thread totally through the thickness of the sandwich preforms. When the needle retracts, the thread is retained within the sandwich preform by simple friction between fibers and core layers, forming a loop under the bottom skin (see Fig. 2). This process is simpler than the conventional stitching process, as it does not require the use of a second thread and does not lock the threads [14][15]. The resin infusion process (LRI process) is proposed after the tufting stage. The liquid resin progressed through the dry tufted fibrous preforms. It allows final parts of very good quality to be obtained with reduced tools.

However, due to the lack of channels through the thickness, the intact foam prevents the liquid resin from entering the nonwoven from the top and bottom sides, and the resin can only enter the area close to the four sides of the preform. As a result, the final sandwich composite part remains dry in some areas (shown in Figure 3.2). The nonwoven layer and foam are not bonded to each other and cannot be compared as a qualified composite sample.

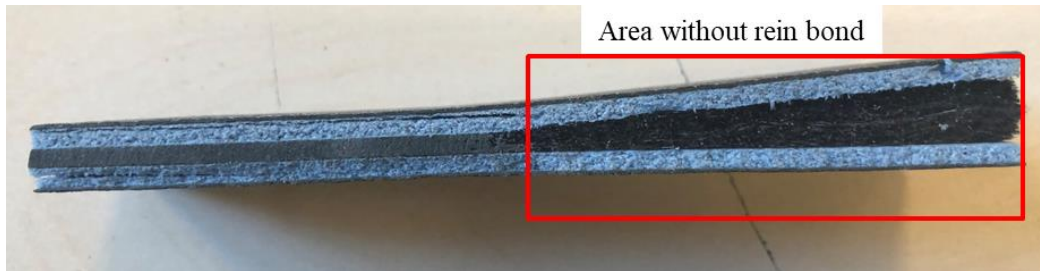


Figure 3.2 Non-tufted sandwich structure with nonwoven core layer.

To study the influence of different core and tufting yarns on composite mechanical properties, four groups of sandwich panels with different core structures are produced and shown in Table 3.1. The fiber volume fraction v_{fiber} of the tested sandwich composites is calculated as the following equation:

$$v_{fiber} = \frac{V_{fiber}}{V_{fiber} + V_{resin}} \quad (3.1)$$

where V_{fiber} and V_{resin} are the volume of fiber and of the resin, respectively.

Table 3.1 Main properties of tufted sandwich composite samples.

Sample ID	Core layer	TT reinforcement	Fiber volume fraction	Thickness (mm)
SW-1	Foam	Carbon fibers/resin column	24%	7.07±0.29
SW-2	Hollow		24%	6.85±0.16
SW-3	Foam/Non-woven	Pure resin column	22%	6.58±0.17
SW-4			18%	5.46±0.15

The resin columns are formed in all sandwich structures due to the holes punched by the tufting needle. Thus, the core structure can be divided into two parts: the superposed core layers and the through-thickness (TT) columns. Different from the SW-1, 2, 3 samples tufted with carbon yarn, the SW-4 preform is tufted without yarn. Therefore, the pure resin columns are presented in the SW-4 composite compared to the carbon fibers/resin columns in SW-1, 2, 3 composites, but the diameter of the columns is considered the same in all of the samples. Regarding the core in sandwich samples, three layers of foam are used in SW-1, 2 structures, but the foam is dissolved by acetone in the final SW-2 sample. Two skins are connected by the carbon fibers/resin columns in the SW-2 structure as shown in Fig. 3. In SW-3, 4 structures, a single layer non-woven mat is employed (see Figure 3.3).

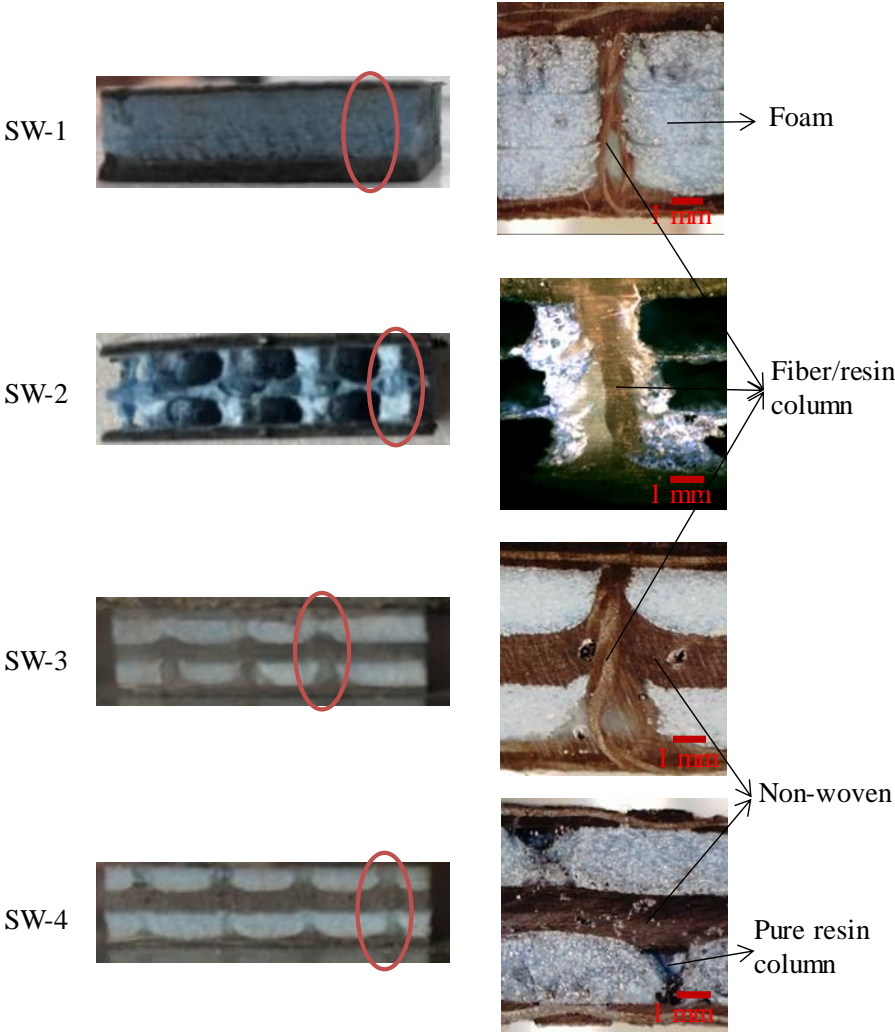


Figure 3.3 Micro-observation of the cross-section of the different samples.

3.2.2 Test methods

Since the added nonwoven layer and tufting thread are expected to enhance the mechanical properties in the thickness direction and also prevent the delamination, core shear test, flatwise compression test, 3-point bending test and Charpy test are conducted.

3.2.2.1 Core shear test

Core shear behavior is one of the important deformation modes for sandwich composites. So the sandwich samples are bonded to the loading metal plates to produce a pure shear stress state as shown in Figure 3.4. The surface dimension of the tested sample is $65 \times 20 \text{ mm}^2$ and the crosshead speed is 2 mm/min. The shear strain γ and the shear stress τ of the sandwich sample can be calculated through the following equations [16]:

$$\tau = \frac{F}{lb} \quad (3.2)$$

$$\gamma = \frac{d}{c} \quad (3.3)$$

where F is the shear load, l and b are the length and width of the sample, c is the thickness of the core part and d is the displacement of the metal plate.

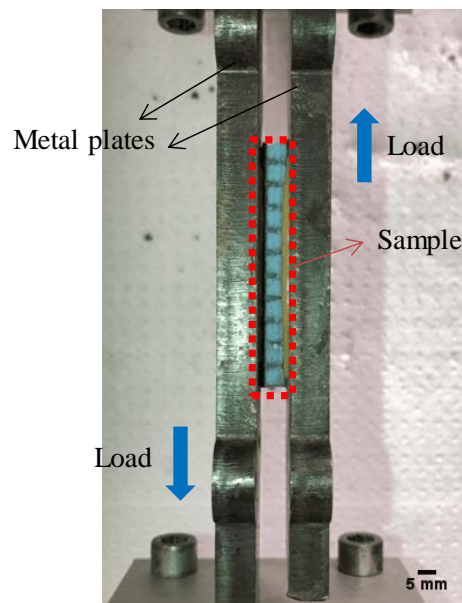


Figure 3.4 Core shear test set-up.

3.2.2.2 Flatwise compression test

To determine the compressive strength in Z-direction, where the core would be placed, in structural construction, the test is designed according to the standard ASTM C365-16 [17]. The general principle of the compression tests is shown in Figure 3.5. The specimens are parallelepipeds at a square base with a dimension of $25 \times 25 \text{ mm}^2$. The construction tested must be placed in the center of the head of the indenter exactly. Each test is repeated five times at a constant speed 2 mm/min to ensure high repeatability of the testing and results. The flatwise compressive strength σ_z and strain are given by:

$$\sigma_z = \frac{F}{b^2} \quad (3.4)$$

$$\tau = \frac{d}{h} \quad (3.5)$$

where F is the measured value of the load, d is the displacement of the loading plate, h and b are the thickness and width of the sample, respectively.

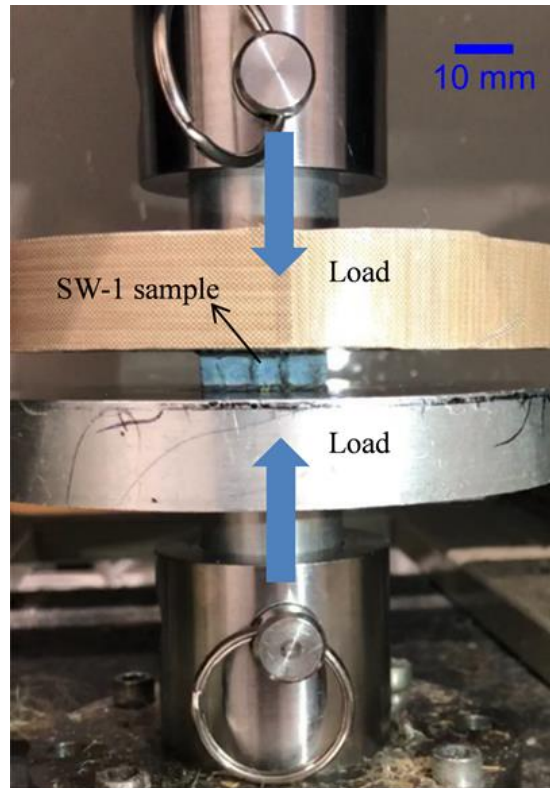


Figure 3.5 Compressive test device.

3.2.2.3 Three-point bending test

Three-point bending test is conducted at a constant crosshead displacement of 1 mm/min according to ASTM D7249 standard [18] (see Figure 3.6). The surface dimension of the tested specimen is 100 (l) \times 20 (b) mm². A load-displacement plot is recorded for each test. The flexural stress σ and core shear strength τ can be determined by equations 3.6 and 3.7:

$$\sigma = \frac{FS}{2t(h+c)b} \quad (3.6)$$

$$\tau = \frac{F}{(h+c)b} \quad (3.7)$$

where F is the value of force, h is the sandwich thickness, c is the core thickness, t is the facing thickness and S is the span length. The shear stress is calculated as a reference value since the sample geometry and span length are restricted to represent the facing bending properties.

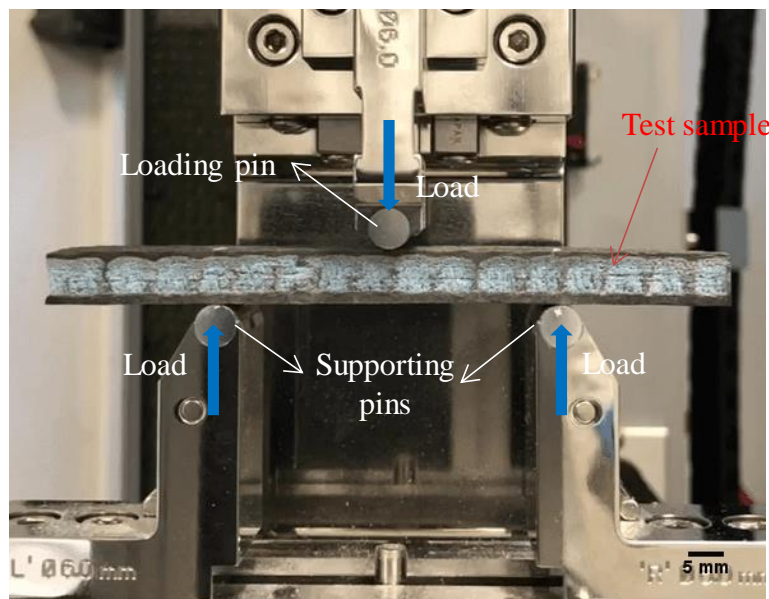


Figure 3.6 Bending test set-up.

3.2.2.4 Charpy impact test

For sandwich composites, normally only the tests in the flatwise direction are carried out. The Charpy impact strength of the composites is tested according to EN ISO 179-1 [19]. This test is designed to measure the resistance to failure of a material to a suddenly applied impact. The value measured is the impact energy or the energy absorbed before fracture. The apparatus consists of a pendulum of known mass and length that is dropped from a known height to impact

a notched specimen of material. The energy transferred to the material can be inferred by comparing the difference in the height of the hammer before and after the fracture (energy absorbed by the fracture event, see Figure 3.7), which is denoted by W . The length (l) and width (b) of specimens are 80 mm and 10 mm, respectively. The resilience K can be computed by:

$$K = \frac{W}{lb} \quad (3.8)$$

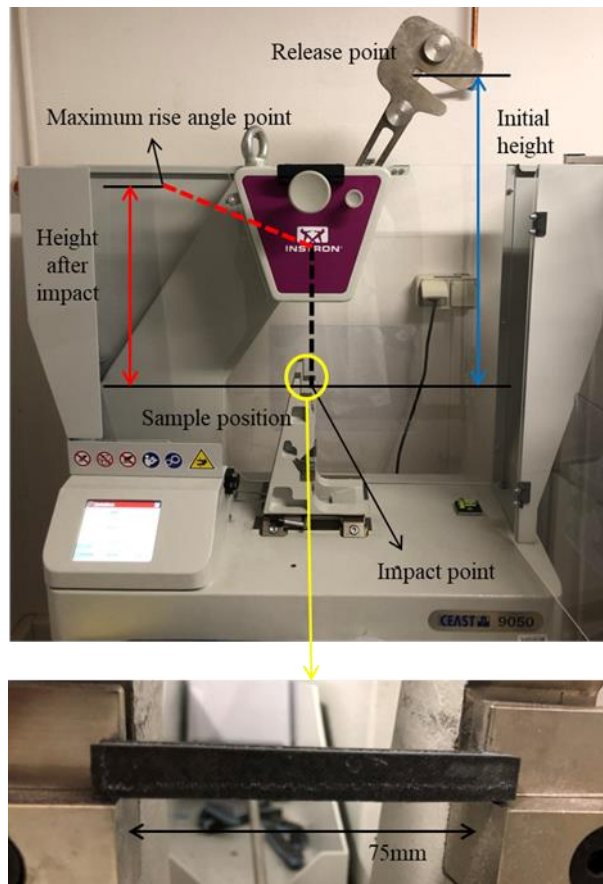


Figure 3.7 Charpy impact test schematization.

3.3 Results and discussion

3.3.1 Core shear test

Figure 3.8 illustrates the shear stress-strain curves of the four tested sandwich samples with different cores. All of the curves increase linearly in the first part between 0 and 0.05 shear strain,

then the SW-1, 2, 3 present a nonlinear behavior up to the failure, while the curve of SW-4 drops suddenly after the structural failure. The difference between SW-4 and the other three sets is the insertion of tufting threads. The columns of SW-4 in Z-direction are made of pure resin while the others are made of carbon fiber/resin (see Table 3.1). This nonlinear portion is attributed to the gradual break of tufting yarns after the solid resin crack.

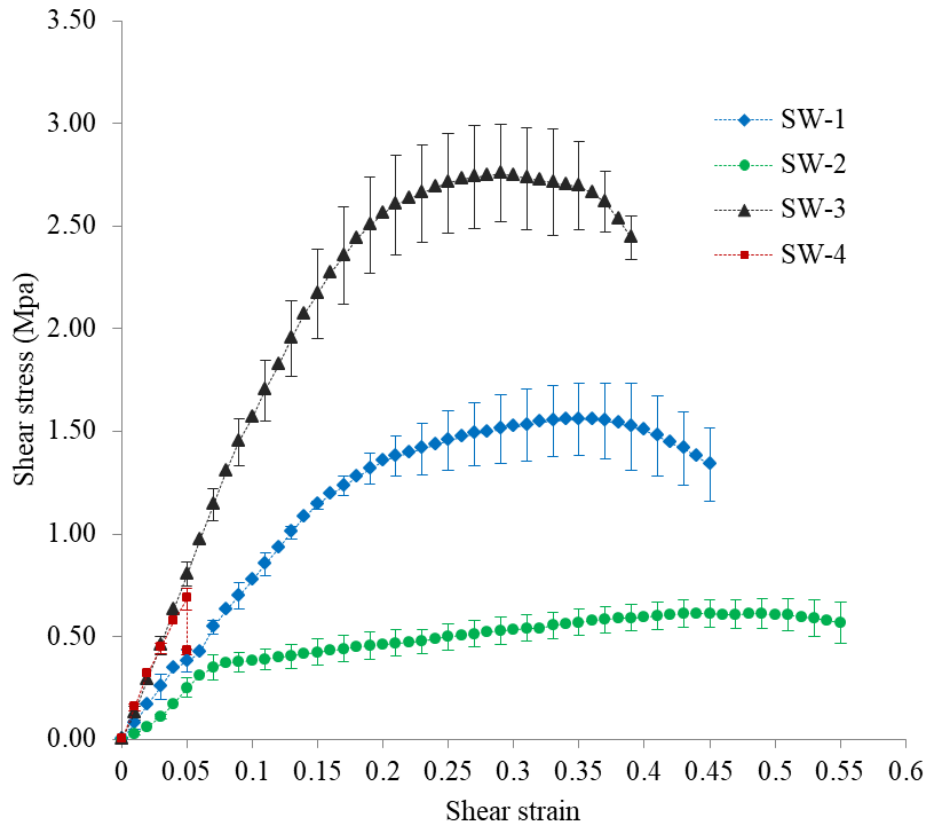


Figure 3.8 Shear stress vs. shear strain curves of the sandwich composite parts.

The shear modulus G_{zx} can be calculated from the slope of the linear part (0-0.05 of the shear strain) on each curve and the maximum shear stress of the linear part can be observed. These values with their coefficients of variation (CV) are noted in Table 3.2. The shear stress of SW-1 is higher than that of SW-2, which shows the shear loading is not only carried by the TT columns, the foam plays an important role to strengthen the core shear resistance. Comparing the SW-3 and SW-4 structures, the SW-3 sample shows higher maximum shear stress in the linear part due to the presence of the tufting yarn (see Figure 3.3). This enhancement depends on whether the mechanical properties of the tufting yarn are higher than that of the resin. The tufted yarn is not

completely straightened in the resin column but exhibits a different degree of bending [20]. Considering the elastic strain is very small, only the resin column is bearing the load, and the yarn is gradually being tensioned at the linear part. After the resin columns are completely broken, the tufting yarn of SW-3 could still bear the load, which resulted in larger maximum shear stress. This phenomenon of winding yarn (see Figure 3.11) can explain why SW-3 and SW-4 have similar shear modulus.

Table 3.2 Mechanical properties of sandwich composites in the core shear tests.

Sample ID	Failure strain	Maximum core shear stress before structure damage (MPa)		Shear modulus G_{zx} (MPa)	
		Average	CV	Average	CV
SW-1	0.36	1.56	8.87%	10.21	9.81%
SW-2	0.45	0.61	6.13%	6.09	8.38%
SW-3	0.29	2.75	8.60%	16.13	6.13%
SW-4	0.05	0.68	7.78%	15.84	5.79%

Figure 3.9 presents the failure modes after the core shear test of the tufted sandwich composites. As the resin column completely penetrates the thickness, no matter what kind of sandwich core structure, all the resin pillars inevitably break before or when the structure fails. As the core of the SW-2 structure is only the TT columns, the main failure mode presents the inclination and fracture of the TT columns. The resin columns are subjected to shear stress but the yarns are stretched. Regarding SW-1 sample, the shear load of the SW-1 is carried by both the TT columns and the foam; consequently, its failure mode mixed the fracture of TT columns and the rupture of the foam. The same phenomenon can be observed in SW-3 and SW-4 structures as the presence of foam in the core. By contrast, the presence of a non-woven layer in SW-3 and SW-4 structures minimized the inclination of the TT yarns under core shear effects. Therefore, the smaller shear strain can be observed in SW-3 and SW-4 structures compared to the SW-1 and SW-2 ones.

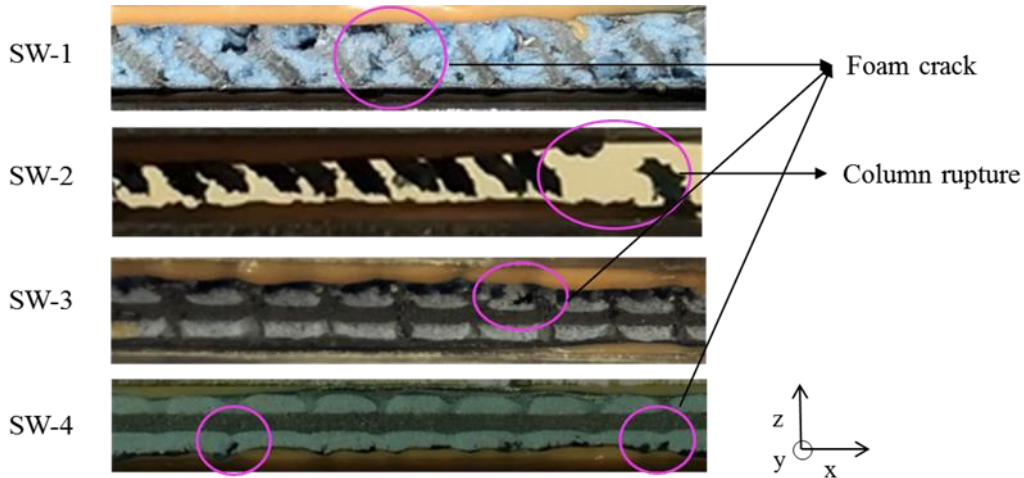


Figure 3.9 Observation of the failure mode in core shear tests.

The shear modulus of the nonwoven layer (346.40 MPa) is much greater than that of foam (4.44 MPa). Consequently, the SW-3 and SW-4 samples have quasi same shear modulus, but the deformation of the foam is much greater than that of the nonwoven layer as shown schematically in Figure 3.10a. Thus the cracks appeared only on the foam. Moreover, the nonwoven layer in the middle has high strength and rigidity; it prevented the cracks in the foam from expanding to the other side. In this case, the fracture of the foam in SW-3 and 4 composites only occur on a single side.

Since the skin sheets are rigid layers and have small thickness and deformation in comparison with the core, the contribution to the core shear properties from skins can be neglected. Thus the shear modulus G_{zx} can be obtained from Equation 3.9:

$$G_{zx} = G_{col}v_{col} + G_l(1 - v_{col}) \quad (3.9)$$

$$v_{col} = \frac{n\pi r^2}{lb} \quad (3.10)$$

where G_{col} and G_l represent the shear modulus of TT columns and core layers respectively, v_{col} is the volume fraction of TT columns in the core, n is the number of TT columns, and r is the radius of the column. The diameter of the TT column in the present work is 1mm. It is different from the rule of mixture, which is applied to estimate the shear modulus of a composite on the assumption that the fibers and the matrix experience equal shear stresses and that the structure is a laminate. Here, the calculation of the shear modulus of the sandwich structure is based on the

assumption that the shear strains of the TT columns in the core and the core layers are equal, and the shear load is carried both by columns and layers.

Figure 3.10 presents schematically the deformation during the core shear test of a sandwich structure. The shear strain (γ_l) and shear modulus (G_l) of core layers can be obtained from Eqs. 3.11 and 3.12.

$$\gamma_l = \frac{2d_f + d_n}{c} = \frac{2d_f}{c_f} \frac{c_f}{c} + \frac{d_n}{c_n} \frac{c_n}{c} = \gamma_f v_f + \gamma_n v_n \quad (3.11)$$

$$G_l = \frac{\tau_l}{\gamma_l} = \frac{G_f G_n}{G_f v_n + G_n v_f} \quad (3.12)$$

where the v is the volume fraction, G is the shear modulus. The subscripts l , n and f represent the core layers, nonwoven layer and foam layers respectively. And τ_l is the shear stress of core layers.

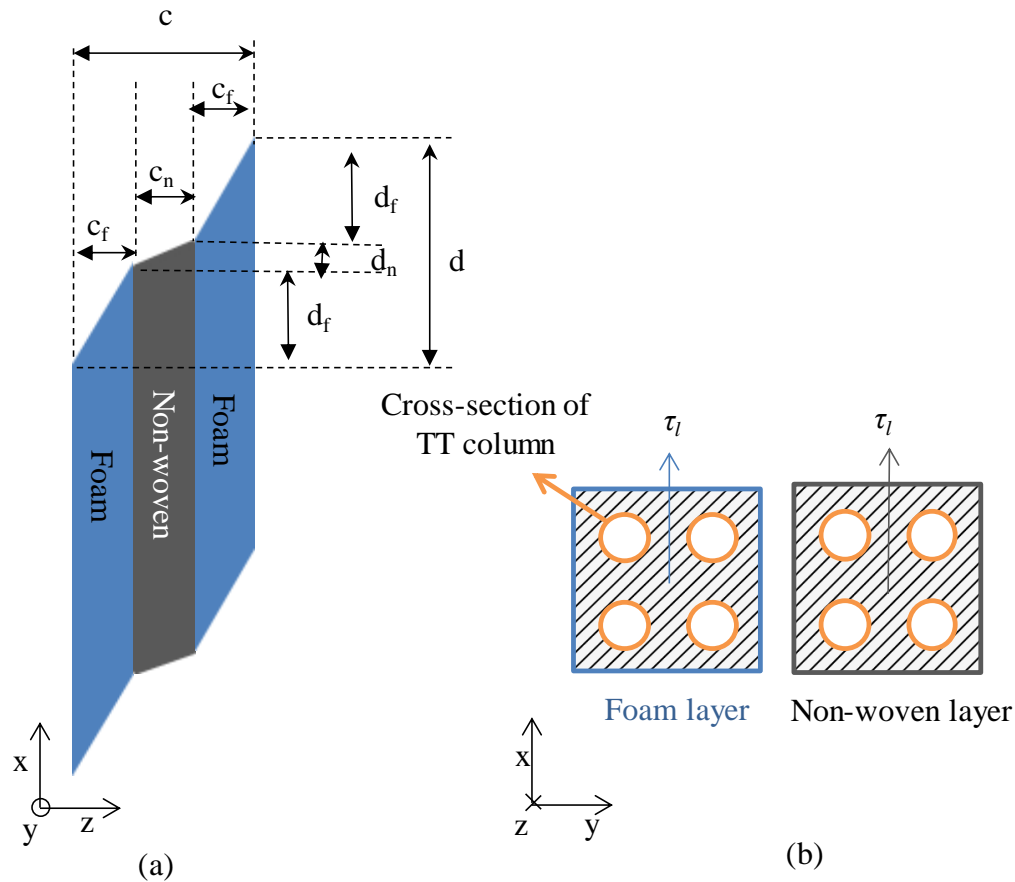


Figure 3.10 The illustration of shear deformation (a) and shear load (b) in SW-3 sample.

The shear modulus of different core constructions is shown as

$$G_{sw1} = G_{col}v_{col} + G_f(1 - v_{col}) \quad (3.13)$$

$$G_{sw2} = G_{col}v_{col} \quad (3.14)$$

$$G_{sw3} = G_{col}v_{col} + \frac{G_f G_n}{G_f v_n + G_n v_f} (1 - v_{col}) \quad (3.15)$$

$$G_{sw4} = G_r v_{col} + \frac{G_f G_n}{G_f v_n + G_n v_f} (1 - v_{col}) \quad (3.16)$$

where G_r is the shear modulus of pure resin.

Based on the Eqs. 3.13-16, the analytical prediction of the core shear modulus of the different sandwich samples is shown in Table 3.3. The difference in percentage between the experimental and analytical results is figured out. It can be remarked that the analytical prediction has a good agreement with experimental results for SW-3 and 4 structures. However, the analytical prediction for SW-1 and 2 composite parts does not match well the experimental investigation. The analytical prediction of SW-1 and 2 structures overestimates the true shear performance of the TT columns. It can be observed that the tufting threads are not straight in the final composite piece as shown in Figure 3.11. The winding threads can be observed in SW-1 and 2 composites as the tufting threads throughout the thickness of the preform are more compressed during the resin infusion process compared to SW-3 and 4 ones. During the shear tests, the winding threads can bring out a sliding before the extension of the threads, this phenomenon can experience more easily in SW-1 and 2 parts due to the non-dense core structure, which can be confirmed by the extracted threads on the rupture surface shown in Figure 3.12.

Table 3.3 Comparison of the experimental and analytical results of the core shearing modulus.

Sample ID	Core shear modulus (MPa)		
	Experimental results (shown in Table 3.2)	Analytical prediction	Difference
SW-1	10.21	12.85	25.86%
SW-2	6.09	8.50	39.57%
SW-3	16.13	15.09	6.89%
SW-4	15.84	14.96	5.56%

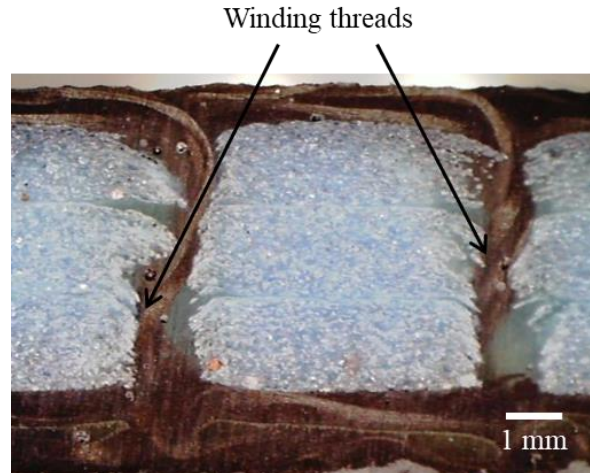


Figure 3.11 Micro-observation of tufting threads in SW-1 sample.

After resin infusion, the non-woven mat and the tufting threads are mixed and integrated into the composite part. It can partly prevent the sliding of the TT threads in the composite. Therefore, the analytical results can well predict the shear response of the SW-3 and 4 structures, in particular the SW-4 sample. There is no sliding in the SW-4 because the preform had no tufting thread in the resin columns. Moreover, the shear modulus of the entire core part (G_{zx}) is positively correlated with the volume fraction of the nonwoven (v_n) according to equation (3.16). Adding non-woven material in the core part provides higher stiffness and strength against shear loadings.

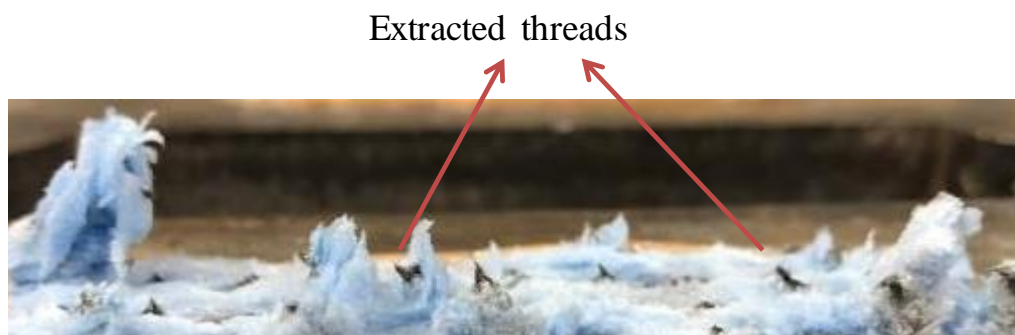


Figure 3.12 Observation of the extracted threads on rupture surface of SW-1 sample.

3.3.2 Flatwise compression test

The effects of core materials and tufting yarns on the resistance to flatwise compression loading are shown in Figure 3.13. The compressive stress-strain curves of the sandwich samples

with four different cores are presented. The curves show an initial elastic stage in which the slope represents the compressive modulus. After the failure of the sandwich structure, due to the continuous compression of each core material, the compressive stress will first decrease and then increase or the stress growth rate (slope of the curve) will decrease. Therefore, its maximum stress value before failure corresponds to the inflection point of each curve rather than the highest point. The maximum stress values before failure of the samples are arranged in descending order: 6.40 MPa in SW-3, 4.42 MPa in SW-1, 3.45 MPa in SW-4, and 3.24 MPa in SW-2 (see Table 3.4).

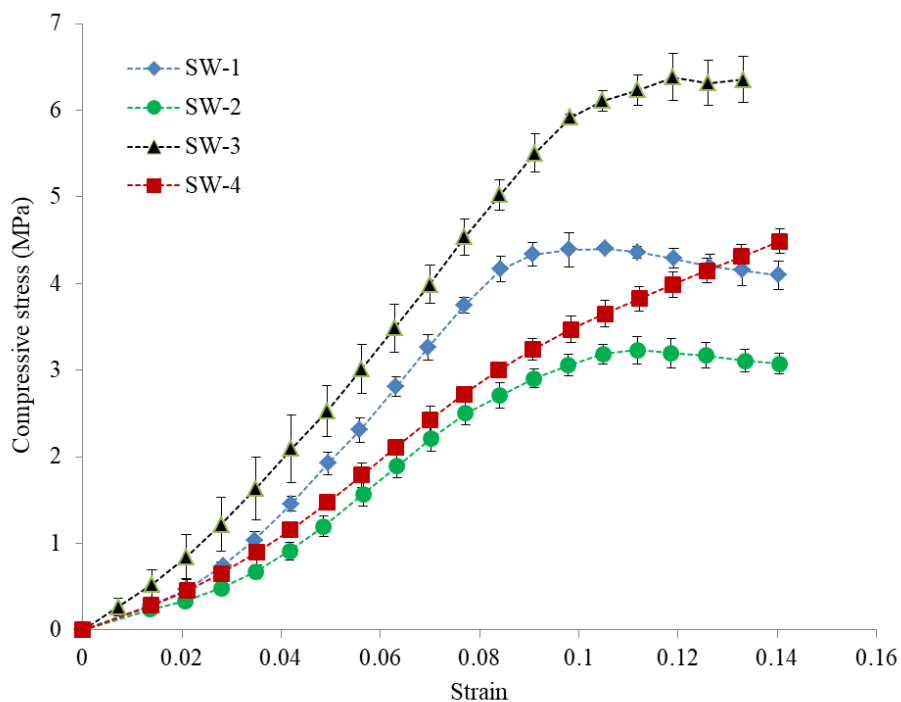


Figure 3.13 Flatwise compression stress-strain curves.

The compressive load is mainly carried by the core materials, thus the analysis of the skins does not have any importance. After the first peak stress, the resin columns buckled or fractured and stress began to decrease. However, the core layers will resist the compression and increase the stress as the compression proceeded because of the densification [1][21]. Thus only the structure failure phase (the first peak stress) is analyzed. The behavior of a sandwich tufted with yarns (SW-1, SW-2 and SW-3) is different from that of a sandwich without tufting threads (SW-4). The curves of the SW-1, SW-2 and SW-3 show a small drop following the ultimate

compression stress due to the breaking of the composite columns. On the contrary, the stress value of the SW-4 has no downward trend after the failure point and keeps increasing, only the slope becomes smaller. Although the SW-3 generally experienced a larger load drop than SW-4 following the failure point, the SW-3 presented higher compressive load-bearing capacity in the entire strain range. The profits from the yarns in Z-direction are clear compared to the sandwich panels with no tufting threads, which can be explained by comparing equations (3.21) and (3.22). The difference is determined by the modulus and the volume fraction in the TT columns of tufting yarn.

Table 3.4 Compressive properties of sandwich composites.

Sample ID	Compressive strength (MPa)	Specific compressive strength (kN·m/kg)	CV (Coefficient of Variation)	Compressive modulus (MPa)
SW-1	4.42	9.52	2.78%	64.32
SW-2	3.24	7.60	5.48%	45.17
SW-3	6.40	9.27	3.40%	67.23
SW-4	3.45	5.55	6.09%	44.82

The effects of foam core on the ultimate stress up to failure and the compressive modulus can be obtained by comparing SW-1 and SW-2. The stress value and the slope of SW-1 are higher, which indicates that compressive strength and modulus increase by the presence of foam core. The columns in Z-direction and the core layers (foam or foam/non-woven) carry the compressive load together. Nevertheless, by using the equations (3.19-21) and (3.23), it can be seen that the gains of stress from non-woven are higher than that from pure foam.

Though the observation of the failure mode from outside is not carried out during the compression process due to the foam or non-woven covered deformation of the columns in the core, the fracture of columns is confirmed after the test. These ruptures occurred almost at the junctions between the skin and the columns. And the foam is critically flattened and it could not recover to its original thickness but the non-woven core remained the same as the beginning. The bulking and the crack of foam and the break of columns are the principal failure mode. The

longitudinal splitting of the columns under compressive load then its deformation caused the foam to crack and collapse, which lead to a large loss of the rigidity of the entire core.

In the case of SW-2, only the fiber/resin columns undergo compressive loading. Thus the failure mode is the buckling of columns. And the failure load F_{sw2} is reached when the columns reached their critical buckling load.

$$F_{sw2} = \frac{\pi^2 E_{col} I}{(Kc)^2} \quad (3.17)$$

where E_{col} is the elastic modulus of columns, I is the area moment of inertia, c is the core thickness, K is the column effective length factor which depends on the conditions of end support of the column. As both ends of the column are considered fixed, the value of K is 1 in this work. Consequently, the equation of the column's compressive strength that fails by buckling can be presented as:

$$\sigma_{col} = \frac{\pi^2 r^2 E_{col}}{4c^2} \quad (3.18) \quad (7)$$

Here, r is the radius of TT columns. The compressive stress σ_z can be predicted by:

$$\sigma_z^{sw1} = \frac{\pi^2 r^2 E_{col} \nu_{col}}{4c^2} + E_f \varepsilon \nu_f \quad (3.19)$$

$$\sigma_z^{sw2} = \frac{\pi^2 r^2 E_{col}}{4c^2} \quad (3.20)$$

$$\sigma_z^{sw3} = \frac{\pi^2 r^2 E_{col} \nu_{col}}{4c^2} + E_c \varepsilon (1 - \nu_{col}) \quad (3.21)$$

$$\sigma_z^{sw4} = \frac{\pi^2 r^2 E_r \nu_{col}}{4c^2} + E_c \varepsilon (1 - \nu_{col}) \quad (3.22)$$

where the superscripts sw1, sw2, sw3 and sw4 represent the four different groups, ε is the compressive strain, E is the Young's modulus, the subscripts r and f represent the resin and the foam, respectively. The Young's modulus of the core with non-woven layers E_c is obtained by using [22]:

$$E_c = \frac{(2c_f + c_n)E_f E_n}{2c_f E_n + c_n E_f} \quad (3.23)$$

where the c is the thickness, the subscript n represents the non-woven (see Figure 3.14).

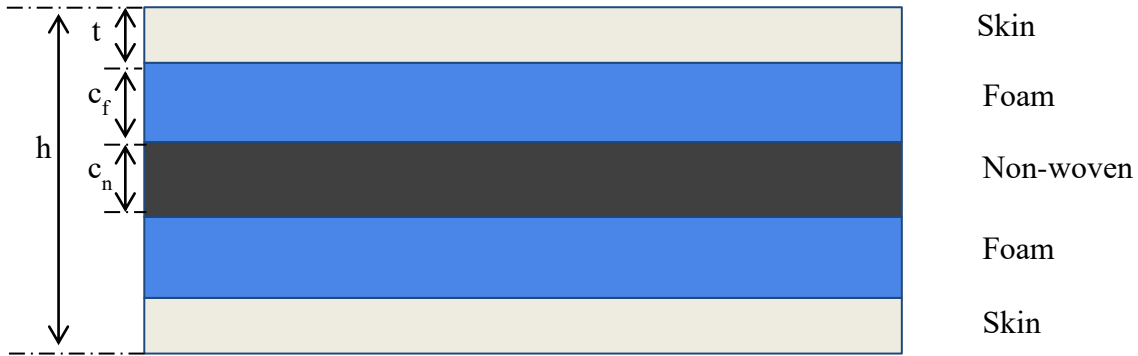


Figure 3.14 Schematic of the analytical calculation of SW-3 and SW-4 samples.

Compressive properties prediction is not performed because the fabric skin and nonwoven layer are anisotropic materials whose moduli of elasticity in the Z-axis direction are presently difficult to measure.

3.3.3 Three-point bending test

The typical bending load *vs.* deflection curves are shown in Figure 3.15. All of the curves have a linear variation between 0 and 0.5 mm deflection which is followed by a non-linear variation. Compared to the curves of SW-1 and SW-2, the curves of SW-3 and SW-4 samples do not have an obvious yield stage before the damage. The main properties of the 3-point bending tests are noted in Table 3.5. It can be observed that the bending modulus of SW-1 and SW-2 are very close. This is because the modulus of foam is very small compared to that of the skin fabric, consequently, the bending stiffness of the foam can be neglected as shown in Eq. 3.24. However, after the elastic deformation stage, the foam is squeezed due to the inconsistent deformation of the upper and lower skins (see Figure 3.16a), so the foam bore more loading. The SW-3 and SW-4 present better 3-point bending results than the SW-1 and SW-2 structures, as the non-woven layer can enhance the mechanical properties of the final sandwich part. Comparing the failure load and maximum flexural strength between the SW-3 and SW-4 structures, it can be remarked the positive influence (an augmentation of 19.7%) of the tufting yarns on the mechanical performances on the interface of the multi-layered composites.

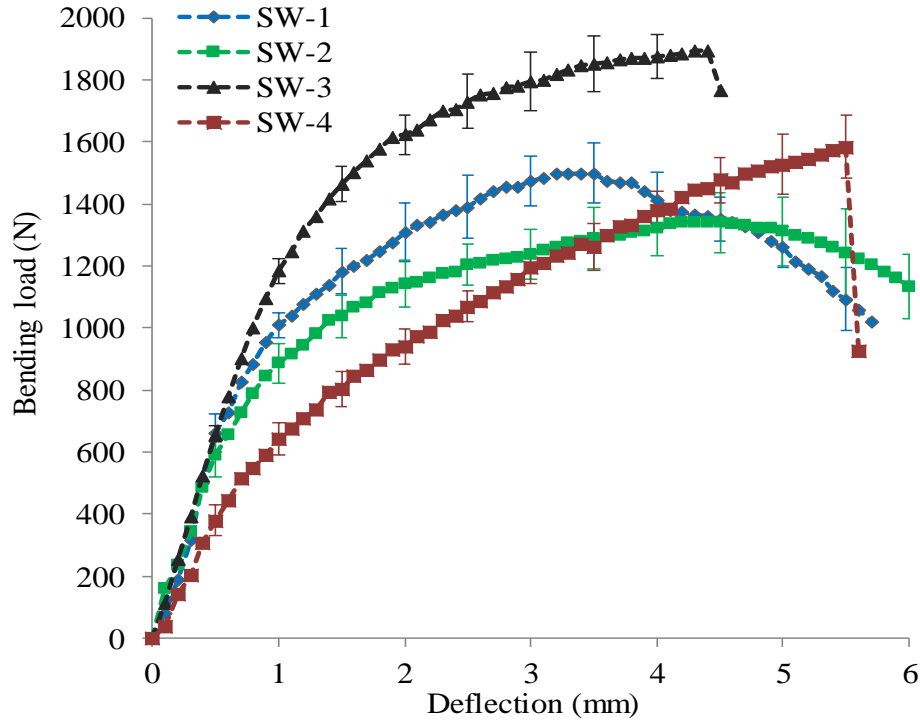
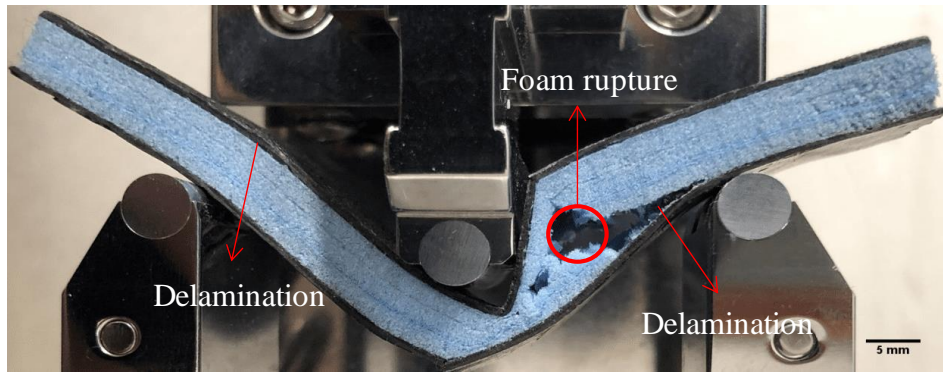


Figure 3.15 Bending load vs. deflection curves of the tested sandwich composites.

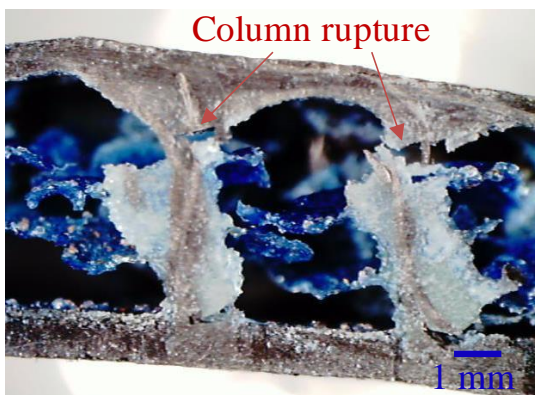
Table 3.5 Main properties of the tested sandwich composites in 3-point bending tests.

Sample ID	Failure load (N)		Maximum flexural strength (MPa)		Bending modulus (0-0.5 mm deflection) (GPa)	
	Average	CV	Average	CV	Average	CV
SW-1	1498.6	6.46%	215.85	6.46%	5.92	7.74%
SW-2	1342.7	8.47%	193.40	8.47%	5.60	8.80%
SW-3	1896.8	6.97%	273.20	6.97%	7.29	4.35%
SW-4	1584.9	6.54%	228.28	6.54%	7.58	7.31%

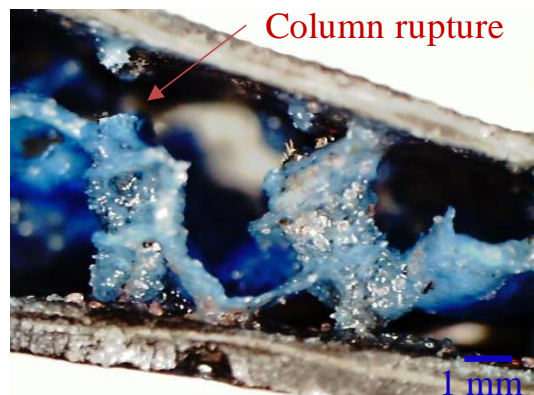
Figure 3.16 shows the structure and core failure modes of the sandwich samples during 3-point bending tests. To observe the failure mode of the core layer and TT columns, the foam is removed from all the samples after bending tests. The cross-section failures for sandwich samples are presented in Figure 3.16b.



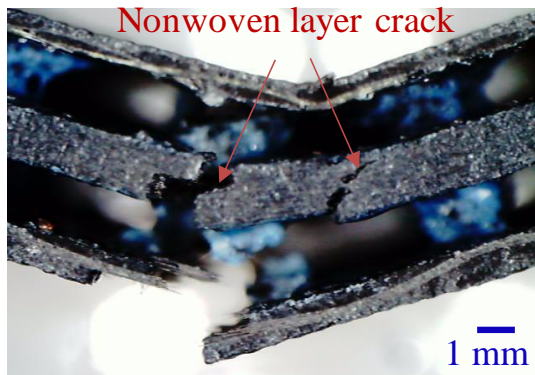
(a)



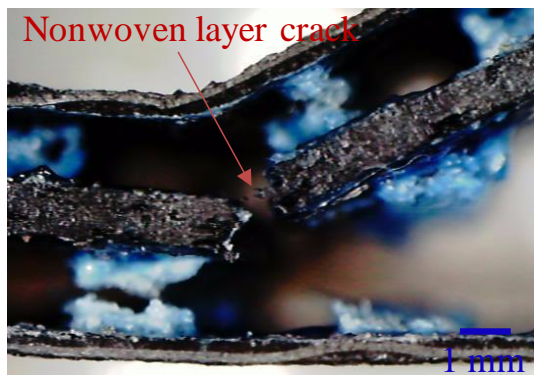
SW-1 sample



SW-2 sample



SW-3 sample



SW-4 sample

(b)

Figure 3.16 (a) Structure failure during 3-point bending test and (b) Observation of the cross-section failures.

Non-woven layer cracks are observed in SW-3 and SW-4 samples. However, the delamination between skin and foam layer is not observed. The ultimate core shear stresses of SW-3 and SW-4 are approximately 146% and 142% of SW-1 (as shown in Figure 3.17), which resulted in the cracks of TT columns. It can be seen from Figure 3.16b that the TT columns have deviated from the Z-direction when it fails. The rupture of the lower skin sheet can be only found in SW-3 and SW-4. Its core part has the highest shear strength (the non-woven as core layer), which will make the bending deflections of upper and lower skins tend to be consistent, resulting in increased deformation of the lower skin.

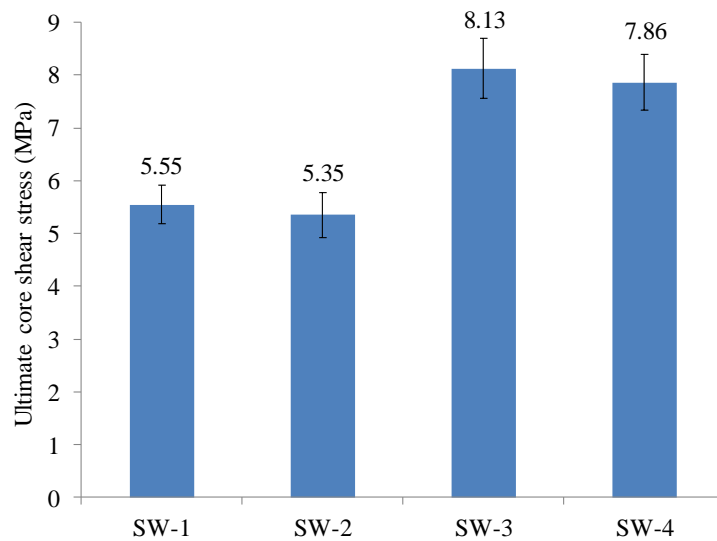


Figure 3.17 Core shear ultimate strength of sandwich samples in bending test.

To investigate the effect of each part in a sandwich beam, the equation of the flexural rigidity EI is used. The flexural rigidity of the core layers in SW-1 $(EI)_{l-1}$ is given as Eq. 21

$$(EI)_{l-1} = E_s \frac{bt^3}{6} + E_s \frac{bt(h-t)^2}{2} + E_f \frac{9bc_f^3}{4} \quad (3.24)$$

where E is the bending modulus, I is the area moment of inertia, E_s is the elastic modulus of the skins, E_f is the elastic modulus of the foam core, t and c_f are the thickness of skin and the single layer of foam, respectively as illustrated in Figure 3.14.

Applying the parallel axis theorem, the outcome for SW-3 and SW-4 samples is:

$$(EI)_{l-3,4} = E_s \frac{bt^3}{6} + E_s \frac{bt(h-t)^2}{2} + E_f \frac{bc_f^3}{6} + E_f \frac{bc_f(c_f + c_n)^2}{2} + E_n \frac{bc_n^3}{12} \quad (3.25)$$

where E_n is the elastic modulus of non-woven, c_n is the thickness of the non-woven layer.

Supposing that the cross-section of the column is square, the flexural rigidity of resin-thread column $(EI)_{col}$ is shown as :

$$(EI)_{col} = E_s \frac{bt^3}{6} + E_s \frac{bt(h-t)^2}{2} + E_{col} \frac{ac^3}{12} \quad (3.26)$$

where E_{col} is the elastic modulus of the resin-thread column, and a is the side length of the square, $a = 2\sqrt{\pi}$.

By using the sum of the rigidities of core layers $(EI)_l$ and the columns $(EI)_{col}$, the flexural rigidity and modulus of the sandwich can be obtained from [11] and shown in Eq. 3.24.

$$EI = (EI)_{col}v_{col} + (EI)_l(1 - v_{col}) \quad (3.27)$$

A comparison between the experimental and analytical results is given in Table 3.6. All the differences between these two series are included in the coefficient of variation; the analytical value gives a good prediction of bending performances. According to the analytical equations, the bending rigidity depends effectively on Young's modulus and the second area moment (I) of the skin sheet.

Table 3.6 Comparison of the experimental and analytical results of the bending.

Sample ID	Bending rigidity (kN·mm ²)			
	Experimental results	CV	Analytical results	Difference
SW-1	3487.50	9.31%	3802.96	9.04%
SW-2	3000.78	8.80%	3248.60	8.26%
SW-3	3462.50	7.35%	3678.79	6.25%
SW-4	2055.16	7.31%	2006.80	2.35%

Compared with the skins, Young's modulus of foam is much smaller (see Table 3.7), and the non-woven layer has a much smaller second area moment. These two small values result in a

limited value influence on the bending rigidity. Since SW-4 does not have tufted yarns, the two skins are flatter and thinner, resulting in smaller errors in the thickness and the second moment of area (I) of the skins, and therefore smaller differences between experimental and analytical predictions. The smaller thickness of SW-4 (resulting in a smaller second moment of area I) could also explain its lower bending stiffness compared to others.

Table 3.7 Material mechanical and physical properties used in the analytical investigation.

Materials	Young's modulus (MPa)	Thickness (mm)			
		SW-1	SW-2	SW-3	SW-4
Skin sheet	14374.43	0.64	0.58	0.75	0.58
Foam	16.00	2.14	-	1.82	1.59
Non-woven/resin layer	4291.20	-	-	1.45	1.12
TT columns	1070.00	6.43	5.70	5.09	4.30

3.3.4 Charpy impact test

The results of Charpy absorbed energy (Kj/m²) of each group are presented in Figure 3.18. The SW-3 has the highest impact strength (23.85 Kj/m²) among these 4 groups of samples. Foam has low fracture toughness (absorbed energy per square meter); it promoted the extension of crack from the top skin to the bottom skin by connecting these two skins. This resulted in a rupture of both two skins (as shown in Figure 3.19) and lower absorbed impact energy. Compared with the hollow structure (SW-2), the presence of the foam core (SW-1) increases the brittleness of the core. The absorbed energy of SW-3 is approximately 66% higher than that of SW-1 (14.38 Kj/m²). Pure epoxy resin and carbon fiber are normally considered brittle materials [23]. But toughness is related to both strength and brittleness. The tensile strength and elongation at break of the resin-infusion non-woven composite are measured as 63.79MPa and 1.49%, respectively. Compared with the parameters of foam (1.02MPa and 6.7%), it can be obtained that the non-woven composite layer has a higher toughness. This can contribute to improving the toughness of the whole sandwich structure. Moreover, the higher absorbed energy of the fiber/resin columns compared with the pure resin columns (SW-4) can be explained by the same mechanism.

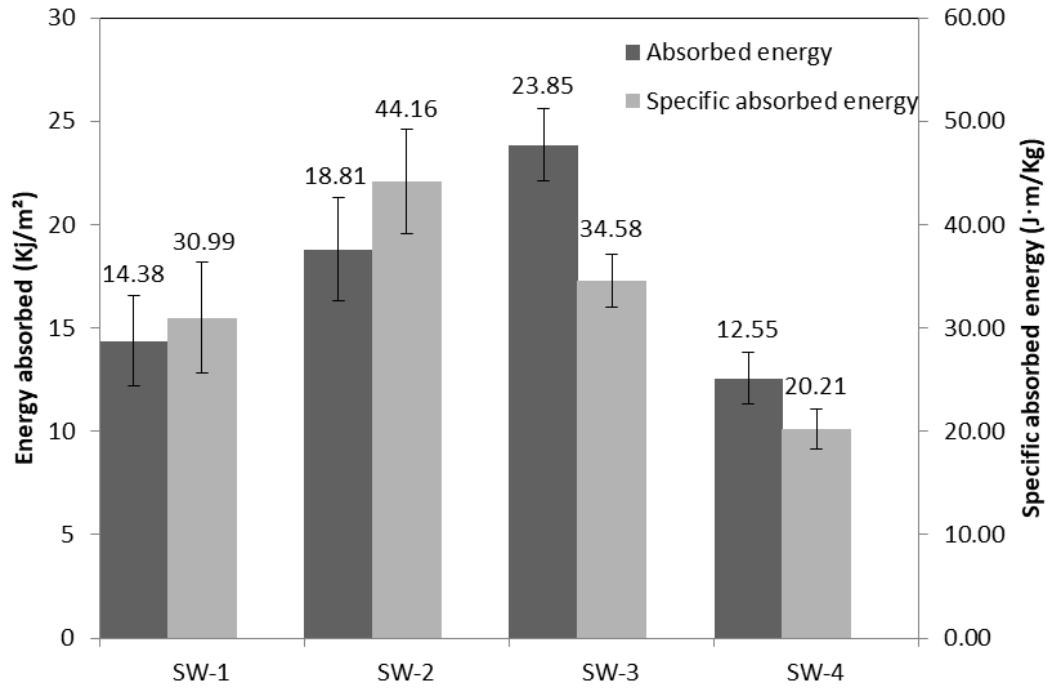


Figure 3.18 Impact energy absorbed during Charpy test.

The photographs of fractured samples of each set are presented in Figure 3.19. A brittle fracture tendency can be seen in the sandwich with core layers (SW-1, SW-3 and SW-4) by visual analysis, which shows more serious damage to the core structure. The delamination between core and skin can be observed in all sandwich groups except SW-1. And the cracks of foam and non-woven layers are determined. Fracture of columns occurred mainly at the connection points between the columns and composite layers (the fabric skin and the non-woven core ply), which is the weak zone of the column mechanical property.

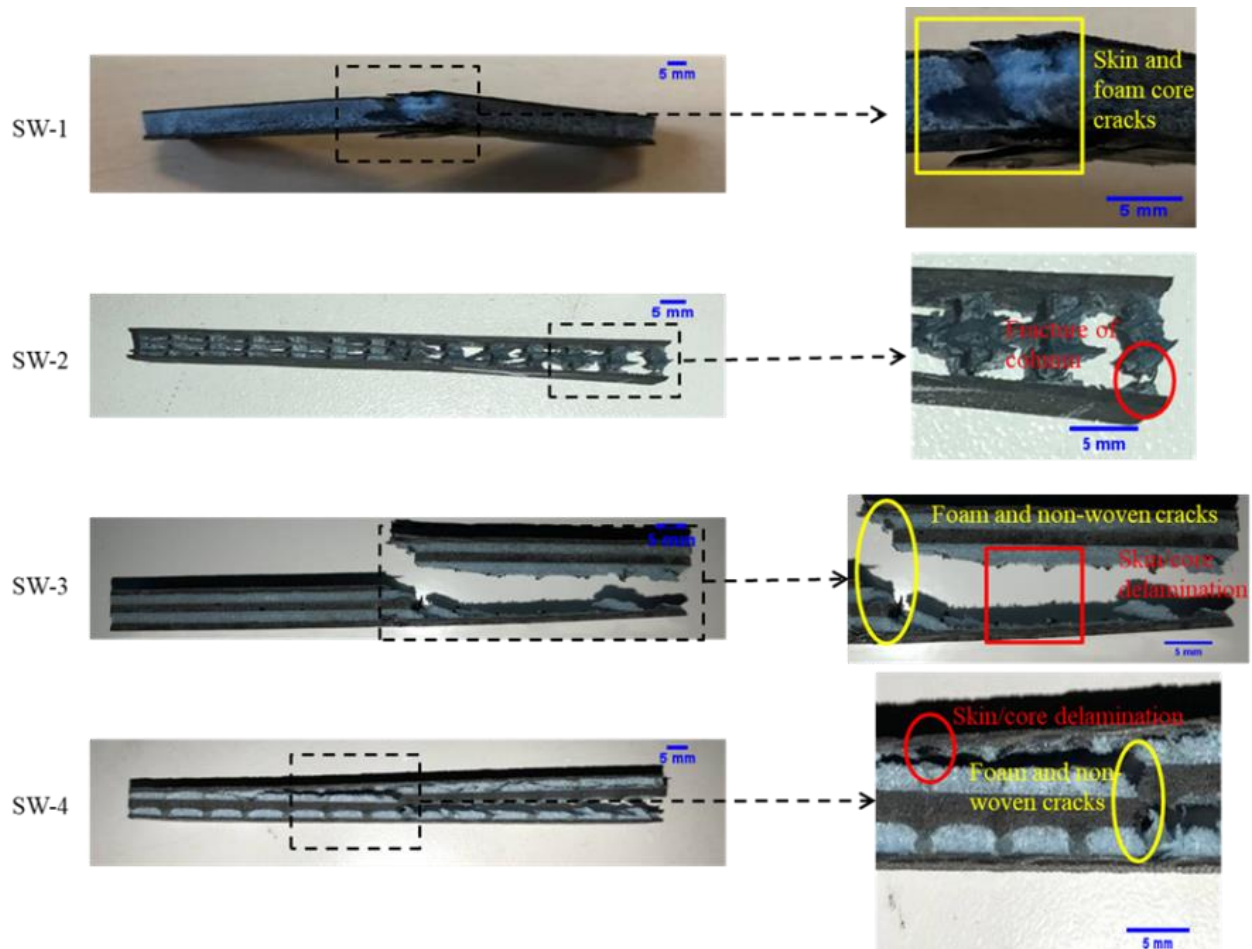


Figure 3.19 Fractured specimens after Charpy impact test.

3.3.5 Specific properties

Though the presence of non-woven and tufting thread can efficiently improve the mechanical performances of the sandwich composites, they also cause an increase in mass, which is not conducive to the lightweight characteristic. It means that the comparison of specific strength and specific modulus is more significant. The specific property can be defined by the following equation:

$$\text{Specific property} = \frac{\text{Measured property (MPa)}}{\text{Density of specimen (kg/m}^3\text{)}} \times 10^{-3} \quad (3.28)$$

Table 3.8 shows the specific stress under shear, compression, bending loadings and the specific fracture toughness of tested sandwich composites. Comparing SW-1 and SW-2 shows that the

specific value of ultimate shear stress, compressive stress and flexural stress of SW-1 are higher. Compared to the mass reduction brought by the removal of the foam (in SW-2 structure), the mechanical performance reduction is more obvious. However, this is reversed in terms of specific impact properties, with SW-2 having a higher specific fracture toughness than SW-1, due to the poor impact properties of the foam itself. In this case, the weight of the foam should not be neglected. The specific core shear stress and fracture toughness of SW-3 have increased by about 19% and 12% than SW-1. But the specific bending stress is reduced by 15%. The specific ultimate compressive stresses of these two are very close. Adding a nonwoven core is beneficial to improve the specific shear and impact performance, but not to the specific bending performance, and has no significant effect on the compression stress. All specific properties of SW-3 are obviously higher than SW-4, which indicates that the tufted yarn can effectively improve the mechanical properties of the sandwich panel and at the same time ensure that the sample weight does not increase much.

Table 3.8 Specific mechanical properties of sandwich composites.

Sample ID	Specific mechanical properties			
	Core shear stress (kN·m/kg)	Compressive stress (kN·m/kg)	Bending stress (kN·m/kg)	Fracture toughness (kJ·m/g)
SW-1	3.36	9.52	465.16	30.99
SW-2	1.42	7.60	454.07	40.16
SW-3	3.99	9.27	396.07	34.58
SW-4	1.09	5.55	367.57	20.21

For specific shear and compressive modulus (see Table 3.9), SW-1 presents higher values than SW-2. And they have a similar specific value of bending modulus (difference about 4%). The hollow sandwich structure SW-2 does not have advantages. Compared with SW-3, the specific compressive modulus and bending modulus are larger but the core shear modulus is smaller. Nonwoven layer is too heavy after absorption of resin. Both specific shear modulus and compressive modulus of SW-3 are higher than SW-4, while the bending modulus is contrast. The main limitation over the specific mechanical properties is the significant increase in weight brought by the nonwoven and tufting yarn. The increase in mass is caused by the absorption of

excessive resin. The nonwoven is due to the high porosity and hygroscopicity itself [24][25], and the tufting thread is due to the formation of channels through the thickness.

Table 3.9 Specific modulus of sandwich composites under different loadings.

Sample ID	Specific modulus (kN·m/kg)		
	Core shear	Flatwise compression	Three-point bending
SW-1	22.00	138.61	$1.27 \cdot 10^4$
SW-2	14.30	95.70	$1.32 \cdot 10^4$
SW-3	23.38	97.46	$1.06 \cdot 10^4$
SW-4	25.50	72.17	$1.22 \cdot 10^4$

Therefore, if the follow-up research can effectively reduce the resin increase caused by non-woven fabrics, it can effectively improve the specific strength and specific modulus of sandwich composites, and increase the potential to replace foam core sandwiches in a wider industrial range.

3.4 Conclusion

As demonstrated in the chapter, the sandwich structures with a non-woven core layer and the tufting threads are successfully designed and manufactured. The mechanical performances under core shear, flatwise compression, flexural and Charpy impact loadings are investigated to understand the effect caused by the foam, tufting yarn, and the non-woven mat as the core layer in a sandwich structure. Tufting yarn in Z-direction and the non-woven core layer can effectively improve the mechanical properties of the sandwich panel. However, the effect of tufted and nonwoven on specific mechanical properties has both advantages and disadvantages. The increase of sample weight by adding non-woven is more significant compared to improved absorbed energy, which results in a lower specific mechanical property. The tufting threads have a positive effect on all specific mechanical properties except specific bending modulus. Therefore, subsequent studies can vary the number of tufting points and determine the optimal tufting density to obtain the best improvement of mechanical properties.

Reference

- [1] Nanayakkara A, Feih S, Mouritz AP. Experimental analysis of the through-thickness compression properties of z-pinned sandwich composites. *Compos Part A Appl Sci Manuf* 2011;42:1673–80. <https://doi.org/10.1016/j.compositesa.2011.07.020>.
- [2] Reis EM, Rizkalla SH. Material characteristics of 3-D FRP sandwich panels. *Constr Build Mater* 2008;22:1009–18. <https://doi.org/10.1016/j.conbuildmat.2007.03.023>.
- [3] Che L, Xu G dong, Zeng T, Cheng S, Zhou X wei, Yang S cai. Compressive and shear characteristics of an octahedral stitched sandwich composite. *Compos Struct* 2014;112:179–87. <https://doi.org/10.1016/j.compstruct.2014.02.012>.
- [4] Yalkin HE, Icten BM, Alpyildiz T. Enhanced mechanical performance of foam core sandwich composites with through the thickness reinforced core. *Compos Part B Eng* 2015;79:383–91. <https://doi.org/10.1016/j.compositesb.2015.04.055>.
- [5] Zheng XT, Zhang JF, Yang F, Chai YN, Li Y. Experimental and analytical study on the mechanical behavior of stitched sandwich composite panel with a foam core. *Adv Mater Res* 2008;33–37 PART:477–82. <https://doi.org/10.4028/www.scientific.net/amr.33-37.477>.
- [6] Reis EM, Rizkalla SH. Material characteristics of 3-D FRP sandwich panels. *Constr Build Mater* 2008;22:1009–18. <https://doi.org/10.1016/j.conbuildmat.2007.03.023>.
- [7] Long D, Guiqiong J, Tao H. Investigation of the effect of Z-pin reinforcement on the collapse of foam-cored sandwich panels. *J Reinf Plast Compos* 2008;27:1211–24. <https://doi.org/10.1177/0731684407087739>.
- [8] Nishi Y, Tsuchikura N, Nanba S, Yamamoto T, Faudree MC. Charpy impact of sandwich structural composites (CFRP/PC/CFRP) of polycarbonate (PC) cores covered with carbon fiber cross textile reinforced epoxy polymer (CFRP) thin sheets as a function of temperature. *Mater Trans* 2012;53:1288–94. <https://doi.org/10.2320/matertrans.M2011357>.
- [9] K. Srivastava V. Impact Behaviour of Sandwich GFRP-Foam-GFRP Composites. *Int J Compos Mater* 2012;2:63–6. <https://doi.org/10.5923/j.cmaterials.20120204.04>.
- [10] Lascoup B, Aboura Z, Khellil K, Benzeggagh M. Prediction of out-of-plane behavior of stitched sandwich structure. *Compos Part B Eng* 2012;43:2915–20. <https://doi.org/10.1016/j.compositesb.2012.07.002>.
- [11] Wang P, Lei Y, Yue Z. Experimental and numerical evaluation of the flexural properties of stitched foam core sandwich structure. *Compos Struct* 2013;100:243–8. <https://doi.org/10.1016/j.compstruct.2012.12.040>.
- [12] Vaidya UK, Kamath M V., Hosur M V., Mahfuz H, Jeelani S. Low-Velocity Impact Response of Cross-Ply Laminated Sandwich Composites with Hollow and Foam-Filled Z-Pin Reinforced Core. *J Compos Technol Res* 1999;21:84–97. <https://doi.org/10.1520/ctr10950j>.
- [13] Zuoguang Z, Jijun H, Min L, Yizuo G, Zhijie S. Mechanical performance of X-truss/foam sandwich construction. *J Reinf Plast Compos* 2009;28:2631–43. <https://doi.org/10.1177/0731684408093319>.
- [14] Liu LS, Zhang T, Wang P, Legrand X, Soulat D. Influence of the tufting yarns on formability of tufted 3-Dimensional composite reinforcement. *Compos Part A Appl Sci Manuf* 2015;78:403–11. <https://doi.org/10.1016/j.compositesa.2015.07.014>.
- [15] Cartié DDR, Dell'Anno G, Poulin E, Partridge IK. 3D reinforcement of stiffener-to-skin T-joints by Z-pinning and tufting. *Eng Fract Mech* 2006;73:2532–40. <https://doi.org/10.1016/j.engfracmech.2006.06.012>.

- [16] ASTM Standard C273. ASTM C393-06 Standard Test Method for Core Shear Properties of Sandwich Constructions by Beam Flexure. *ASTM Int* 2010;i:1–7. <https://doi.org/10.1520/C0273>.
- [17] Materials C. Standard Test Method for Flatwise Compressive Properties of Sandwich Cores 1. *Current* 2003;i:2–4. <https://doi.org/10.1520/C0365>.
- [18] International A. ASTM D7264 Standard Test Method for Flexural Properties of Polymer Matrix Composite Materials. *Annu B ASTM Stand* 2007;i:1–11.
- [19] ISO-Committee. *Plastics - Determination of Charpy impact properties (ISO 179-1)*. 2010.
- [20] Liu LS, Wang P, Legrand X, Soulat D. Investigation of mechanical properties of tufted composites: Influence of tuft length through the thickness reinforcement. *Compos Struct* 2017;172:221–8. <https://doi.org/10.1016/j.compstruct.2017.03.099>.
- [21] Tita V, Caliri MF. Numerical simulation of anisotropic polymeric foams. *Lat Am J Solids Struct* 2012;9:259–79. <https://doi.org/10.1590/s1679-78252012000200005>.
- [22] May-Pat A, Avilés F, Aguilar J. Mechanical properties of sandwich panels with perforated foam cores. *J Sandw Struct Mater* 2011;13:427–44. <https://doi.org/10.1177/1099636210379769>.
- [23] Junaedi H, Albahkali E, Baig M, Dawood A, Almajid A. Ductile to Brittle Transition of Short Carbon Fiber-Reinforced Polypropylene Composites. *Adv Polym Technol* 2020;2020. <https://doi.org/10.1155/2020/6714097>.
- [24] Mao N, Russell SJ. *Fibre to Fabric: Nonwoven Fabrics*. Elsevier Ltd; 2015. <https://doi.org/10.1016/B978-1-84569-931-4.00013-1>.
- [25] Albooyeh A, Eskandarzadeh S, Mousavi A. Influence of different foaming conditions on the mechanical, physical, and structural properties of polypropylene foam. *Mech Adv Compos Struct* 2019;6:225–37. <https://doi.org/10.22075/MACS.2019.15614.1160>.

**CHAPTER 4. CHARACTERIZATION
OF THE MECHANICAL BEHAVIOR
OF TUFTED FLAX FIBER
REINFORCED SANDWICH
COMPOSITES**

4.1 Introduction

There has been an increasing interest in using natural fibers to replace glass fibers for composite reinforcement in recent years [1]. Among a number of natural fibers, flax fiber has been considered as a replacement because of its outstanding mechanical properties and low cost [2–4]. In Chapter 3, replacing the foam with a nonwoven mat has been verified to enhance the mechanical properties of the tufted sandwich composite. The presence of both nonwoven layer and tufting thread can effectively improve the shear, bending and impact behaviors.

Therefore, this sandwich structure is adopted to manufacture a green sandwich panel and the effect of tufting density is investigated in this chapter. Several experimental and numerical studies have been conducted concerning the flax fiber-reinforced sandwich. In most of them, the sandwich structures had a homogeneous core [5-9]. The authors adopted other methods to enhance the interfacial bond strength rather than avoiding delamination damage by adding z-directional reinforcement.

As mentioned in the literature of Chapter 3, a number of investigations have been done to analyze the mechanical performance of sandwich composite with through-the-thickness reinforcement, such as z-pin [10][11], stitching [12–14] and tufting [15–20]. However, these studies mostly focused on the optimization of the tufting process and less on the improvement of the core layer structure. In this chapter, both core layer improvement and tufting reinforcement are investigated to verify the specific mechanical property of this sandwich structure and analyze the influence of tufting density.

4.2 Materials and methods

4.2.1 Sandwich panel manufacture

As the two aims of this study are respectively to fabricate a green tufted sandwich composite and to improve the specific mechanical performance, a bio-based epoxy resin is adopted as a matrix in addition to the flax fiber textile reinforcement. This sandwich structure is developed from the structure in Chapter 3 and considers the tufting density as an independent variable. The stacking order from top to bottom is flax weaving fabric, foam, nonwoven mat; foam and one more layer of flax weaving fabric (see Figure 4.1).

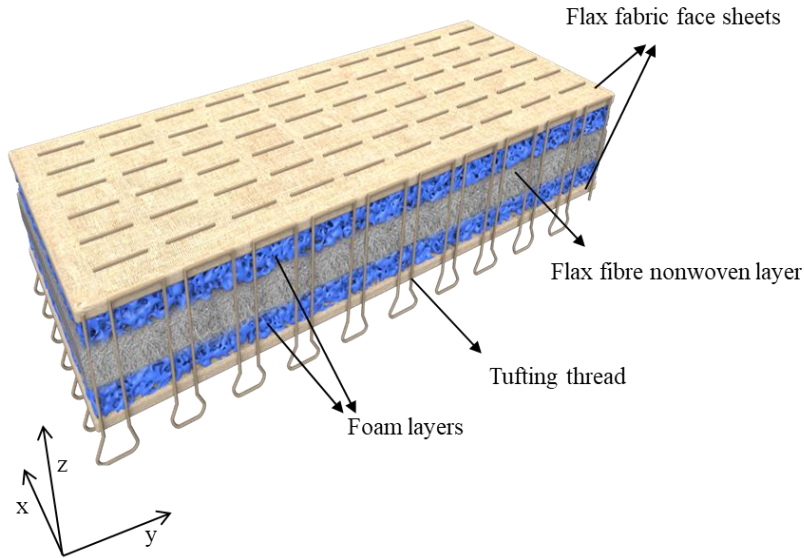


Figure 4.1 Schematic of a flax fiber reinforced sandwich panel.

For all different groups, the skins are one layer of weaving fabric, and the core includes at least one layer of nonwoven. After stacking, the flax thread is tufted into the dry fabrics through a hollow needle of 2 mm diameter. This yarn is twisted with a single spindle hand reeling machine and its linear density is 500 Tex. Parameters of the core, skin, and tufting thread are presented in Table 4.1.

Table 4.1 Parameters of sandwich raw materials.

Composition of structure	Density	Young's modulus
Weaving fabric skin	189 g/m ²	98.42 MPa
Nonwoven core	354 g/m ²	23.45 MPa
Tufting thread	Linear density: 500 Tex	4233.68 MPa
Foam	138 g/m ²	10.46MPa

Five groups of sandwich panels are prepared in different tufting densities (spacing of 6 mm, 8 mm, 10 mm, 12 mm and no tufting thread). The final flax-fiber reinforced sandwich panels are manufactured by LRI process. Given the hygroscopic nature of flax fibers, all dry fibrous preforms needed to be allowed to stand for at least 24 hours at constant temperature and humidity before resin impregnation. The loops are cut off to prevent excessive yarn build-up at the bottom,

resulting in increased panel thickness and resin over-absorption. A bio two-component epoxy system (InfuGreen resin 810/hardener SD 8825.2), produced by Sicomin, is used as the matrix. As explained in Chapter 3, if both foam and nonwoven are used but without tufting, the resin infusion process cannot be carried out smoothly. This is because the foam on both two sides of the nonwoven will isolate the resin, resulting in no adhesion between the nonwoven and the foam. Therefore, the non-tufted sandwich preform with the same layers as the tufted sandwich structure is not adopted as a contrast. The foam is all replaced by nonwoven with the approximate dimensions to realize the resin infusion for the non-tufted sandwich sample. The thickness of the non-tufted sandwich panel can be controlled by modifying the number of nonwoven layers. Once the liquid matrix is well cured, the sandwich composite panels are cut in different dimensions with a saw machine.

As described in Chapter 2, the tufting density is the number of tufting points per unit area, it can be obtained by the tufting spacing (as shown in Table 4.2). SW in the table represents the sandwich composite. For facilitating the identification, a characteristic label is used for each group. For instance, T0 indicates that the sandwich is not tufted; T6, T8, T10 and T12 show that the tufting spaces are 6 mm, 8 mm, 10 mm and 12 mm, respectively. The volume fraction is calculated by the inverse method: measure the exact weights of fiber reinforcement and of resin, then their volumes are obtained by the weight and knowing fiber and matrix density.

Table 4.2 Relation between tufting density and tufting spacing.

Sample ID	Tufting spacing	Tufting density for different tests			Thickness	Fiber volume fraction
		Core shear test	Three-point bending test	Charpy Impact test		
SW-T0		No tufted			7.03±0.12 mm	30%
SW-T6	6 mm	32	54	16	7.50±0.53 mm	30%
SW-T8	8 mm	24	20	12	7.34±0.60 mm	31%
SW-T10	10 mm	21	16	10	7.42±0.68 mm	35%
SW-T12	12 mm	10	12	8	7.27±0.65 mm	35%

*SW: Sandwich composite

4.2.2 Test methods

The sandwich panels are tested under core shear, three-point bending and Charpy impact loadings (as shown in Figure 4.2). Core shear tests are conducted in accordance with ASTM C 273 [21]. A series of coupons, 65 mm × 25 mm, are prepared with the different five tufting configurations and tested. The load is applied at a constant crosshead displacement of 2 mm/min. The applied force is used to calculate the stress imparted to the sandwich structure, while the shear strain is simply the displacement divided by the thickness of the sandwich core.

Static three-point bending tests of all the sandwich beams are performed in accordance with the ASTM D 7264 standard [22]. Five coupons are tested to determine their flexural properties. Due to the similar thicknesses of the sandwich panels, all the sample dimensions and test setups are uniform to achieve the same span-to-depth ratio. According to the standard, a support span-to-depth ratio of 16:1 is used and the load is applied at the center point of the length of the span. The length of the samples is 160 mm and their width is 15 mm. All of the tests are performed at a constant crosshead displacement of 1 mm/min.

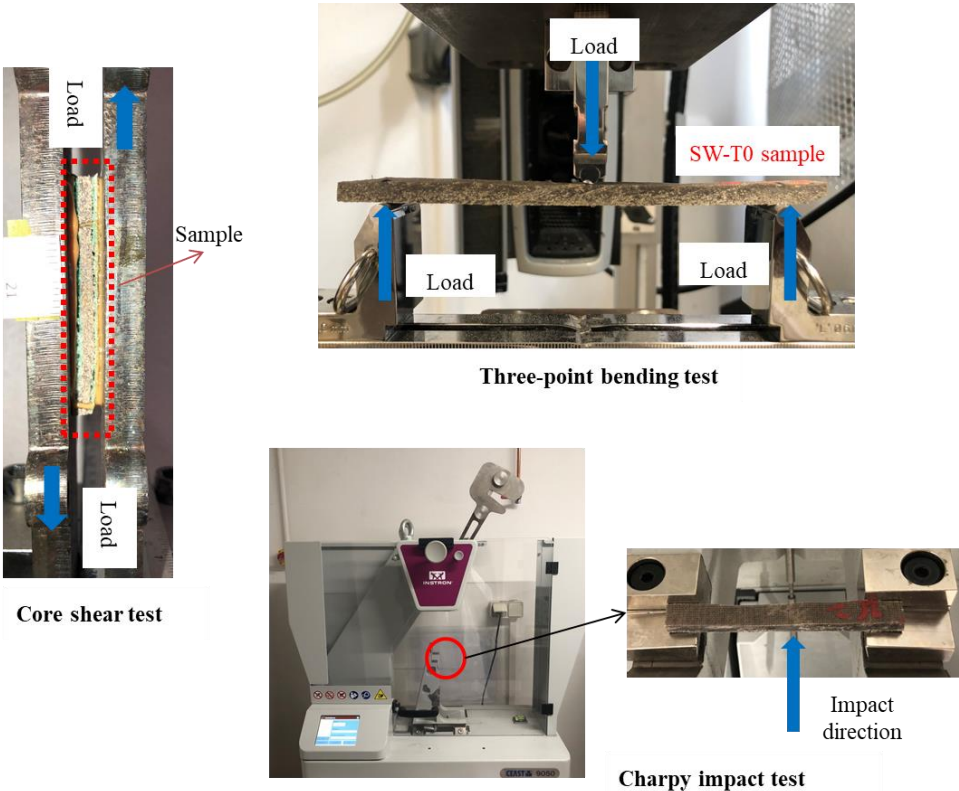


Figure 4.2 Experimental set-ups for different loadings.

In order to evaluate the impact fracture toughness, the Charpy impact values of the sandwich panels are measured according to EN ISO 179-1 [23]. The sandwich samples are cut with dimensions 100 mm × 10 mm.

Since the test standards adopted are the same as those in Chapter 3, the calculation methods of these test results are also in accordance with the equations of the previous chapter (Equations 3.1-3.6) are not listed separately here.

4.3 Results and discussion

4.3.1 Core shear test

Shear stress-shear strain curves of tufted sandwich composites can be seen in Figure 4.3. The shear modulus, maximum shear stress and the coefficient of variation (CV) are listed in Table 4.3. It can be obtained that the ultimate shear stress and shear modulus of the sandwich structure increases with the increase of tufting density. In addition, the cracking sound is already heard during the linear stage, indicating that the resin columns in the specimen are cracked at this point. As the loading continued, cracking sound increased, shear stress continued to rise and finally the failure occurred. But the structure still bore the loading because of the presence of flax thread. The figure also shows that the linear phases of the curves for SW-T6, SW-T8 and SW-T10 are overlapping and thus their shear moduli are close.

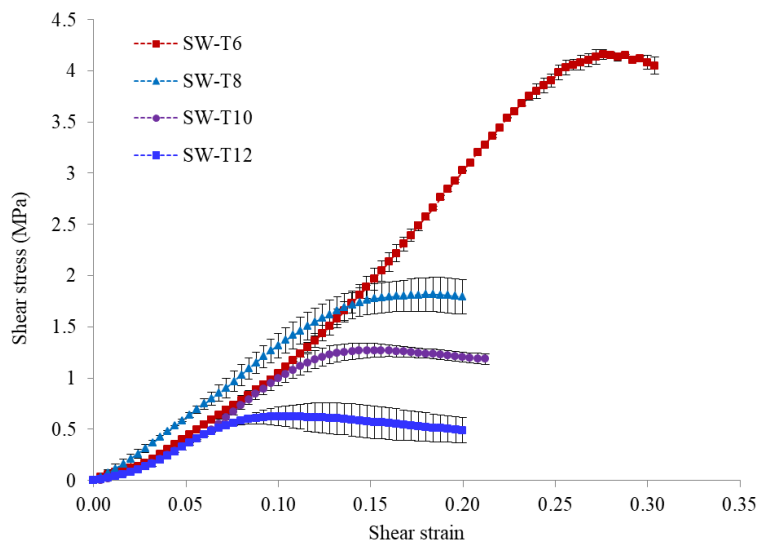


Figure 4.3 Typical stress-strain curves of core shear behavior of tufted sandwich panels.

Shear stress-strain curves of SW-T0 and SW-T6 can be seen in Figure 4.4. First, it can be seen that both shear stress and shear modulus of the sandwich panel with the pure nonwoven core is much higher. And the curve shows a typical brittle fracture characteristic as it suddenly drops after reaching the highest point. This is attributed to the fact that SW-T0 had no fiber reinforcement in the thickness direction and the interface between the nonwoven core layers had similar properties to the resin which exhibits a high brittleness.

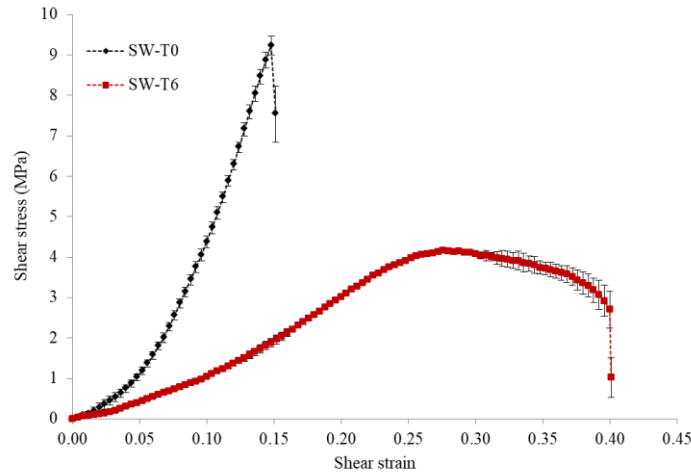


Figure 4.4 Typical core shear stress-strain curves of SW-T0 and SW-T6.

Although considering the weight of the sample, the sandwich with foam layer showed a much lower specific property than the sandwich panel without foam. The foam with a low shear modulus (measured as 3.3Mpa) severely weakens the shear resistance of the sandwich structure. For those tufted sandwich panels, both specific ultimate shear stress and specific shear modulus are positively correlated with tuft density.

Table 4.3 Mechanical properties of sandwich composites in the shear test.

Sample ID	Ultimate core shear stress			Shear modulus		
	Average (MPa)	CV	Specific value (kN·m/kg)	Average (MPa)	CV	Specific value (kN·m/kg)
SW-T0	9.37	3.29%	11.34	85.89	8.81%	103.99
SW-T6	4.16	1.17%	7.31	17.68	3.38%	31.06
SW-T8	1.81	14.36%	3.59	10.98	6.13%	28.34
SW-T10	1.27	4.96%	2.71	10.46	5.79%	29.02
SW-T12	0.63	14.30%	1.48	9.47	3.56%	22.23

The failure mechanisms of these different samples under shear loading are illustrated in Figure 4.5. For the tufted cores, the dominant mode of failure is that of the core/skin interface, including the column tips cracks, the foam cracks and fiber pull-out. During shear testing, the top skin, bottom skin and central nonwoven absorbed liquid resin and formed composite layers which presented better mechanical performance than foam. Complete cracks of foam are observed in all tufted sandwich specimens before the final structure failure. The rotation of columns caused by shear force made the matrix around column tips crack relatively easy. This also resulted in the fiber of tufting thread being pulled out from resin. This would suggest that the effect on the shear resistance of column reinforcements is much stronger than the foams under shear loading. Increasing the tufting density can efficiently enhance the shear properties of the structure.

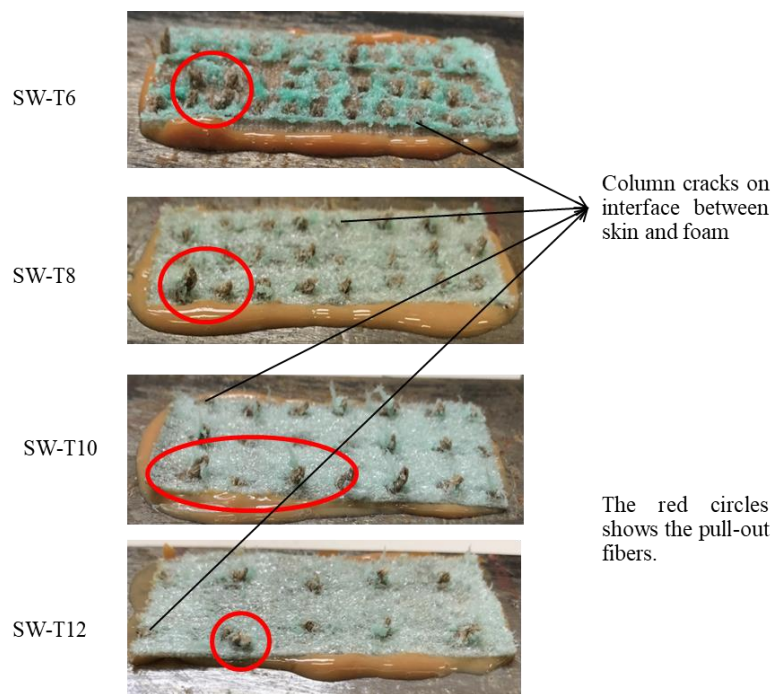


Figure 4.5 Fracture modes of tufted sandwich panels.

The SW-T6 has the same tufting density and core structure as SW-3 in Chapter 3. The fiber reinforcement of the former is made of flax fiber, while the latter is made of carbon fiber. The comparisons of the basic bending properties of these two sandwich panels are listed in Table 4.4. The higher value of flax fiber-reinforced sandwich panels can be attributed to the higher modulus of the resin (1.34 GPa) than that of the resin for carbon fiber reinforced sandwich panel (1.07 GPa). The diameter of the flax yarn (500 Tex) is much larger than that of the carbon fiber yarn (2

× 67 Tex), while the diameters of the tufting needles adopted are equal. Therefore, in the final fiber/resin columns, there are fewer winding flax yarns and the slippage is less, which reduced the strain range and increased the slope (shear modulus).

Table 4.4 Core shear properties of flax fiber-reinforced and carbon fiber-reinforced sandwich panels.

Sample ID	Ultimate core shear stress			Shear modulus		
	Average (MPa)	CV	Specific value (kN·m/kg)	Average (MPa)	CV	Specific value (kN·m/kg)
SW-3	2.75	8.60%	3.99	16.13	6.13%	23.38
SW-T6	4.16	1.17%	7.31	17.68	3.38%	31.06

As described in last chapter, the shear modulus of tufted sandwich with both nonwoven and foam core layers G_{zx} can be presented as:

$$G_{zx} = G_{col}v_{col} + \frac{G_f G_n}{G_f v_n + G_n v_f} (1 - v_{col}) \quad (4.1)$$

where v is the volume fraction, G is the shear modulus. The subscripts col , n and f represent the tufting column reinforcement, nonwoven layer and the foam layer respectively.

Obviously, the overall shear modulus of the sandwich panel is proportional to the shear modulus of tufting thread/resin columns and also of the core layers, and is positively correlated with the volume fraction of which component has a higher shear modulus. In this work, the shear modulus of columns is much larger than that of integration of nonwoven and foam layers. Therefore the higher is the volume fraction of the column; the larger is the shear modulus of the sandwich panel, which is consistent with the above results. The comparison between experiment and prediction results is shown in Table 4.5.

Table 4.5 Experiment and prediction results of the core shear modulus.

Sample ID	Shear modulus (MPa)			
	Experimental result	CV	Prediction value	Difference
SW-T6	17.68	3.38%	19.72	11.51%
SW-T8	10.98	6.13%	16.06	12.56%
SW-T10	10.46	5.79%	14.69	8.04%
SW-T12	9.47	3.56%	9.67	2.12%

It can be found that the prediction values of all samples are higher than their experimental results, except for the SW-T12 whose prediction value is inside the error range. The equations presented better predictions for carbon fiber reinforced sandwich composite in Chapter 3. Compared with carbon fiber, flax fiber is discontinuous and has a larger variation in yarn number [24][25]. Thus it resulted in a large error of mechanical properties of sandwich panels.

4.3.2 Three-point bending test

The flexural load-deflection curves of sandwich panels tufted in different densities are shown in Figure 4.6, respectively. It is found that the augmentation of tufting density had a very obviously positive effect on the bending properties of the sandwich structure. In order to clearly compare the differences, the failure load, flexural stress and flexural modulus are listed in Table 4.6. The improvement of the flexural modulus and maximum flexural stress brought by increasing tufting points is obvious. This is because, under the bending testing condition, the delamination is the main fracture mode of the structure. In this case, the through-the-thickness reinforcements which can effectively prevent the delamination had a positive effect on increasing ultimate flexural stress. Similar to the core shear experimental results, these curves can be also roughly divided into two stages before the failure. The first stage starts from the initial point to the complete breaking of the resin. In this stage, the load increases linearly with the increase of displacement. The second stage starts after the resin crack. During the stage the foam, nonwoven and bottom skin all fractured.

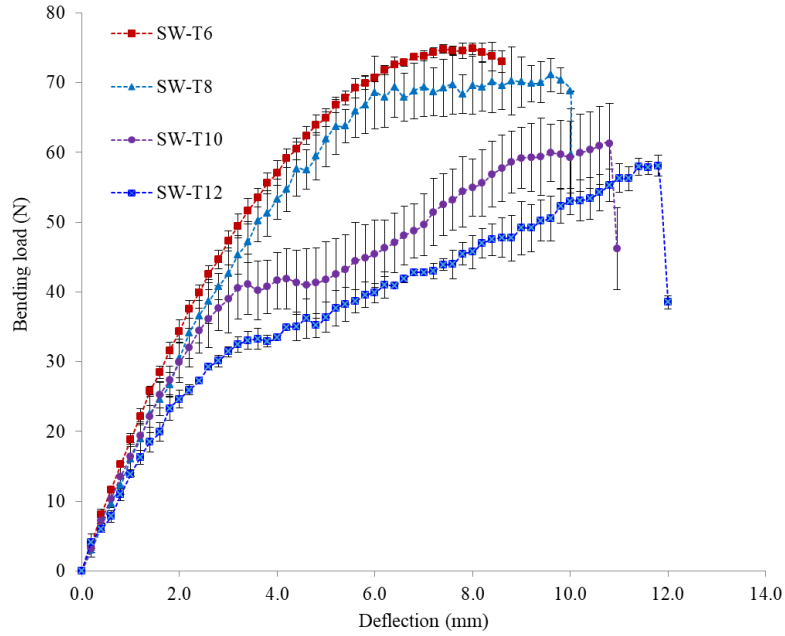


Figure 4.6 Typical bending load-deflection curve plots for each tufting density.

Regarding the core type, the sandwich with pure nonwoven core showed a much higher failure load as the higher mechanical properties of nonwoven/resin composite layers than foam layer (see Figure 4.7). The weak mechanical properties of the foam severely limited the flexural performance of the sandwich structure.

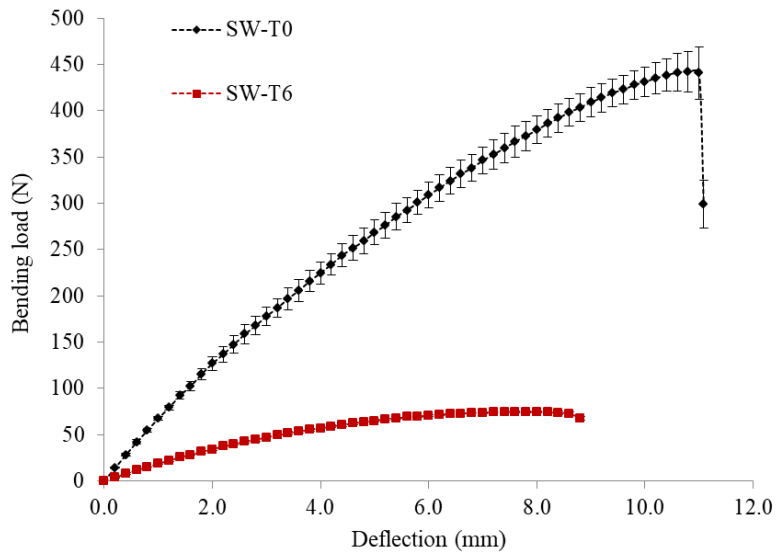


Figure 4.7 Typical bending load-deflection curves of SW-T0 and SW-T6.

From Table 4.6 it can be obtained that the specific ultimate stress and bending modulus decreased with tufting density increasing. The increased weight is more obvious compared to the improved mechanical properties brought by the tufted threads. Tufting density of spacing 8 mm presented the highest improvement on specific ultimate stress. While for the bending modulus, SW-T10 showed the highest value.

Table 4.6 Flexural properties of each group of sandwich panel.

Sample ID	Failure load (N)		Maximum flexural stress (MPa)		Specific stress (kN·m/kg)	Bending modulus (MPa)		Specific modulus (kN·m/kg)
	Average	CV	Average	CV		Average	CV	
SW-T0	442.15	4.88%	100.20	4.88%	121.32	4423.47	4.74%	5355.64
SW-T6	74.84	1.15%	14.90	1.15%	26.18	1015.96	2.13%	1784.91
SW-T8	71.06	3.41%	14.46	3.41%	28.71	946.75	9.12%	1879.98
SW-T10	61.23	9.46%	12.73	9.46%	27.16	909.41	10.33%	1940.57
SW-T12	56.43	2.59%	11.96	2.59%	28.08	785.35	3.89%	1844.24

Figure 4.8 presents the main failure mode of each group of the sandwich sample. The complete rupture of bottom skin can be observed in almost all the panels. The major failure modes of SW-T0 are fiber fracture and fiber pull-out, which is probably due to its high resin content. Besides, delamination occurred in all tufted sandwich panels except SW-T6. The resistance of the tufted reinforcement to delamination is obvious. The fracture of the nonwoven layer becomes less and less pronounced as the tufting density decreases. Its complete fracture can still be observed in SW-T6. However, in the other three groups of samples, there is partial fracture or only the resin matrix fracture. On the one hand, the higher resin content of SW-T6 increased the brittleness of the structure; on the other hand, the high tufting density makes the shear strength of the core layer of the samples increase, and the deformation in the Z-axis direction of each layer under flexural load tended to be uniform, increasing the deformation of the foam layer, the non-woven layer and the bottom skin layer, which are more prone to fracture. For the SW-T10 and SW-T12, their main fracture modes are delamination between foam and other layers, rupture of columns and of the bottom skin. In SW-T8, besides the three modes, the crack of foam is also obvious. As for SW-T6, the same failure modes as the other samples are bottom skin layer fracture and foam cracking, with the difference that complete fracture of the nonwoven layer is also observed.

The purple circles show pull-out fiber, the red is delamination.

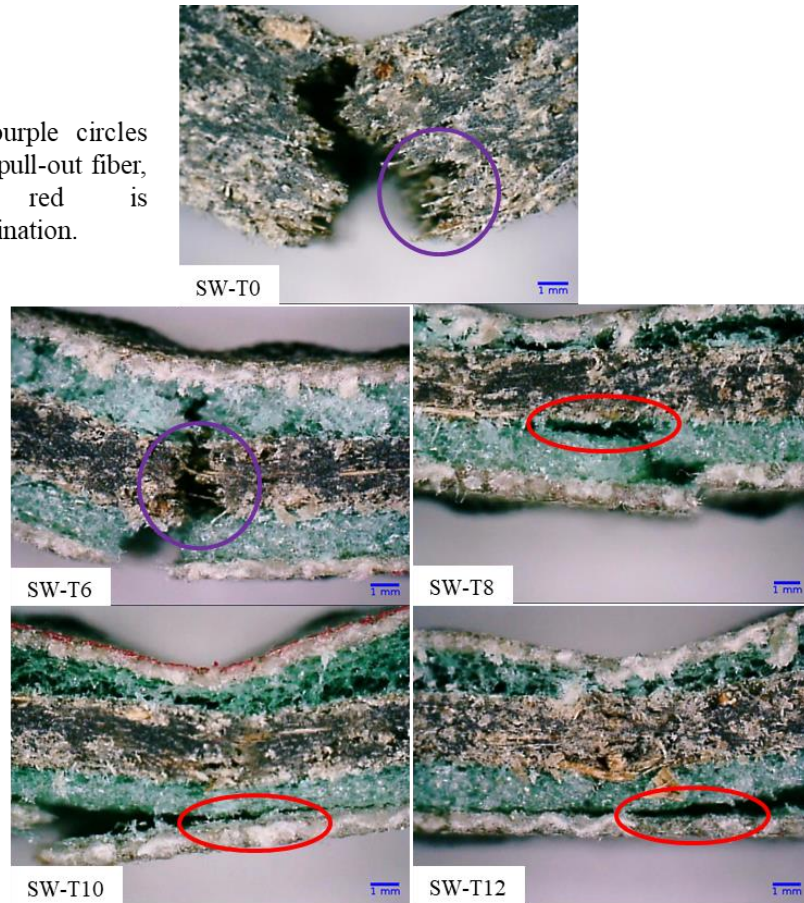


Figure 4.8 Fracture modes of each group of sandwich panel.

The comparisons of the basic bending properties between SW-T6 and SW-3 are listed in Table 4.7. It can be seen that the values of SW-3 are much higher than SW-T6. Since the bending performance is most affected by the tensile modulus of the skin and its cross-sectional moment of inertia, the carbon fiber skin will result in a larger bending modulus of the sandwich panel due to its larger tensile modulus ($1.44 \cdot 10^4$ MPa) than that of flax fiber skin (1479 MPa).

Table 4.7 Bending properties of tufted sandwich panels in carbon fiber and in flax fiber.

Sample ID	Ultimate bending stress			Bending modulus				
	Average (MPa)	CV	Specific value (kN·m/kg)	Average (MPa)	CV	Specific value (kN·m/kg)	Prediction value (MPa)	Difference
SW-3	273.20	6.97%	396.07	7292.28	4.35%	$1.06 \cdot 10^4$	7749.21	6.25%
SW-T6	14.90	1.15%	26.18	1015.96	2.13%	1784.91	1139.24	12.13%

As the tufted sandwich structure is similar to the carbon fiber reinforced sandwich composite SW-3, the equations 3.25-27 can be also applied in this section. However, the difference between the experimental results and the predicted values of SW-T6 is beyond the error range (see Table 4.7).

$$(EI)_l = E_s \frac{bt^3}{6} + E_s \frac{bt(h-t)^2}{2} + E_f \frac{bc_f^3}{6} + E_f \frac{bc_f(c_f + c_n)^2}{2} + E_n \frac{bc_n^3}{12} \quad (3.25)$$

$$(EI)_{col} = E_s \frac{bt^3}{6} + E_s \frac{bt(h-t)^2}{2} + E_{col} \frac{ac^3}{12} \quad (3.26)$$

$$EI = (EI)_{col}v_{col} + (EI)_l(1 - v_{col}) \quad (3.27)$$

where E_s is the elastic modulus of the skins in MPa, E_f is the elastic modulus of the foam layer, E_n is the elastic modulus of non-woven, c_f is the thickness for one layer of foam, c_n is the thickness of non-woven. v is the volume fraction, the subscript *col* and *l* represent the columns and layers, respectively. And h and t are the sandwich panel thickness and skin thickness. EI represents the bending rigidity, E is the bending modulus, I is the area moment of inertia of sandwich panel.

Only SW-T0 has a different structure, its shear rigidity can be predicted by:

$$EI = E_s \frac{bt^3}{6} + E_s \frac{bt(h-t)^2}{2} + E_n \frac{bc_n^3}{12} \quad (4.2)$$

To confirm the applicability of the equations, all samples are compared and the results are shown in Table 4.8. All tufted sandwich structures showed large differences, but the prediction value of the non-tufted sandwich panel (SW-T0) provided a reasonably good correlation with the experimental result. Since the flax fiber yarn usually shows a great variability [26], the error range or CV of the sandwich panel without tufting thread (SW-T0) is smaller. The linear density of the tufted flax fiber yarn used in this section is 500 Tex, which is much thicker than the carbon fiber yarn (2×67 Tex) in Chapter 3. As a result, fewer tufting threads on the skin lead to the rough surface and thus larger manual thickness measurement errors, while the bending stiffness is

sensitive to changes in thickness. Thus it is most probably attributed to the large thickness error introduced by the tufted thread. Relevant parameters need to be introduced to correct the equation. The layers can be divided into two parts according to thickness.

Table 4.8 Comparison of the results from experiments and analytical equations.

Sample ID	Bending modulus (kN·m/kg)			
	Experimental result	CV	Analytical result	Difference
SW-T0	4423.47	7.74%	4792.96	8.35%
SW-T6	1015.96	7.13%	1139.24	17.23%
SW-T8	946.75	9.12%	1080.39	14.12%
SW-T10	909.41	10.33%	1057.91	16.33%
SW-T12	785.35	6.89%	952.82	18.61%

The equation 3.25 can be modified as:

$$EI = (EI)_{col}v_{col} + [k(EI)_i^{thick} + (1 - k)(EI)_i^{thin}](1 - v_{col}) \quad (4.3)$$

where $(EI)_i^{thick}$ and $(EI)_i^{thin}$ are the bending stiffness of layers with larger thickness and with smaller thickness, respectively. And k is the volume fraction of the layers with larger thickness. Note that k is estimated by the assumption that the larger thickness is due to the presence of tufting thread on the skin surface.

The prediction values calculated from the corrected equations are shown in Table 4.9. All differences have been effectively reduced and are inside or close to the error range. Due to the high proportion of foam layer (about 0.5-0.6), $(EI)_i$ is slightly smaller than $(EI)_{col}$. Therefore, when the volume fraction of the column increases, its bending rigidity also increases accordingly. The influence of each layer on the flexural properties of the overall structure is determined by its own tensile modulus and its position in the interlayer. Specifically, it is related to the thickness of the interlayer structure, its own thickness and the distance from the neutral plane. Therefore, in the subsequent research, the quantity of nonwoven layers used needs to be first determined according to the requirements of thickness and weight; then, without affecting the resin infusion, their lay-up positions can be placed close to the skin on both sides to obtain a larger area moment of inertia, thus improving the bending stiffness of the sandwich structure.

Table 4.9 Comparison of the results from experiments and analytical equations.

Sample ID	Bending modulus (kN·m/kg)			
	Experimental result	CV	Analytical result	Difference
SW-T6	1015.96	7.13%	939.67	8.12%
SW-T8	946.75	9.12%	902.49	4.90%
SW-T10	909.41	10.33%	888.75	2.33%
SW-T12	785.35	6.89%	852.71	7.90%

4.3.3 Charpy impact test results

The results of Charpy impact tests of the flax fiber-reinforced sandwich panels are shown in Figure 4.9. Results show overall, the non-tufted sandwich specimen had higher values of energy absorbed than the tufted sandwich panels. The added foam and tufting reinforcement didn't present a positive effect on the impact behavior. Since it has been verified in the previous part that the stitching thread is beneficial to the impact performance, it can be known that the reduction of the energy absorption by foam is greater compared to the increase of energy caused by the tufting thread. The figure reveals a slight increase in absorbed energy with the tufting density of sandwich panels.

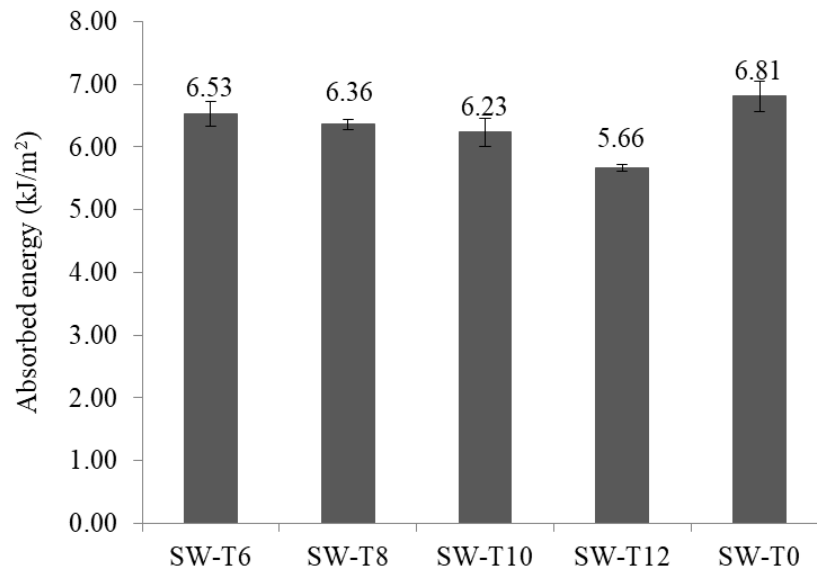


Figure 4.9 Impact behaviors of different sandwich panels.

However, in Figure 4.10 the specific value shows the reverse trend. The specific energy absorbed first increases with the decrease in the tufting density, then SW-T10 and SW-T12 have the same value. If the tufting density continues to decrease we can assume that the value also decreases because the specific energy of the untufted sandwich (SW-T0) is the smallest. The best tufting space should be between 0 and 10 mm.

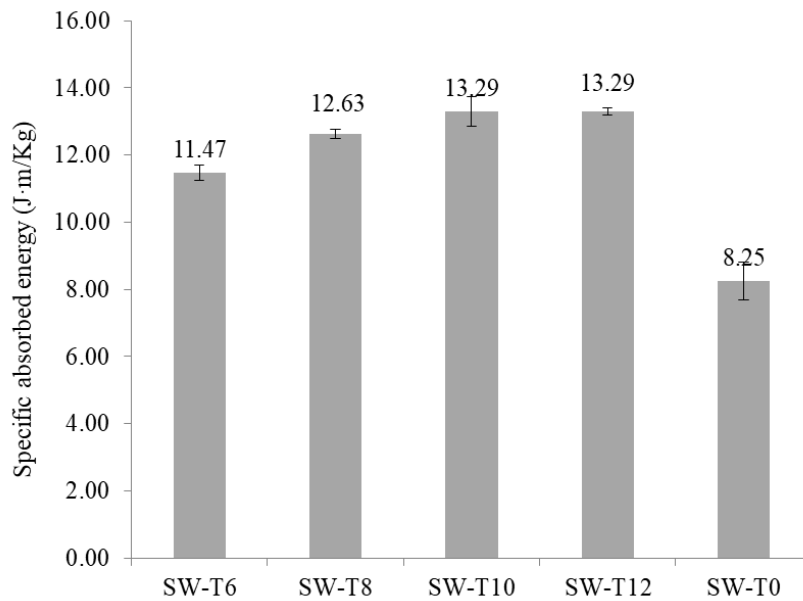


Figure 4.10 Specific impact properties of each sandwich panels.

Another important aspect to be discussed is the characteristic macroscopic rupture of the specimens after the test. Figure 4.11 illustrates typical views of broken specimens of sandwich panels with different tufting densities. It is shown that only the specimen with the pure nonwoven core is separated into two parts after the impact. The more the resin absorbed by the sandwich preform during the LRI process, the more brittle the sandwich panel. Both the less fiber and the presence of foam in tufted sandwich panels could decrease the liquid resin absorption.

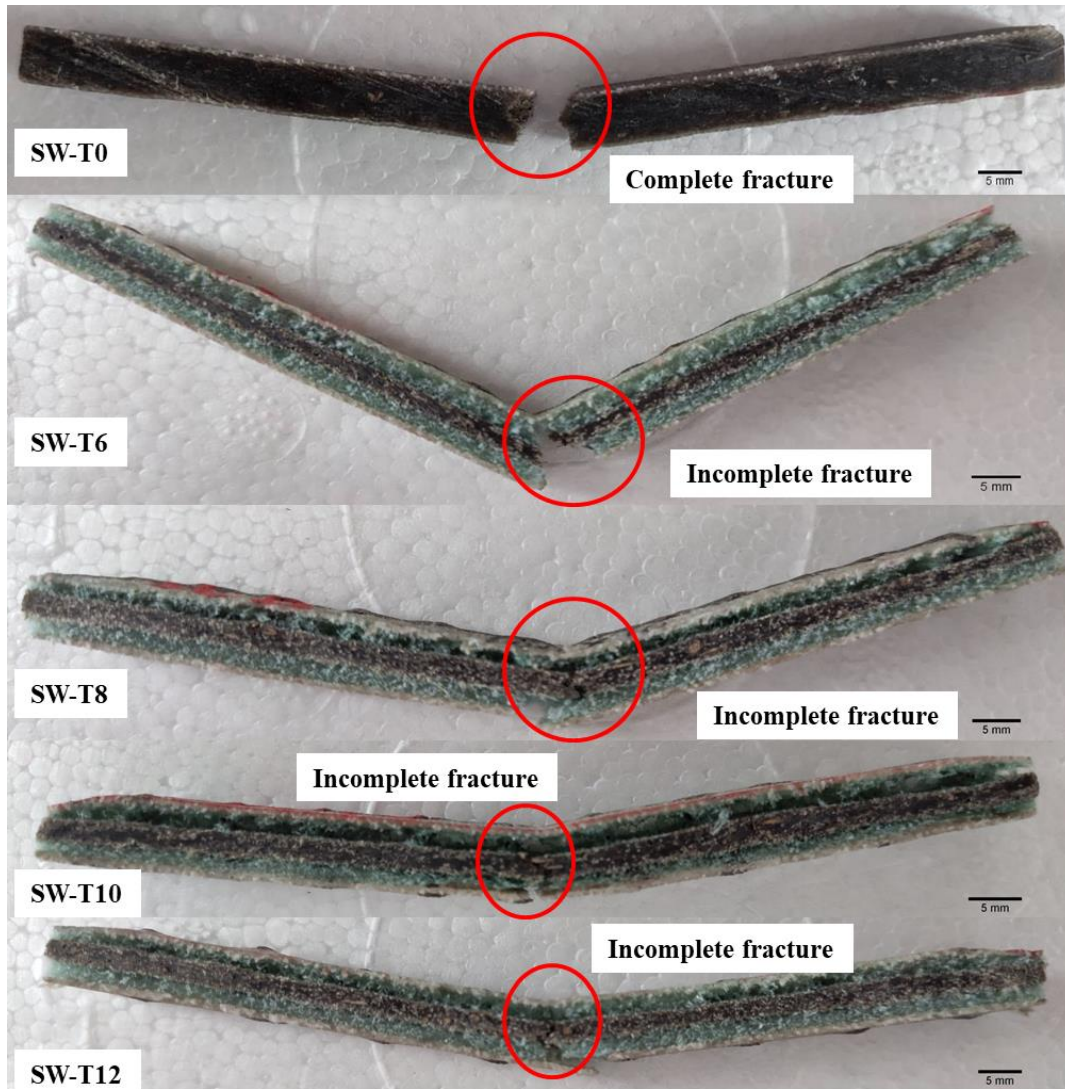


Figure 4.11 Typical ruptured sandwich panels by Charpy impact tests.

The failure mode analysis of the Charpy impact allows a better comprehension of the mechanism responsible for the higher fracture toughness. Figure 4.12 shows the fracture surface of each series of specimens. With lower magnification, the fiber fracture, debonding, delamination, and core damage are observed. In the sample of SW-T0, the fiber fracture and fiber pull-out are the failure modes. Besides these, foam crushing and crack also occurred in the tufted sandwich panels. However, the presence of foam resulted in delamination between the foam and skin. This is most evident in the photo of SW-T12 and became less pronounced as the tufting density increased. Until SW-T6, the delamination is almost not visible. It indicates that the tufting reinforcement can effectively prevent delamination. According to the conclusion of Chapter 3,

tufting reinforcement can effectively improve the impact behavior. With the increase of tufting density, the sample impact resistance is enhanced due to the increase of tufting reinforcements on the one hand; on the other hand, the weight increased, thus decreasing the specific energy absorption of impact. The result differences of tufted sandwich panels caused by different tufting densities are not obvious in this experiment. These results are very close if the error range is taken into account. Therefore, increasing the tufting density obviously increased the weight and thus decreased the specific impact performance.

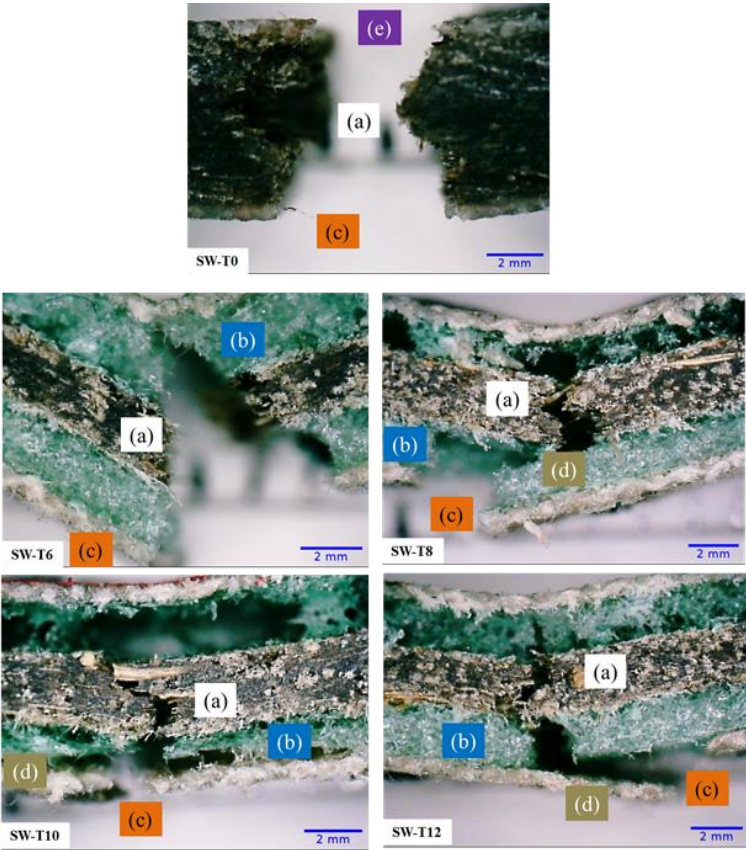


Figure 4.12 Fracture modes: (a) fiber of nonwoven, (b) foam, (c) fiber of bottom skin, (d) delamination and (e) fiber of top skin.

Due to the high brittleness of the resin after curing, the nonwoven core breaks completely into two pieces in all considered cases. Different from the sandwich panel without foam, only matrix cracks occurred in the skin of the impacted side for the tufted sandwich panels with foam layers, and fiber fracture is limited. Hence the energy dissipated by fiber fracture is reduced. In the tufted sandwich panels, the deformation of the skin on the impact side is more obvious than the others.

The fiber volume fractions of the tufted samples are higher; the crack is prevented by the fibers and then the specimen bent around the impact point. The rupture occurred only along with the interface fiber/matrix due to the flexibility of the fibers that are not broken.

Compared to the impact properties of SW-3 in Chapter 3 (23.85 kJ/m² and 34.58 J·m/kg), neither the absorbed energy (6.53 kJ/m²) nor its specific value (11.47 J·m/kg) of SW-T6 is dominant. The prediction of the fracture toughness of fiber-reinforced sandwich composite is quite complicated. It is associated with the work of fiber fracture, matrix fracture, foam fracture and fiber/matrix interfacial debonding, including the post-debonding friction and fiber pull-out. It also depends on the properties of the constituents as well as the fiber length and the fiber orientation. Moreover, the impact energy of the fiber-reinforced composites increases with the augmentation of the fiber length in the final composites [27], which is conducive to carbon fiber.

4.4 Conclusion

This work aimed to manufacture a green sandwich composite by flax fiber reinforcement and bio epoxy resin. Moreover, in this chapter, the effect of tufting density of sandwich with nonwoven core has been studied. The mechanical performances such as bending modulus and maximum force under bending loading, shear modulus and shear stress under shear loading, and absorbed energy under impact loading are examined in comparison with non-tufted sandwich composite with pure nonwoven core.

Comparing the shear stress-strain results, a clear improvement of ultimate shear stress with increased tufting density is observed. Although considering the weight augmentation, the specific stress value of the sandwich panel with the highest tufting density is still the largest. Nevertheless, their shear property is much lower than that of the non-tufted sandwich with the only nonwoven core. Columns through the thickness of the sandwich composites restrict the deformation and movement of the core. This implies that the foam has a negative effect on the core shear behavior of sandwich composite.

The flexural performance of the composites with tufted cores increases with the increase in the count of tufting threads. The sandwich composite with pure nonwoven core presented much higher bending stress and modulus than the tufted sandwich panel with foam layers. It also

satisfies the comparison of specific bending properties. However, the specific shear modulus decreased with increasing tufting density.

Same as the bending test, the impact property is enhanced with increased tufting points, while the change in specific impact property is the opposite. It shows that the improvement from increasing the tufting density is not sufficient to offset the weight increase caused by it.

The foam layer limits the mechanical properties of the sandwich panel in all the test conditions. Consequently, further reduction of the volume fraction of the foam is of potential interest for subsequent studies. And meanwhile, controlling and optimizing the parameters of the tufting and LRI process are important to obtain the expected structural parameters. These parameters need to be investigated to improve theoretical equations.

Due to the similar core structure, the prediction equations of SW-3 in Chapter 3 for shear modulus and bending rigidity are also applicable to the tufted sandwich structure in this chapter. Nevertheless, it should be noted that the large variation of the area moment of inertia (I) caused by the excessive error in the thickness of the skin requires the introduction of relevant correction factors to correct the bending stiffness equation. The equation of shear modulus does not involve the thickness of the skin, so the prediction is closer to the experimental results.

Reference

- [1] Wambua P, Ivens J, Verpoest I. Natural fibres: Can they replace glass in fibre reinforced plastics? *Compos Sci Technol* 2003;63:1259–64. [https://doi.org/10.1016/S0266-3538\(03\)00096-4](https://doi.org/10.1016/S0266-3538(03)00096-4).
- [2] Xue D, Hu H. Mechanical properties of biaxial weft-knitted flax composites. *Mater Des* 2013;46:264–9. <https://doi.org/10.1016/j.matdes.2012.10.019>.
- [3] Mahboob Z, Bougherara H. Fatigue of flax-epoxy and other plant fibre composites: Critical review and analysis. *Compos Part A Appl Sci Manuf* 2018;109:440–62. <https://doi.org/10.1016/j.compositesa.2018.03.034>.
- [4] El-Sabbagh A, Steuernagel L, Ziegmann G, Meiners D, Toepfer O. Processing parameters and characterisation of flax fibre reinforced engineering plastic composites with flame retardant fillers. *Compos Part B Eng* 2014;62:12–8. <https://doi.org/10.1016/j.compositesb.2014.02.009>.
- [5] Rashid M, Hanus JL, Chetehouna K, Khellil K, Aboura Z, Gascoin N. Investigation of the effect of tufts contribution on the in-plane mechanical properties of flax fibre reinforced green biocomposite. *Funct Compos Mater* 2021;2. <https://doi.org/10.1186/s42252-021-00019-z>.
- [6] Lachaud F, Boutin M, Espinosa C, Hardy D. Failure prediction of a new sandwich panels based on flax fibres reinforced epoxy bio-composites. *Compos Struct* 2021;257. <https://doi.org/10.1016/j.compstruct.2020.113361>.

- [7] Betts D, Sadeghian P, Fam A. Experiments and nonlinear analysis of the impact behaviour of sandwich panels constructed with flax fibre-reinforced polymer faces and foam cores. *J Sandw Struct Mater* 2020. <https://doi.org/10.1177/1099636220925073>.
- [8] CoDyre L, Mak K, Fam A. Flexural and axial behaviour of sandwich panels with bio-based flax fibre-reinforced polymer skins and various foam core densities. *J Sandw Struct Mater* 2018;20:595–616. <https://doi.org/10.1177/1099636216667658>.
- [9] Monti A, EL Mahi A, Jendli Z, Guillaumat L. Quasi-static and fatigue properties of a balsa cored sandwich structure with thermoplastic skins reinforced by flax fibres. *J Sandw Struct Mater* 2019;21:2358–81. <https://doi.org/10.1177/1099636218760307>.
- [10] Zuoguang Z, Jijun H, Min L, Yizuo G, Zhijie S. Mechanical performance of X-truss/foam sandwich construction. *J Reinf Plast Compos* 2009;28:2631–43. <https://doi.org/10.1177/0731684408093319>.
- [11] Nanayakkara A, Feih S, Mouritz AP. Experimental analysis of the through-thickness compression properties of z-pinned sandwich composites. *Compos Part A Appl Sci Manuf* 2011;42:1673–80. <https://doi.org/10.1016/j.compositesa.2011.07.020>.
- [12] Potluri P, Kusak E, Reddy TY. Novel stitch-bonded sandwich composite structures. *Compos Struct* 2003;59:251–9. [https://doi.org/10.1016/S0263-8223\(02\)00087-9](https://doi.org/10.1016/S0263-8223(02)00087-9).
- [13] Drake DA, Sullivan RW, Lovejoy AE, Clay SB, Jegley DC. Influence of stitching on the out-of-plane behavior of composite materials – A mechanistic review. *J Compos Mater* 2021. <https://doi.org/10.1177/00219983211009290>.
- [14] Wang P, Lei Y, Yue Z. Experimental and numerical evaluation of the flexural properties of stitched foam core sandwich structure. *Compos Struct* 2013;100:243–8. <https://doi.org/10.1016/j.compstruct.2012.12.040>.
- [15] Cartié DDR, Dell’Anno G, Poulin E, Partridge IK. 3D reinforcement of stiffener-to-skin T-joints by Z-pinning and tufting. *Eng Fract Mech* 2006;73:2532–40. <https://doi.org/10.1016/j.engfracmech.2006.06.012>.
- [16] Hui C, Wang P, Legrand X. Improvement of tufting mechanism during the advanced 3-dimensional tufted composites manufacturing: To the optimisation of tufting threads degradation. *Compos Struct* 2019;220:423–30. <https://doi.org/10.1016/j.compstruct.2019.04.019>.
- [17] Liu LS, Zhang T, Wang P, Legrand X, Soulat D. Influence of the tufting yarns on formability of tufted 3-Dimensional composite reinforcement. *Compos Part A Appl Sci Manuf* 2015;78:403–11. <https://doi.org/10.1016/j.compositesa.2015.07.014>.
- [18] Hartley JW, Kratz J, Ward C, Partridge IK. Effect of tufting density and loop length on the crushing behaviour of tufted sandwich specimens. *Compos Part B Eng* 2017;112:49–56. <https://doi.org/10.1016/j.compositesb.2016.12.037>.
- [19] Henao A, Carrera M, Miravete A, Castejón L. Mechanical performance of through-thickness tufted sandwich structures. *Compos Struct* 2010;92:2052–9. <https://doi.org/10.1016/j.compstruct.2009.11.005>.
- [20] Blok LG, Kratz J, Lukaszewicz D, Hesse S, Ward C, Kassapoglou C. Improvement of the in-plane crushing response of CFRP sandwich panels by through-thickness reinforcements. *Compos Struct* 2017;161:15–22. <https://doi.org/10.1016/j.compstruct.2016.11.034>.
- [21] ASTM Standard. ASTM C273 Standard Test Method for Shear Properties of Sandwich Core Materials. *ASTM Int* 2010;i:1–7.
- [22] International A. ASTM D7264 Standard Test Method for Flexural Properties of Polymer Matrix Composite Materials. *Annu B ASTM Stand* 2007;i:1–11.
- [23] ISO. ISO 179-1: Plastics. Determination of Charpy impact properties. Part 1: Non-instrumented impact test. vol. ns-1. 2006.

- [24] Andersons J. Tensile Strength Model of Ud Flax Fiber Reinforced Polymer Composites. 4th Int Conf Exp Model 2011;II:343–676.
- [25] Omrani F, Soulat D, Ferreira M, Wang P. Effects of needle punching process and structural parameters on mechanical behavior of flax nonwovens preforms. *Adv Aircr Spacecr Sci* 2019;6:157–68. <https://doi.org/10.12989/aas.2019.6.2.157>.
- [26] Wang MP. Caractérisation de la variabilité des propriétés mécaniques aux échelles fils , renforts et composites à base de lin. Université de Lille 1, 2017.
- [27] Fu SY, Lauke B, Mäder E, Hu X, Yue CY. Fracture resistance of short-glass-fiber-reinforced and short-carbon-fiber-reinforced polypropylene under Charpy impact load and its dependence on processing. *J Mater Process Technol* 1999;89–90:501–7. [https://doi.org/10.1016/S0924-0136\(99\)00065-5](https://doi.org/10.1016/S0924-0136(99)00065-5).

CHAPTER 5. GENERAL CONCLUSION

5.1 Conclusions

Sandwich composites have been applied for many decades in many industrial fields. As a structure developed from the conventional laminates, the sandwich composite presents the same defect of delamination due to the lack of through-the-thickness reinforcement. And common polymer foam core with low mechanical properties results in a poor through-the-thickness property and poor impact toughness of sandwich panel. Measures are taken for these two defects. As described in Chapters 1 and 2, reinforcement in the z-axis direction is inserted by tufting on the one hand; on the other, non-woven is used instead of foam to enhance the mechanical properties of the structure. The current works mainly focus on the improvement and optimization of the through-the-thickness reinforcement structure and distribution. However, there are fewer studies on the improvement of the core layer in the X-Y plane.

This thesis addresses the manufacturing and mechanical characterization of tufted sandwich panels with nonwoven layers. This novel structure design is firstly realized for carbon fiber reinforced sandwich composite and is validated beneficial to enhance the mechanical performance. Four groups of sandwich panels with different core architectures are tested under shear, compression, bending and impact loadings. The effect of both tufting thread and nonwoven layer on the mechanical behavior of sandwich specimen are respectively analyzed and discussed. By analyzing and comparing all the results, it can be concluded that the profits brought by the presence of the tufting threads and the nonwoven layer are considerable in all types of mechanical tests. However, the nonwoven core facilitates the resin absorption, which results in an increase in sandwich panel weight. Therefore the specific values of mechanical properties are calculated and compared. It shows that the influence of the tufting thread is still positive on the specific ultimate stress and impact toughness, while the nonwoven presents both advantages and disadvantages.

Since the resin columns connect the top and bottom skins and run through the entire thickness, the final failure mode of the sandwich structure must necessarily involve fracture or buckling of the columns. The fractures mainly occur at the connection point between through-the-thickness resin columns and composite skin or core layers.

Two series of equations are applied to predict the core-shear modulus and bending rigidity, and the majority of the prediction values are found close to the experimental results except for the shear test. The presence of the twisted wire in the resin column leads to the thread not being straightened at the initial stage, which increases the strain and causes large dispersion.

Because of the proven advantages of nonwovens and tufted threads, this structure is used directly in the manufacture of flax fiber reinforced sandwich composite. The effect of tufting density on shear, bending and impact behaviors is studied. The shear, three-point bending and Charpy impact performance of the tufted sandwich composites are enhanced as the count of tufting threads increases. This improvement is not significant for the absorbed impact energy so that if the weight gain from increasing the tufting density is also considered, the sandwich panel with the lowest tufting density has the highest specific value of absorbed energy. For both core shear and three-point bending tests, the tufting density shows significant improvements in mechanical properties except the specific bending modulus. Nevertheless, their performance is much lower than that of the non-tufted sandwiches with the only nonwoven core. Based on the observation of the failure mechanism, it is the foam layer that limits the mechanical properties of the sandwich panel in all test conditions.

The shear modulus prediction equation used for the carbon fiber reinforced sandwich composite also exhibits favorable applicability to the flax fiber sandwich panel. The calculation results of the equation for bending stiffness, however, have large errors. This could be mainly due to the large dispersion of skin thickness caused by the large linear density of tufting thread. A correction factor is introduced to represent the variation of the moment of inertia of the section. The corrected equations offer predictions much closer to the experimental results.

5.2 Perspectives

The mechanical tests with different tufted sandwich panels indicate that accurate control of basic parameters of sample is important regarding the mechanical behavior and characterization. All the problems are focused on one contradiction, finding a compromise between mechanical properties and the weight of the sandwich panel.

The limitations are mainly caused by the low mechanical properties of polymer foam and the excessive resin absorption of the preform. Further optimization of both tufting and LRI process

can be explored, such as minimizing the amount of liquid resin while keeping the complete impregnation. The presence of foam for flax fiber reinforced sandwich composite is due to its isolation of resin. However, the specific mechanical properties of the sandwich with pure nonwoven core are still much higher than the sandwich with foam layers, which indicates the reduction of mechanical property brought by foam is more significant than the decrease of the sample weight. It is worth trying a thinner material instead of foam to isolate the resin, and to insert more nonwovens in the space left.

The failure mechanisms under different test conditions are determined by cross-sectional low magnification micrographs of the sandwich specimens. But it is not able to observe the changes inside the sample during the test. The cracks or deformation are not confirmed. Other observation tools or methods would obtain the status inside the specimen such as the ultrasonic inspection. These methods can also be used to detect the porosity of composite which is neglected in this study because of its low estimated value. However, the distribution of the porosities may concentrate in the tufting area, which could affect the mechanical performance of sandwich composite panel. The next work should consider the effect of this parameter and link it with the optimization of manufacturing process.

The length and arrangement of tufting thread are different on the top skin and bottom skin, which results in different thicknesses of two skin sheets. Though this difference is minimized by removing the tufting loops, a more accurate measurement is conducive. The tensile and shear properties of each component of the sandwich panel are obtained by testing the material without structural damage. Thus the larger errors occur. During the test for each component material, the material should be made as close as possible to its state in the sandwich panel. The measurement of the resin column diameter should also be optimized. The diameter of the tufting needle cannot simply be equated with the diameter of the resin column, because when the tufting needle is retracted, each ply recovers partial deformation. By using a scale in the microscope photos, it was found that the diameter of the resin column is only about half the diameter of the needle.

Present equations are derived based on the classical sandwich theory and can only allow the prediction of shear modulus and bending rigidity. The prediction of failure load or ultimate stress is also needed in future work. The explanation and analysis of the mechanical behavior of

sandwich panels in terms of energy accumulation and release is also interesting and can be applied to verify each other with other mechanisms.

RÉSUMÉ ÉTENDU

Le matériau composite renforcé de fibres est principalement appliqué dans l'aérospatiale, les transports, la construction et l'ingénierie mécanique pour remplacer les matériaux métalliques en raison des rapports résistance/poids et rigidité/poids plus élevés. Il existe deux types courants de structures : le composite stratifié et le sandwich composite. Le premier est constitué de plusieurs couches textiles dans différentes orientations et a été développé plus tôt et a un plus large éventail d'applications. Les composites en sandwich sont développés selon la structure stratifiée, dont le but est de réduire encore le poids du matériau. Cette structure est normalement fabriquée en joignant deux peaux externes minces et rigides à une âme interne légère et épaisse. La couche d'âme du composite sandwich est responsable de la connexion des peaux supérieure et inférieure, améliorant la capacité portante en flexion de la structure et transférant la contrainte de cisaillement entre deux peaux. Par conséquent, des matériaux de densité inférieure telle que la mousse polymère sont souvent utilisés afin de garantir que la structure est suffisamment légère. En tant qu'une structure développée à partir de stratifié, le composite sandwich présente le même problème de délaminage causé par les faibles propriétés mécaniques de l'interface entre l'âme et la peau. La solution actuelle consiste à insérer des renforts à travers l'épaisseur des structures sandwich. Le composite sandwich avec renfort dans l'axe Z a été validé avec succès pour améliorer la résistance au cisaillement et à la flexion. Plusieurs techniques ont été proposées et développées telles que le tissage 3D, le z-pinning et la couture/piquage. Néanmoins, le tissage 3D a une capacité limitée de la machine. Les broches de Z-pinning sont indépendantes, il n'y a donc pas d'ancrages sur les peaux supérieure et inférieure. En conséquence, ils présentent moins efficace pour empêcher le délaminage. Comparé à d'autres procédés, le piquage est plus efficace et moins coûteux. Les faibles propriétés mécaniques de l'âme en mousse polymère conduisent généralement à une mauvaise résistance aux dommages par impact. En plus du délaminage, la rupture de mousse est un autre mode de défaillance courant du composite sandwich. Cependant, les gains de la mousse pour réduire le poids du composite sont considérables. Le non-tissé est adopté comme substitut en raison de ses meilleures performances mécaniques que la mousse polymère et une densité inférieure à celle de tissu. Cette adoption est d'abord validée en utilisant des matières premières en fibre de carbone.

La conception d'une nouvelle structure sandwich et son procédé de fabrication sont présentés en détail dans le chapitre 2. Tous les panneaux composites sandwich dans le présent travail sont fabriqués par les procédés de piquage et d'infusion de résine liquide (LRI). Les paramètres pertinents sont identifiés et les variables parmi celles-ci sont étudiées dans les chapitres suivants.

Dans le chapitre 3, l'influence de la couche de non-tissé et du fil de piquage sur le comportement mécanique est étudiée sous des charges de cisaillement, de compression, de flexion et de résilience Charpy. Et la faisabilité d'utiliser du non-tissé au lieu de la mousse comme couche centrale de la structure sandwich est initialement vérifiée en fonction des résultats expérimentaux. Le fil de piquage dans la direction Z et la couche d'âme en non-tissé peuvent améliorer efficacement les propriétés mécaniques du panneau sandwich. Cependant, l'âme non tissée facilite l'absorption de la résine, ce qui entraîne une augmentation du poids du panneau sandwich. Par conséquent, les valeurs spécifiques des propriétés mécaniques sont calculées et comparées. Des études ultérieures dans la section suivante sont sur la variation du nombre de points de piquage pour obtenir la meilleure amélioration des propriétés mécaniques. Étant donné que les colonnes de résine relient les peaux supérieure et inférieure et traversent toute l'épaisseur du composite sandwich, le mode de défaillance doit nécessairement impliquer la rupture des colonnes. Les fractures se produisent principalement aux points de connexion entre les colonnes de résine et les couches composites de peau ou d'âme. Le module de cisaillement et la rigidité en flexion sont prévus par les équations. Les valeurs du premier présentent une grande erreur et la rigidité en flexion prédite est proche du résultat. La présence du fil torsadé dans la colonne de résine conduit à ce que le fil ne soit pas redressé au stade initial, ce qui augmente la déformation et provoque des erreurs importantes.

Les préoccupations environnementales croissantes ont encouragé les chercheurs à adapter des matériaux recyclables pour remplacer les matériaux traditionnels pour la fabrication de composites sandwichs. Le bio composite à base de fibres naturelles connaissent aujourd'hui une évolution croissante dans tous les secteurs industriels en raison de son faible coût, sa faible densité, sa résistance spécifique élevée, sa faible consommation d'énergie lors de sa fabrication, ses caractéristiques biodégradables et sa recyclable. Parmi les fibres naturelles telles que le chanvre, le jute et le bambou, les fibres de lin présentent un grand intérêt en tant que renfort pour les bio composites en raison de leurs meilleures propriétés mécaniques.

En raison des avantages prouvés des non-tissés et des fils de piquage, cette structure est utilisée directement dans la fabrication de composite sandwich renforcé en fibres de lin. L'effet de la densité de piquage sur les comportements de cisaillement, de flexion et d'impact est étudié. Les performances de cisaillement, de flexion en trois points et d'impact Charpy du composite sandwich sont améliorées à mesure que le nombre de fils de piquage augmente. Cette amélioration n'est pas significative pour l'énergie d'impact absorbée. De sorte que si le gain de poids résultant de l'augmentation de la densité de piquage est également pris en compte, le composite sandwich avec la densité de piquage la plus faible a la valeur spécifique d'énergie absorbée la plus élevée. Pour les essais de cisaillement d'âme et de flexion trois points, la densité de piquage montre des améliorations significatives des propriétés mécaniques, à l'exception du module de flexion spécifique. Néanmoins, leurs performances sont bien inférieures à celles des sandwiches non piqués avec uniquement une âme de non-tissé. Sur la base de l'observation du mécanisme de défaillance, c'est la couche de mousse qui limite les propriétés mécaniques du panneau sandwich dans toutes les conditions d'essai. La réduction des propriétés mécaniques du composite sandwich est plus évidente que la diminution du poids apportée par la mousse. Cela vaut la peine d'essayer un matériau plus fin au lieu de mousse pour isoler la résine et insérer plus de non-tissés dans l'espace laissé.

L'équation de prédiction du module de cisaillement utilisée pour le composite sandwich renforcé en fibres de carbone présente également une applicabilité favorable au panneau sandwich en fibres de lin. Cependant, il existe une grande erreur entre la valeur calculée par l'équation de rigidité en flexion et les résultats expérimentaux. Cela pourrait être principalement dû à une grande erreur d'épaisseur de peau causée par la grande densité linéaire du fil de piquage. La rigidité et le module de flexion sont très sensibles aux variations du moment quadratique. Un facteur de correction est introduit pour représenter la variation du moment quadratique. Les équations corrigées offrent des prédictions plus proches des résultats expérimentaux.

Development, characterization and optimization of sustainable green composites with advanced sandwich structure

ABSTRACT

Sandwich composites normally consist of two skins with high mechanical properties and a lightweight core that undergoes mainly the shear loading. They are employed in many industries, such as construction, automotive, sports and aerospace, due to their advantage in weight saving and stiffness. At the request of being lightweight, polymer foam is one of the most common core materials. Developed on the base of traditional laminate, the sandwich composite presents the same delamination problem caused by the weak mechanical properties of the interface between the core and the skin. The common method is inserting the reinforcement through the thickness of the sandwich, which has been successfully validated to improve the shear and bending strength and stiffness. A number of processes have been proposed and developed such as z-pinning, 3D weaving, stitching and tufting. Compared with the other techniques, tufting presents a higher efficiency and less cost. Another common failure mechanism is the rupture of the crack of foam core because of its lower mechanical properties than composite skins. However, the gains of foam to reduce the weight of composite are considerable. Thus, the nonwoven is adopted as a substitute due to its better mechanical performance than polymer foam and lower density than weaving skins. This adoption is first validated by using carbon fiber raw materials. The influence of nonwoven layer and tufting thread are investigated under shear, compression and bending loadings. Both nonwoven and tufting threads are capable of effectively enhancing the mechanical properties of the sandwich composite. In recent years, increasingly stringent environmental requirements have prompted researchers to develop green sandwich composites. After verifying the feasibility of adding nonwoven layers, the novel sandwich structure is realized by using flax fiber reinforcements because the flax fiber exhibits normally higher mechanical properties among the natural fibers. And bio based epoxy resin is selected to replace epoxy resin and fabricate the green sandwich composite.

Key words: Sandwich composite, Nonwoven, Tufting, Mechanical properties

Développement, caractérisation et optimisation de composites durables avec une structure sandwich avancée

RÉSUMÉ

Les sandwichs composites se composent normalement de deux peaux aux propriétés mécaniques élevées et d'une couche d'âme légère qui subit principalement le cisaillement. En raison de leur avantage sur la réduction de poids et l'augmentation de rigidité, ils sont utilisés dans de nombreuses industries, telles que la construction, l'automobile, le sport et l'aérospatiale. A la demande d'être léger, la mousse polymère est l'un des matériaux d'âme les plus courants. Développé à base de la structure stratifiée traditionnelle, le sandwich présente le même problème de délaminage causé par les faibles propriétés mécaniques de l'interface entre l'âme et la peau. La méthode courante consiste à insérer le renfort à travers l'épaisseur du sandwich, ce qui a été validé avec succès pour améliorer la résistance au cisaillement et à la flexion. Un certain nombre de procédés ont été proposés et développés tels que le z-pinning, le tissage 3D, la couture et le piquage. Comparé aux autres techniques, le piquage présente une efficacité plus élevée et un coût moindre. Un autre mécanisme de défaillance commun est la rupture de l'âme en mousse en raison de ses propriétés mécaniques plus faibles que les peaux composites. Cependant, les gains de la mousse pour réduire le poids du composite sont considérables. Ainsi, le non-tissé est adopté comme substitut en raison de ses meilleures performances mécaniques que la mousse polymère et une densité inférieure à celle des peaux de tissu. Cette adoption est d'abord validée en utilisant des matières premières en fibre de carbone. L'influence de la couche non-tissé et du fil de piquage est étudiée sous des charges de cisaillement, de compression et de flexion. Le non-tissé et le fil de piquage sont capables d'améliorer efficacement les propriétés mécaniques du sandwich composite. Ces dernières années, les exigences environnementales de plus en plus strictes ont incité les chercheurs à développer des sandwichs composites écologiques. Après avoir vérifié la faisabilité de l'ajout d'une couche de non-tissé, la nouvelle structure est réalisée en utilisant des renforts en fibre de lin car elle présente des propriétés mécaniques normalement plus élevées parmi les fibres naturelles. Et la bio résine époxy est sélectionnée pour fabriquer le sandwich composite écologues.

Mots-clefs : Sandwich composite, Non-tissé, Piquage, Propriétés mécaniques